



THE UNIVERSITY  
*of* ADELAIDE

# **Vibration signatures of defective bearings and defect size estimation methods**

**Alireza Moazen-ahmadi**

School of Mechanical Engineering

The University of Adelaide

Adelaide, South Australia, 5005

Australia

A thesis submitted in fulfilment of the requirements for the degree  
of Ph.D. in Mechanical Engineering  
on the 18th March 2016

## **Abstract**

Rolling element bearings are widely used in rotary machinery, often with extremely demanding performance criteria. The failure of bearings is the most common reason for machine breakdowns. Machine failures can be catastrophic, resulting in costly downtime and sometimes in human casualties. The implementation of condition monitoring systems, which use data from various sources to determine the state of bearings, is commonly used to predict bearing failure. Hence, a considerable amount of attention has been devoted to bearing failure modes, fault detection, fault development and life expectations of bearings. The focus of this research is on the fault detection and defect size estimations of ball and cylindrical rolling element bearings with outer race defects.

In classic bearing vibration condition monitoring methods, the trend of vibration amplitudes is often used to determine when a bearing should be replaced. As a defect on the surface of a bearing raceway enlarges, the changes in the size and shape of the defect due to successive passes of the rolling elements can result in a fluctuation of the averaged measured values of the vibration amplitude. As an alternative to studying measures of vibration severity in order to determine the size of the defect indirectly, the actual geometric arc length of a bearing defect can be determined from the vibration signal and used to decide when to replace the bearing. The research in this project provides an insight into both the stiffness behaviour of a defective bearing assembly, with ball and cylindrical rolling elements, and the characteristics of the vibration signature in defective bearings in order to identify the vibration features associated with the entry and exit events of bearing defect. The ultimate aim of this research is to develop methods to accurately estimate the size of a defect on the outer raceway of a bearing, which are not dependent on the

magnitude of the vibration response, but instead use these features for tracking defect size in bearings.

In the research conducted here, the vibration excitation of a bearing associated with line-spall defects is studied both experimentally and analytically. An improved nonlinear dynamic model of the contact forces and vibration responses generated in defective rolling element bearings is proposed to study the vibration characteristics in defective bearings. It is demonstrated that previous models are not able to predict these events accurately without making significant assumptions about the path of rolling elements in the defect zone. Similar to the results of the analytical modelling, the experimental results show that there are discrepancies in previous theories describing the path of the rolling elements in the defect zone that have led to poor results in simulating the vibration response and the existing defect size estimation methods. The parametric study presented here shows that the relative angular extents between the entry and exit events on the vibration results decrease with increasing load. Significant speed dependency of these angular extents is shown by simulation and experimental measurements of defective bearings as the operational speed increases. The sources of inaccuracy in the previously proposed defect size estimation algorithms are identified and explained. A complete defect size estimation algorithm is proposed that is more accurate and less biased by shaft speed when compared with existing methods.

A method is presented for calculating and analysing the quasi-static load distribution and varying stiffness of a bearing assembly with a raceway defect of varying load, depth, length, and surface roughness. It has been found that as the shaft and rollers in a defective bearing rotate, it causes the stiffness of the bearing assembly to vary, which cause parametric vibration excitations of the bearing assembly. It is shown that when the defect

size is greater than one angular roller spacing, signal aliasing occurs and the vibration signature is similar to when the defect size is less than one angular roller spacing. Using the results from simulations and experimental testing, signal processing techniques are developed to distinguish defect sizes that are less than or greater than one angular roller spacing.

The results of this study provide an improved hypothesis for the path of a rolling element as it travels through a defect and its relationship to the vibration signature in a bearing.

# Contents

<b>Abstract</b>	<b>i</b>
<b>Declaration</b>	<b>vi</b>
<b>Acknowledgments</b>	<b>vii</b>
<b>Nomenclature</b>	<b>viii</b>
<b>Chapter 1. Introduction</b>	<b>1</b>
1.1 Background .....	1
1.2 Aims and objectives .....	4
1.3 Thesis outline .....	5
1.4 Publications arising from this thesis .....	9
1.5 Format .....	10
References	
<b>Chapter 2. Literature review</b>	<b>13</b>
2.1 Background.....	13
2.1.1 Rolling element bearings .....	13
2.1.2 Parametric excitation in bearings .....	14
2.1.3 Excitation due to defects .....	15
2.2 Vibration signature and condition monitoring in defective bearings .....	18
2.2.1 Detection.....	19
2.2.2 Severity analysis.....	21
2.2.3 Vibration signature and defect size estimation methods .....	23
2.2.4 Effect of slippage.....	27
2.2.5 Effect of clearance .....	28
2.2.6 Stiffness of the bearing assembly .....	29

2.3 Models of defective bearings.....	31
2.4 Conclusion of literature review and objectives .....	38
<b>Chapter 3. Nonlinear dynamic model of defective rolling element bearings</b>	<b>51</b>
Paper 1: A nonlinear dynamic vibration model of defective bearings – the importance of modelling the finite size of rolling elements.....	55
<b>Chapter 4. Parametric studies</b>	<b>73</b>
Paper 2: The path of rolling elements in defective bearings: Observations, analysis and methods to estimate spall size.....	77
<b>Chapter 5. Stiffness analyses in rolling element bearings</b>	<b>93</b>
Paper 3: The importance of bearing stiffness and load when estimating the size of a defect in a rolling element bearing .....	97
<b>Chapter 6. Defect size estimation in rolling element bearings</b>	<b>123</b>
Paper 4: A defect size estimation method based on operational speed and path of rolling elements in defective bearings .....	127
<b>Chapter 7. Conclusion and Future Work</b>	<b>153</b>
7.1 Conclusion.....	153
7.1.1 Multi-body nonlinear dynamic model of a defective bearing .....	153
7.1.2 Experimental testing.....	154
7.1.3 Stiffness analyses in defective bearings .....	156
7.1.4 Comprehensive defect size estimation algorithm.....	157
7.2 Recommendations for future work.....	157
7.2.1 Effect of defect entry and exit geometry on the vibration signature .....	159
7.2.2 Deformable components.....	160
7.2.3 Time-frequency signal processing algorithms.....	160

## **Declaration**

I certify that this work contains no material which has been accepted for the award of any other degree or diploma in my name, in any university or other tertiary institution and, to the best of my knowledge and belief, contains no material previously published or written by another person, except where due reference has been made in the text. In addition, I certify that no part of this work will, in the future, be used in a submission in my name, for any other degree or diploma in any university or other tertiary institution without the prior approval of the University of Adelaide and where applicable, any partner institution responsible for the joint-award of this degree.

I give consent to this copy of my thesis, when deposited in the University Library, being made available for loan and photocopying, subject to the provisions of the Copyright Act 1968.

The author acknowledges that copyright of published works contained within this thesis resides with the copyright holder(s) of those works.

I also give permission for the digital version of my thesis to be made available on the web, via the University's digital research repository, the Library Search and also through web search engines, unless permission has been granted by the University to restrict access for a period of time.

Alireza Moazen-ahmadi

Date: 27/9/2016

## **Acknowledgment**

I would firstly like to acknowledge my principal supervisor Dr Carl Howard for his endless support and guidance during the course of this study; I continue to learn a lot from him. I would also like to thank the co-supervisors of the project, Dr Dick Peterson and Dr Steven Grainger who have shared their knowledge and expertise. I thank you all sincerely.

I would also like to thank all of my friends, (of whom there are many), who have supported me throughout my research endeavours. I would like to extend my thanks to the technicians of the Mechanical and Electrical workshops in the School of Mechanical Engineering at the University of Adelaide, who have assisted in the fabrication of the designed models as well as the provision of the required equipment. You have all been a source of knowledge, fun and friendliness, and to you all I express my thanks.

Finally I save the biggest thanks to my parents Abdolhai Moazen ahmadi and Homa Dohan and to my sister Nazanin Moazen-ahmadi whose love and support have led me to this point. This journey has been as much hard work for you as it has been for me and through your support we have made it, together. Words cannot express my thanks and appreciation.



## Nomenclature

$c$	linear contact damping
$c_s$	damping of the support, subscript “s” defines the component ‘Support’
$cl$	bearing clearance
$D_b$	roller diameter. Subscript “b” is used for ‘Ball’
$D_p$	nominal pitch diameter. Subscript “p” means “Pitch”
$F$	contact forces
$g$	acceleration of gravity
$K$	load-deflection factors
$k$	nonlinear contact stiffness
$k_s$	stiffness of the support. Subscript “s” is used for ‘Support’
$m_b$	mass of the rolling elements, subscript “b” is used for ‘Ball’
$m_i$	mass of the inner ring plus the shaft, subscript “i” is used for “Inner”
$m_o$	mass of the outer ring plus the support structure. Subscript “o” is used for “Outer”
$m_r$	equivalent mass associated with the high frequency bearing resonance. Subscript “r” is used for “resonance”
$N_b$	number of rolling elements
$Q$	radial contact force
$T$	total kinetic energy
$t_i$	time to impact
$V$	total potential energy
$W$	static load

## Symbols

$\phi$	angular position
$\alpha_i$	angle of impact
$\omega_s$	run speed of the shaft
$\omega_c$	run speed of the cage
$\delta$	contact deformations
$\delta_{\max}$	maximum contact deformations
$\gamma$	defect shape function

## Subscripts

in	denotes the inner raceway
$j$	denotes the $j^{th}$ rolling element
out	denotes the outer raceway
$r$	denotes the $r^{th}$ row of the bearing

# Chapter 1

## Introduction

### 1.1. Background and motivation

Rolling element bearings are widely used in rotary machinery, often with extremely demanding performance criteria. The failure of bearings is the most common reason for machine breakdowns [1-3]. Machine failures can be catastrophic, resulting in costly downtime and sometimes human casualties. The implementation of condition monitoring systems, which use data from various sources to determine the state of bearings, is commonly used to predict bearing failure. Hence, a considerable amount of attention has been devoted to bearing failure modes, fault detection, fault development and life expectations in bearings. The focus of this research in this project is on the detection of faults and estimation of the size of defects in bearings, by analysing vibration signals.

Defects in bearings are commonly categorised as either localized or distributed defects. Unlike the distributed defects, localized defects do not extend completely across the raceway. Distributed defects, such as waviness, surface roughness, or off-size rolling elements, are usually the result of manufacturing errors [4, 5]. Localized defects are often initiated by insufficient lubrication film between the surfaces that are in contact or normal fatigue failure, and the defects grow in size and change shape over time. Metal-to-metal contact between the rolling elements and the raceways, which generate stress waves, in time lead to the formation of sub-surface cracks. The large forces in bearings cause the sub-surface cracks to grow into surface defects. This phenomenon is called pitting or spalling [6]. In this thesis the term “Extended defect” is used for localized defects that are larger than

the angular spacing between two rolling elements. In the present study, attention has been given to localized defects on the outer raceway of rolling element bearings.

In classic bearing vibration condition monitoring methods, the trend of vibration amplitudes is often used to determine when a bearing should be replaced after exceeding a nominated threshold level. As a defect on the surface of a bearing raceway enlarges, the changes in the size and shape of the defect due to successive passes of the rolling elements can result in a fluctuation of the averaged measured values of the vibration amplitude [7-11]. As an alternative to studying measures of vibration severity in order to determine the size of the defect indirectly, the actual geometric arc length of a bearing defect can be determined from the vibration signal and used to decide when to replace the bearing. Bearing vibration condition monitoring to estimate the arc length of a defect is relatively new and requires detailed analyses of the vibration signature. Therefore, extensive experiments and accurate models to study the dynamic behaviour and the vibration response in defective bearings are necessary.

Generally speaking, models that are adaptable to represent the dynamics of different bearing configurations and capable of predicting the path of rolling elements in the defect zone without making major assumptions have not been found. Thus the objective of this thesis is to present a general approach for physical multi-body modelling of rolling element bearings. An improved nonlinear dynamic model of the contact forces and vibration responses generated in defective rolling element bearings is proposed to study the vibration characteristics in defective bearings. In the model developed in this research, the path of a rolling element is predicted by taking into account its mass and finite size, and the actual defect geometry is used in the model. Unlike the current bearing models, the proposed model does not make assumptions about the path of the rolling elements or artificially modify the simulated defect geometry. Similar to the results of the analytical modelling, the

experimental results show that there are discrepancies in previous theories describing the path of the rolling elements in the defect zone that have led to poor results when simulating the vibration response and in the existing defect size estimation methods. The model developed here can be used to simulate the vibration response of bearings with a raceway defect to aid in the development of new diagnostic algorithms. The model has the potential to consider modelling different defect profiles on different bearing components. However, the developed model is used for studying the dynamic behaviour and vibration response of defective bearings with localized defects on the outer raceway.

The stiffness of the bearing assembly directly affects the vibration signature in rolling element bearings. Therefore, analysing the stiffness in bearings, and defective bearings in particular, is essential when the vibration signature in bearings is studied. Several defect size estimation methods have been suggested previously for localized defects in bearings, based on detecting the time separation between entry and exit events from the vibration signal [12, 13]. These defect size estimation methods underestimate the size of a defect that is larger than at least one roller angular spacing. This is because the time separations between entry and exit events are similar on the vibration signal. The stiffness behaviour of a defective bearing assembly is studied and a signal processing method, which is based on analyses of stiffness variations in defective bearings, is proposed in this research.

The main motivation for this PhD project is to improve the reliability and accuracy of condition monitoring systems for rolling element bearings by developing a comprehensive vibration analysis and by improving understanding of the interactions between different components in rolling element bearings to develop defect size estimation algorithms. The ultimate aim of this research is to develop reliable and accurate defect size estimation methods that are not dependent on the magnitude of the vibration response, but instead use features of the vibration signal that are generated when a rolling element enters and exits a

defect. This has been achieved by identifying the gaps in the associated literature, and addressing them in order to make a comprehensive defect size estimation method for localized defects in bearings.

## **1.2. Aims and objectives**

Note that the format of this PhD thesis is by publication, where several chapters comprise published or submitted journal papers. The start of each chapter contains an introductory summary about the journal publication, including a list of the aims from the journal paper. An overall list of aims from all the technical chapters is included in this section, so that the reader has a “global view” of the aims of this thesis. The aims of this research project are:

- To develop an improved nonlinear dynamic model of the contact forces and vibration responses generated in defective rolling element bearings to study the vibration characteristics in defective bearings. The focus of this research is on the fault detection and defect size estimations of ball and cylindrical rolling element bearings with outer race defects.
- To provide an insight into the stiffness behaviour of a defective bearing assembly and analyse the static load distribution and varying stiffness of a bearing with a raceway defect of varying parameters.
- To provide insights into the characteristics of the vibration signature in defective bearings in order to identify the vibration features associated with the entry and exit events into a defect in bearings.
- To propose a signal processing technique based on the stiffness variation in defective bearings to distinguish defect sizes that vary in size by at least one ball angular spacing.

- To undertake a parametric study on the vibration characteristics of the defective bearings in order to address the sources of errors in the current defect size estimation methods.
- To develop reliable and accurate defect size estimation methods that are not dependent on the magnitude of the vibration response, but instead use features of the vibration signal that are generated when a rolling element enters and exits a defect.

### **1.3. Thesis outline**

This thesis is presented in a number of chapters, the sequence of which highlights the chronology of the knowledge-development and the research undertaken to meet the project aims. The first chapter, which is the introduction, provides an overview of the subject matter as well as the principal aims and specifies briefly the gaps in the related knowledge. Chapter 2 provides a comprehensive literature review and explains the gap in knowledge as well as the importance of the research in more detail. The main body of the thesis, Chapters 3 to 6, is a collection of four manuscripts that have been published, or are currently under review. These publications present the progress made in the course of this study and explain the achievements of this research. Finally, the conclusions of the research performed, in addition to some basic recommendations for future work, are given in Chapter 7. In the following paragraphs the content of each chapter and the alignment of the research with the specified aims are explained.

Chapter 2 provides a review of the vibration excitation mechanisms in healthy and defective bearings, followed by an extensive literature review of the characteristics of the vibration signature in defective bearings. It is followed by a brief discussion of the existing condition monitoring techniques used to detect defects and to determine the severity of defects in bearings. This chapter includes a comprehensive literature review of bearing models that

allow for the study of the bearing vibration response under certain operational conditions. The review identifies the primary research gaps that have been addressed by the current work.

Chapter 3 is the first of four journal publications that has been published [14]. In this chapter, an improved nonlinear dynamic model of the contact forces and vibration responses generated in rolling element bearings, with an outer raceway defect, is developed. The improvement comes about by considering the finite size of the rolling elements, which overcomes the limitations exhibited by previous models caused by the modelling of rolling elements as point masses. For line spall defects, a low frequency event occurs in the measured vibration response when a rolling element enters the defect. Previous models were not able to accurately predict this event without making the simulated and actual defect geometries significantly different. The chapter also presents comparisons between the proposed model, previous models and experimental results carried out to show that the low and high frequency events are more accurately predicted. This analysis identifies and explains the mechanisms leading to the inaccuracies of the previous models. The outcome of this chapter is a hypothesis to explain the path of rolling elements in the defect zone, which explains the discrepancies in the previous assumptions of the path of rolling elements in the defect zone and the corresponding features on the vibration response to the entry and exit events. The model presented in this chapter is used in subsequent analyses presented in this thesis.

Chapter 4 is the second of four journal publications that has been published [15]. This chapter presents an experimental investigation of the vibration signature generated by rolling elements entering and exiting a notch defect in the outer raceway of a bearing. The hypothesis of the path of rolling elements in the defect zone and the corresponding features on the vibration response to the entry and exit events, developed in Chapter 3, is tested

experimentally by simultaneously measuring the vibration generated by a defective bearing on a bearing housing, and the shaft displacement. These key features can be used to estimate the size of a defect and are demonstrated in this paper for a range of shaft speeds and bearing loads. It is shown that existing defect size estimation methods include assumptions that describe the path of the rolling elements in the defect zone, leading to poor estimates of the size of a defect. A new method is proposed to estimate the size of a defect, and is shown to be accurate for estimating a range of notch defect geometries over a range of shaft speeds and applied loads.

Chapter 5 is the third of four journal papers (submitted). In this chapter the hypothesis of using the low frequency variation in stiffness to distinguish defects that vary in size by exactly one angular ball spacing is investigated, based on analytical and experimental results. This hypothesis was initially suggested by Petersen et al. [16] based on numerical simulations, in which the author of this thesis is a co-author. However, this hypothesis was not validated with experimental test results and is the subject of the third journal paper and this chapter of the thesis. Moreover, the hypothesis suggested by Petersen et al. [16] is further improved to include the important effects of the applied load on the static stiffness in defective bearings, which were ignored previously. A time-frequency technique to detect the variation in the frequency response of the vibration signal due to stiffness variations of the bearing assembly is suggested, and the importance of including the effect of load in developing an accurate defect size estimation method is demonstrated in this chapter. Recommendations for condition monitoring are given, based on the analyses presented in this chapter. The new method that is proposed does not rely on prior historical vibration data for assessing the damage in a bearing, unlike previously suggested methods.

The methods and results presented in this chapter contribute to the wider experimental investigation of the effects of load on the varying static stiffness in defective bearings and



their effects on measured vibration signatures. The force-displacement relationships for defective bearings under various static radial loadings at various cage angular positions are analytically estimated, experimentally measured and then they are compared. The study shows the importance of the effect of the applied load on the static stiffness variations in defective rolling element bearings. These findings are presented in the third of the four journal publications. The experimental measurements of the effect of the defect size and the applied load on the varying stiffnesses of bearing assemblies has not been shown previously and provides valuable knowledge for developing methods to distinguish between bearings with defects that vary in size by exactly one angular ball spacing.

Chapter 6 is the fourth of four journal papers (submitted) and presents investigations into the effect of the centrifugal and inertia forces acting on the rolling elements on the measured vibration signature in defective bearings. The sources of inaccuracy and the speed-dependency in the existing defect size estimation algorithms are identified and explained. The speed dependency of the angular extents between the low frequency entry events and the high frequency exit events on the vibration signal have been shown by experimental measurements and simulation. The simulation in this chapter is carried out using the model developed in Chapter 3. The analyses presented in this study are essential to develop accurate and reliable defect size estimation algorithms, which are also suitable for bearings under various operational speeds. The simulations and experimental measurements in this study have led to the derivation of a hybrid method to more accurately estimate the size of a defect in a bearing, which is shown not to be biased for operational speed, unlike previous methods. The hybrid method, presented in Chapter 6, uses the analyses presented in this chapter; the model presented in Chapter 3 and the defect size estimation algorithm proposed in Chapter 4.

In Chapter 7, the key conclusions that have been documented throughout the thesis will be summarised. Potential works still exist for future investigations, and are listed in the final chapter.

#### **1.4. Publications arising from this thesis**

The research presented in this thesis has led to the generation of five journal manuscripts and three peer reviewed conference articles. The journals and conferences in which the papers are published or submitted are closely related to the field of the research of this thesis and will be cited in the following section. Following is a list of the manuscripts resulting from the current research:

##### **Journal papers**

Main author:

1. A. Moazen Ahmadi, D. Petersen, C.Q. Howard, A nonlinear dynamic vibration model of defective bearings – the importance of modelling the finite size of rolling elements, *Mechanical Systems and Signal Processing* 52–53 (2015) 309-326. published online (DOI: 10.1016/j.ymsp.2014.06.006). [Current total number of citations: 13].
2. A. Moazen Ahmadi, C.Q. Howard, D. Petersen, The path of rolling elements in defective bearings: Observations, analysis and methods to estimate spall size, *Journal of Sound and Vibration* 336 (2016) 277-292. published online (DOI: 10.1016/j.jsv.2015.12.011).
3. A. Moazen Ahmadi, C.Q. Howard, The importance of bearing stiffness and load when estimating the size of a defect in a rolling element bearing, *Journal of Sound and Vibration* (Submitted to *Journal of Sound and Vibration* on 17/03/2016).

4. A. Moazen Ahmadi, C.Q. Howard, A defect size estimation method based on operational speed and path of rolling elements in defective bearings, *Journal of Sound and Vibration* (Submitted to *Journal of Sound and Vibration* on 17/03/2016).

Co-author:

5. D. Petersen, C.Q. Howard, N. Sawalhi, A. Moazen Ahmadi, S. Singh, Analysis of bearing stiffness variations, contact forces and vibrations in radially loaded double row rolling element bearings with raceway defects, *Mechanical Systems and Signal Processing* 50-51 (2015) 139-160. [Current total number of citations: 19].

### **Refereed conference papers**

1. A. Moazen Ahmadi, D. Petersen, C.Q. Howard, A nonlinear dynamic model of the vibration response of defective rolling element bearings, *Proc of Australian Acoustical Society*, Victor Harbor, Australia, 2013.

2. A. Moazen Ahmadi, D. Petersen, C.Q. Howard, N. Sawalhi , Defect size estimation and analysis of the path of rolling elements in defective bearings with respect to the operational speed, *Inter.noise 2014*, Melbourne, Australia, 2014.

3. A. Moazen Ahmadi, C.Q. Howard, Observation and analysis of the vibration and displacement signature of defective bearings due to various speeds and loads, *Inter.noise 2015*, San Francisco, USA, 2015.

### **1.5. Format**

The thesis has been submitted as a portfolio of the publications, according to the formatting requirements of The University of Adelaide. The printed and online versions of this thesis are identical. The online version of the thesis is available as a PDF and can be viewed using Adobe Reader 9.

## References

1. J.M. Erdman, R.J. Kerkman, D.W. Schlegel, and G.L. Skibinski, *Effect of PWM inverters on AC motor bearing currents and shaft voltages*. Industry Applications, IEEE Transactions on, 1996. **32**(2): p. 250-259.
2. S. Grubic, J.M. Aller, B. Lu, and T.G. Habetler, *A survey on testing and monitoring methods for stator insulation systems of low-voltage induction machines focusing on turn insulation problems*. Industrial Electronics, IEEE Transactions on, 2008. **55**(12): p. 4127-4136.
3. O.V. Thorsen and M. Dalva, *A survey of faults on induction motors in offshore oil industry, petrochemical industry, gas terminals, and oil refineries*. Industry Applications, IEEE Transactions on, 1995. **31**(5): p. 1186-1196.
4. Y.T. Su, M.H. Lin, and M.S. Lee, *The effects of surface irregularities on roller bearing vibrations*. Journal of Sound and Vibration, 1993. **165**(3): p. 455-466.
5. C. Sunnersjö, *Rolling bearing vibrations-the effects of geometrical imperfections and wear*. Journal of Sound and Vibration, 1985. **98**(4): p. 455- 474.
6. T.A. Harris, *Rolling Bearing Analysis*. 2001, USA: Wiley.
7. N.S. Swansson and S. Favaloro, *Applications of vibration analysis to the condition monitoring of rolling element bearings*. 1984, DTIC Document.
8. P. Boto, *Detection of bearing damage by shock pulse measurement*. Ball Bearing Journal, 1971(167): p. 1-8.
9. T. Williams, X. Ribadeneira, S. Billington, and T. Kurfess, *Rolling element bearing diagnostics in run-to-failure lifetime testing*. Mechanical Systems and Signal Processing, 2001. **15**(5): p. 979-993.
10. N. Gebraeel, M. Lawley, R. Liu, and V. Parmeshwaran, *Residual life predictions from vibration-based degradation signals: a neural network approach*. Industrial Electronics, IEEE Transactions on, 2004. **51**(3): p. 694-700.
11. N. Gebraeel, A. Elwany, and J. Pan, *Residual life predictions in the absence of prior degradation knowledge*. Reliability, IEEE Transactions on, 2009. **58**(1): p. 106-117.
12. S. Zhao, L. Liang, G. Xu, J. Wang, and W. Zhang, *Quantitative diagnosis of a spall-like fault of a rolling element bearing by empirical mode decomposition and the approximate entropy method*. Mechanical Systems and Signal Processing, 2013. **40**(1): p. 154-177.

13. N. Sawalhi and R.B. Randall, *Vibration response of spalled rolling element bearings: observations, simulations and signal processing techniques to track the spall size*. Mechanical Systems and Signal Processing, 2011. **25**(3): p. 846-870.
14. A. Moazen Ahmadi, D. Petersen, and C.Q. Howard, *A nonlinear dynamic vibration model of defective bearings – the importance of modelling the finite size of rolling elements*. Mechanical Systems and Signal Processing, 2015. **52–53**: p. 309-326.
15. A. Moazen Ahmadi, C.Q. Howard, and D. Petersen, *The path of rolling elements in defective bearings: observations, analysis and methods to estimate spall size*. Journal of Sound and Vibration, 2016. **336**: p. 277-292.
16. D. Petersen, C.Q. Howard, N. Sawalhi, A. Moazen Ahmadi, and S. Singh, *Analysis of bearing stiffness variations, contact forces and vibrations in radially loaded double row rolling element bearings with raceway defects*. Mechanical Systems and Signal Processing, 2015. **50-51**: p. 139-160.

## **Chapter 2**

### **Literature Review and Background**

This chapter introduces basic concepts of rolling element bearings, defects that can occur in bearings, vibration generation mechanisms in rolling element bearings, vibration signatures and current fault diagnosis techniques in rolling element bearings, using vibration signals and simulations of defective rolling element bearings. The chapter concentrates on three main aspects of rolling element bearings, namely, the characteristics of the vibration signal generated in defective bearings, numerical simulations of defective bearings, and algorithms that use vibration signals to estimate the size of a defect in a bearing.

#### **2.1. Background**

##### **2.1.1. Rolling element bearings**

Rolling element bearings allow relative rotary movements and are widely used in industry. As opposed to journal or plain bearings, the main loads are transferred through moving rolling elements. The main components of rolling element bearings are rolling elements (in the form of balls or rollers), a cage, which sometimes is referred to as a separator, an inner ring, and an outer ring. The hardened surfaces of the inner and outer rings that are in contact with the rolling elements are called inner and outer raceways. The most important geometrical quantities of rolling element bearings are the pitch diameter, the number of rolling elements and the roller diameter. Figure 1 shows the arrangement of a ball bearing and the above-mentioned important components. The load zone shown in Figure 1 is associated with the horizontal load applied to the centre of the inner ring. In bearings under load, some rolling elements lose contact with one or both raceways and the system becomes

highly nonlinear [1]. The area within which the rolling elements are still in contact with both raceways and carrying load, is generally referred to as the loaded zone.

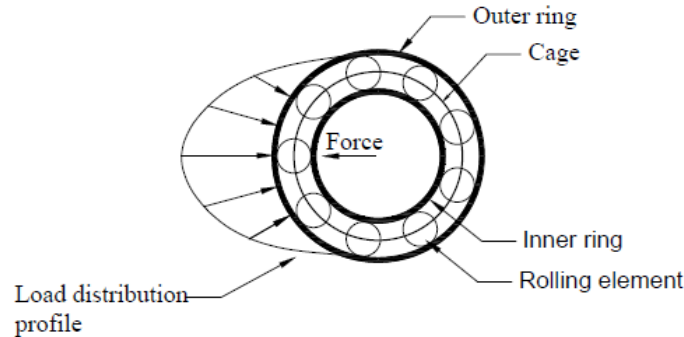


Figure 1: Schematic view of a rolling element bearing and its components.

Bearings that are subjected to an externally applied axial load and bearings subjected to preloading have uniformly distributed contact loads. However, the load distributed in bearings that are subjected to an externally applied radial load is not uniform and the profile of the load distribution depends on both the geometry of the bearing and the direction of the applied load.

### 2.1.2. Parametric excitation in bearings

The rotation of the cage in rolling element bearing causes variations in the number of loaded rolling elements in the load zone over time. As the contacts between the rolling elements and the raceways are elastic, the bearing stiffness becomes explicitly dependent on time. Since the time varying stiffness is considered a system parameter, it leads to a phenomenon known as parametric excitation. This phenomenon causes vibration generation in rolling element bearings even if the geometry of a ball bearing is perfect [2]. The characteristic frequency of the generated vibration due to the parametric excitation that is transmitted through the outer ring is called the ball pass frequency. This frequency in a rolling element

bearing with the cage constant angular velocity,  $\omega_c$ , equals  $N_b \omega_c / 2\pi$  (Hz), where the parameter  $N_b$  denotes the total number of rolling elements in the bearing.

Vibration modes of a ring can be extensional, flexural or rigid body modes; see Figure 2. The contacts between a rolling element and raceways in a ball bearing can be represented by nonlinear springs [1]. The vibrations in a healthy bearing are mostly a combination of flexural vibrations of the outer ring and the housing, along with the rigid body vibrations of the shaft.

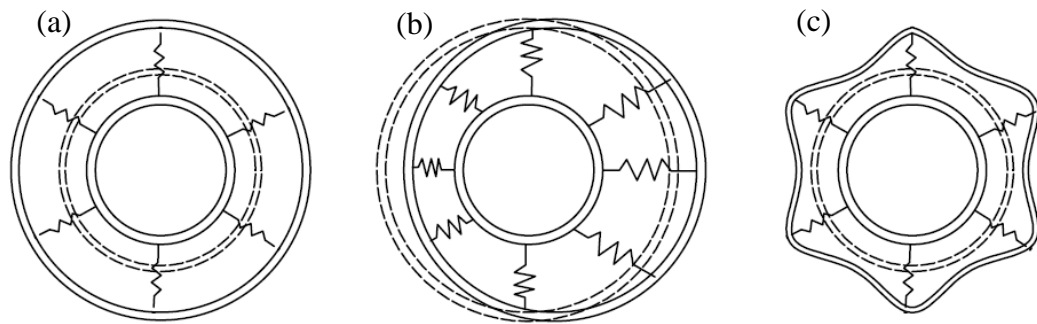


Figure 2: (a) Radial extensional mode. (b) Rigid body mode. (c) Deformation of the outer ring due to equally spaced rolling elements (flexural mode).

### 2.1.3. Excitation due to defects

Rolling element bearings may become defective by several means and at different stages through the service life of the bearing. At the early stage of the service life, bearing defects may be a result of inappropriate design, manufacturing error, misalignment, overload and faulty installation [3]. Defects in bearings are commonly categorised into localised and distributed defects. Distributed defects, such as waviness, surface roughness, or off-size rolling elements, are usually the result of manufacturing errors [4, 5]. Whereas, localised defects do not cover the entire surface of a raceway. Localised defects are often initiated by



insufficient lubrication film between the surfaces in contact or normal fatigue failure and grow in size and shape over time.

Waviness is one of the common distributed defects and are sinusoidal-shaped imperfections on the outer surface of the bearing components. The characteristic wavelengths of the waviness defects are much larger than the dimensions of the contact Hertzian deformation areas between rolling elements and the raceways. Waviness causes variations in the contact forces during operation which, in turn, generate vibrations in the bearing. The amplitude of these variations depends on the amplitude of the waviness defects and the contact stiffness. The resulting vibration modes of the rings can be either extensional, flexural or rigid body modes (see Figure 2). Waviness defects cause vibrations at distinct frequencies which depend on the wavenumber of the defect, the number of waves per circumference, the rotational speed and the location of the defect. The formulas for these distinct frequencies are included in Appendix 2A at the end of this chapter. A comprehensive overview of the vibrations generated in ball bearings was given by Wardle [6] and Yhland [7].

A fault in a bearing is described as localised when it does not extend completely across the raceway. Localised defects in rolling element bearings are often caused by insufficient lubrication film between the surfaces in contact, contamination, presence of moisture, corrosive or abrasive substances or improper loading and fatigue, and grow in size over time [3]. Metal-to-metal contact between the rolling elements and the raceways generates stress waves, which in time, form sub-surface cracks. In an ideal condition where the bearing is free from any contamination and it is properly loaded and lubricated, the repeating stresses acting on the load carrying surfaces can be extremely high and cause fatigue [1]. Fatigue in rolling element bearings is caused by the application of repeated stresses on a finite volume of material [1]. Fatigue failure outcomes include peeling, pitting, flaking, pitting and spalling and results in the removal of the material from the inner raceway, the outer raceway or the

rollers. By definition, fatigue pitting is relatively shallow; approximately 10  $\mu\text{m}$  and appears on the contact surfaces with a maximum depth of the hardened section of the surface, whereas spalling is typically deeper in size (20 $\mu\text{m}$  to 100  $\mu\text{m}$ ) [8]. Through the formation and development of defects into spalls or cracks, localised faults will be formed. As the defect deteriorates due to the pitting effect, it grows into an extended defect. In this research, ‘extended defect’ refers to those defects where the angular extent of the defect is equal to or larger than the angular spacing between the rolling elements. Examples of line-spall defects on different bearing components that have occurred from operational use are shown in Figure 3.

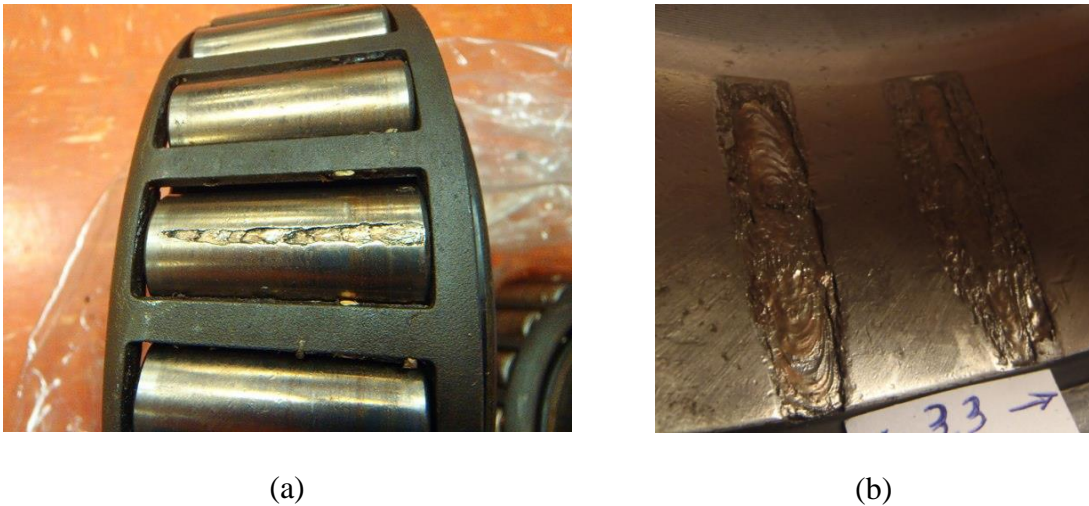


Figure 3: Common line-spall bearing faults. (a) Line spall on the roller. (b) Line-spall on the outer raceway.

Bearings that have defects with sharp edges produce impulses at known defect fault frequencies, and are functions of the geometry of the bearing, the rotational speed of the bearing and the location of the fault (inner-raceway, outer-raceway or rollers) [9-11]. Depending on the stage of the fault development on a bearing component, the impulsive signals can be weak and difficult to detect. In classic bearing fault detection methods, often called vibration condition monitoring, defects, locations (raceways or rolling elements) and

defect severity, are identified by detection of vibration occurring at the bearing fault frequencies that are listed in Appendix 2A at the end of this chapter.

## **2.2. Vibration signature and condition monitoring in defective bearings**

Rolling element bearings are widely used in rotating machinery and bearing failure is one of the most common reasons for machinery breakdowns. The common measure of bearing life is the number of revolutions or the number of hours before the first defects appear under specific operation conditions [12].

To estimate the remaining useful life of bearings, fatigue life prediction theories have been developed [13, 14]. In these theories, the geometry of the bearing and other factors, such as material properties, lubricant, temperature, load, and speed, are considered for the estimation of the fatigue life probability in bearings. These models have been improved over time [15, 16]. Some modifications were based on discrete finite element methods [17, 18] and some account for the debris inside a bearing [19]. The objective of all of these bearing failure criteria is to estimate the bearing life before the first evidence of fatigue or characterising the fatigue with a severity level. The acceptable fatigue severity determines the bearing life criterion, which may differ case by case. For example Timken Company laboratories define the fatigue criterion and life expectancy based on pitting of an area of  $0.01\text{in}^2$  [12, 20]. However, Timken also observe that the useful bearing life of the bearing may extend considerably beyond this point. Therefore, bearing failure criteria that pre-determines the service life of a bearing may not ensure the optimum useful life of the bearing in service. Moreover, no single failure criterion is applicable for all situations, where the bearing is operating under different conditions.

With condition monitoring systems in place, the unnecessary costs due to scheduled maintenance can be reduced by only addressing bearings that have been identified as

potentially faulty, without any assumption of the bearings' life expectancy. Effective bearing condition monitoring systems should be able to detect and, more importantly, determine the severity of the defect in bearings correctly at the early stages of defect development in order to enable remedial action to be taken.

### **2.2.1. Detection**

In classic bearing fault detection methods, the amplitude of the signals at the bearing fault frequencies (described in Section 2.1.3) are compared against threshold levels and, when the amplitude exceeds the threshold level, an alarm is triggered to replace the faulty bearing [21]. Conventional signal processing methods applied on the vibration signal to detect the bearing fault frequencies include Power Spectral Density (PSD), envelope analysis [22], sonogram [23] and cyclo-stationary analysis [24]. The Envelope analysis is the most commonly used technique to detect impact type faults in bearings. It was initially developed to transfer the very high resonant carrier frequency components to the lower frequency range, and can provide a good frequency resolution [22]. Since the successful application of this technique depends on the existence of impulses in the signal, which in turn excite the natural frequencies of the system, bearings with weak or no impact type faults are difficult to identify using Envelope analysis.

Antoni and Randall [25], and Immovilli [26] showed where defective bearings do not have a deterministic vibration signature, fault frequency components cannot be identified using a demodulation process. Immovilli [26] proposed utilising the Kurtogram, which is a 3D spectrum of the kurtosis value of a signal (the z-axis) on a frequency resolution (the y-axis) versus frequency (x-axis) plot, to identify the fault related bandwidth and conduct statistical analyses of the vibration signal. In his method, the energy of the bandwidth which maximises the kurtosis will be used as a diagnostic index. This method relies on the assumption that

each transient event in the signal is associated with an optimal frequency resolution pair, which maximises its kurtosis.

Randall [27] measured the vibration from a gearbox which had combinations of extended faulty bearings with very weak impacts and faulty worn gears. He suggested that the cyclo-stationary property of the vibration signal can be used to distinguish bearing faults, which have cyclo-stationary property, from gear faults that have periodic properties. They observed that envelope analysis failed to show the ball-pass frequency because of the dominant presence of the vibration occurring at the shaft speed and harmonics in the spectrum. Although the proposed method is claimed to be effective in distinguishing bearing faults on the inner raceway from gear-mesh faults, it should be noted that the only interfering signal (gear-mesh signal) is periodic. In their proposed method, fault identification is based on the fact that other machine signals (the periodic gear-mesh signal in this case) was modulated by the bearing fault signal. If the length of the recorded data is insufficient to capture the cyclo-stationary property of the bearing fault, for example data captured for only  $180^\circ$  of shaft rotation, Sawalhi's and Randall's method [27] would fail to distinguish the bearing faults from other signals.

Sawalhi and Randall [28] conducted experimental testing on roller ball bearings that had extended faults on the inner raceway and outer raceway, where faults were artificially manufactured using an electric etching pencil. They showed that using an envelope analysis in conjunction with a Kurtogram, failed to identify the faults at the bearing fault frequencies. However, they showed that the Spectral Correlation Function (SCF), a tool to analyse cyclo-stationary signals, can be used in conjunction with Envelope analysis to improve the detection process. At a given cyclic frequency, the Power Spectral Density (PSD) can be calculated. This spectrum is called the Cyclic Spectral Density. Sawalhi and Randall [28]

used the Cyclic Spectral Density at the cyclic frequency equivalent to the rotational frequency of the inner ring and thereby improved the detection results.

### **2.2.2. Severity analysis**

Bearing failure begins where a spall develops on the surface, thus exciting the fundamental defect frequency and its harmonics (multiple integers of the defect frequency). Effective bearing condition monitoring systems should be able to detect and assess the severity or estimate the size of defects in bearings at the early stages of defect development, either to enable remedial action to be taken, or to schedule the replacement of the bearing at a convenient time. Conventionally, the severity of defects is related to the magnitude of the transient oscillations, as each rolling element strikes the fault at different locations within the load zone. Alternatively, the geometric arc length of a bearing defect from the vibration signal can be determined to assist replacement decision making. The presence of the harmonics of the defect frequency is another indication of the formation and growth of a spall in a bearing [1].

The study by Igarashi and Hamada showed the width and shape of pulses in both time signals and the frequency spectrum of the vibration signals generated by different defects changes [29, 30]. Redistribution of energy in the frequency spectrum, as a fault progresses, causes the magnitude of the characteristic frequency components to increase [31]. The relationship between the magnitude of the measured vibration response and defect growth has been investigated on bearings in run-to-failure studies [32-36]. In these studies, the trend of traditional vibration and acoustic metrics such as Root-Mean-Square (RMS) and kurtosis are measured. The results of these studies show that the RMS of vibration and acoustic signals has a general increasing trend to the end of life of the bearing, regardless of the location of the fault. However, at some stage, the RMS value decreases and rises again. Figure 4

illustrates the fluctuation in the averaged RMS values of the amplitude of the defect frequency and its first six harmonics as the defect propagates along the surface of the raceway [35]. This fluctuation can be explained by a phenomenon known as ‘healing’. The term is applied when the sharp edges of the fault zone are smoothed. This phenomenon overpowers the increase of the signal level because of the fault growth. However, as the fault develops further, the overall vibration level increases again. Therefore, the RMS value cannot be used as a measure to track the true trend of the defect growth reliably. This is because the bearing might be at the stage where it exhibits low RMS values while the bearing fault has grown in size.

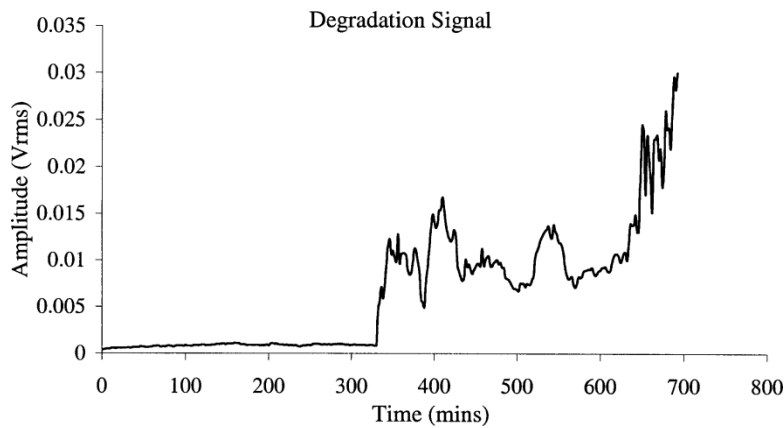


Figure 4: Evolution of the averaged amplitude of the defective frequency and its first six harmonics [35]

Williams et al. [34] conducted run-to-failure experiments on bearings and monitored the trend of the kurtosis value for both vibration and acoustic data. This value fluctuates in time as the fault grows, and depends on both the size of the fault and the geometry of the edges of the fault. Since impulses in the vibro-acoustic signature of bearings are generated for line spall faults with sharp entrance and exit edges, this results in high values of kurtosis. However, once the fault grows beyond the spacing of the rollers, the distribution of the signal becomes closer to a normal distribution, and the Kurtosis value decreases. The reduction of

the value of kurtosis could also be due to the gradually worn sharp edges of the fault. Therefore, while the kurtosis value might be a good indicator for detection of impact type bearing faults with fixed areas, it cannot be used to detect non-impact type bearing faults as the kurtosis value fluctuates with the size of the fault.

As an alternative to studying severity measures, to indirectly determine the size of a defect, the actual geometric arc length of a bearing defect from the vibration signal can be determined and used for deciding when to replace a bearing. This study aims to consider the characteristics of the vibration signal in defective bearings and propose new defect size estimation methods that are not dependant on the magnitude of the vibration response. The following section contains an overview of defect size estimation methods.

### **2.2.3. Vibration signature and defect size estimation methods**

Measurement studies of defective ball bearings with a line spall defect show that the passage of a rolling element over the spall generates two main vibration characteristics: entry and exit events [37]. Several defect size estimation methods suggested previously are based on determining the time between these two events, and are reviewed in this section.

Sawalhi and Randall [28] conducted experimental testing on rolling element bearings with machined defects and developed a hypothesis to explain the characteristics of the measured vibration signal in defective bearings. Shown in Figure 5, Sawalhi and Randall [37] assumed that point A (the local maxima of the low frequency event) corresponds to the entry point, while the largest high frequency responses in magnitude, shown as point B in Figure 5(b), in the multiple impact region, correspond to the exit point of the defect. The entry of a rolling element into a line spall defect produces a vibration signal with low frequency content [37, 38]. The exit of the rolling element excites a much broader range of frequencies, including the high frequency bearing resonances. These resonances are excited by the impact of the



rolling element mass on the exit point of a defect, as well as the parametric excitations caused by rapid changes in the bearing stiffness, which occur when the rolling element re-stresses between the raceways [2]. The high frequency event observed in experimental results [38, 39] often appears to have been caused by multiple impacts rather than a single impact. Simulation results of defective bearings presented by Singh et al. [40] indicate that multiple impacts occur when a rolling element strikes the inner and outer raceways successively as it is re-loaded at the exit point. Sawalhi and Randall [37] suggest that the high frequency impulsive event in the measured vibration response occurs when the centre of a rolling element is halfway through the defect. These researchers claim that the defect size can be estimated by finding points A (the low frequency local maxima) and B (the high frequency event) and doubling the distance between points A and B in order to estimate the defect size.

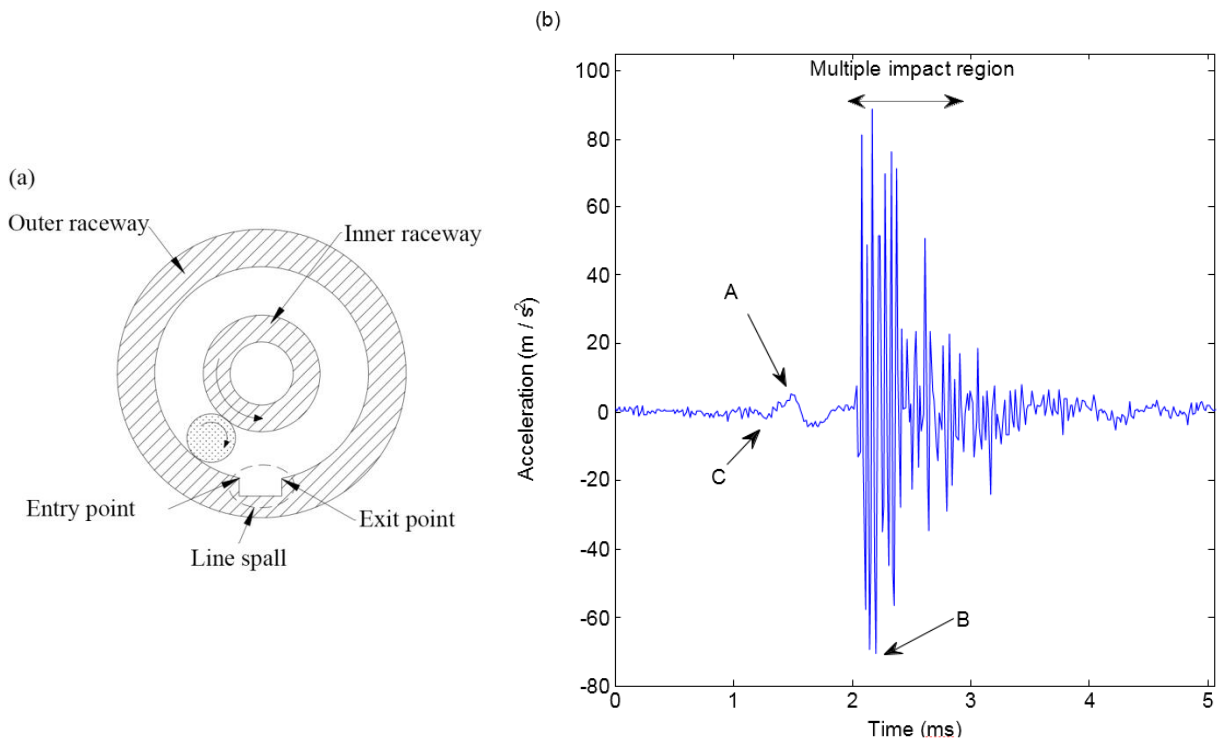


Figure 5: (a) Diagram of a rolling element travelling into a line spall defect located on the outer raceway. (b) A typical measured vibration response. Points A and B are typically identified as entry and exit points, as suggested by previous studies [37, 41], whereas the analysis in this paper shows that points C is the entry point and the exit point happens in the multiple impact region.

Figure 6 shows the estimated size of a bearing defect for two test bearings (with 0.6mm and 1.2mm defect sizes) using the hypotheses of the path of rolling elements developed by Sawalhi and Randall [37]. The inaccuracy and speed dependency of the estimated defect size indicate that the previous hypotheses describing the path of rolling elements and the explanation for high-frequency vibration is inadequate. Previous studies that investigated the speed dependence of the path of a rolling element from point A, the end of the entry transient event, to the first impact point of a rolling element at the exit. Smith et al. [42] tried to identify systematic errors in conventional spall size estimation methods being speed dependent. However, detailed simulations have not been done to explain and investigate the physics of the interaction between rolling elements and defects. In order to develop an accurate defect size estimation method based on the detection of the high-frequency event, detailed analyses of the effect of speed on the angular extent between entry and first exit impact events are essential and is addressed in the study presented here. In this thesis, the analyses have been undertaken experimentally and analytically by modelling the path of rolling elements in defective bearings.

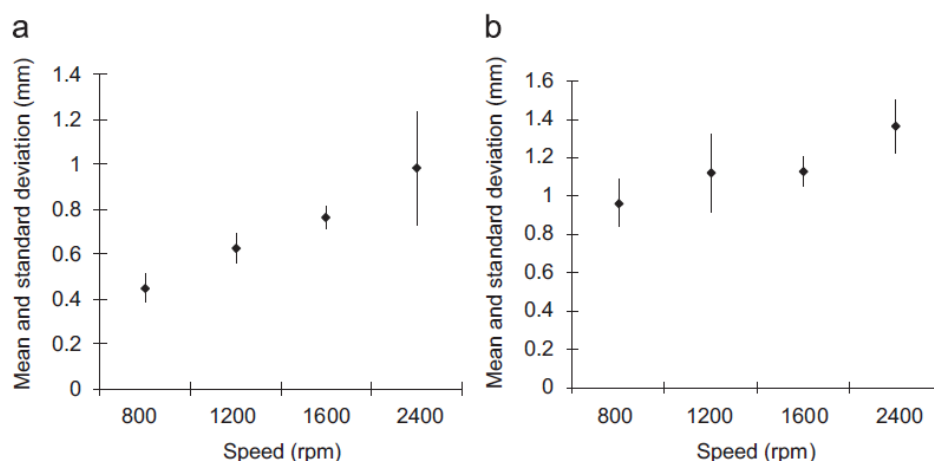


Figure 6: The mean spall size estimate (mm) and the standard deviation (error) around each estimate for outer race faults: (a) small spall (0.6 mm) and (b) large spall (1.2 mm) [37].

Figure 7 shows two experimental test results of the acceleration measured on a bearing housing, for two defective ball bearings with localised defects that vary in size by exactly one angular ball spacing as a function of the cage angular position. The figure shows the sizes (in degrees) of the defects on each test bearing. It can be seen that the angle between any two successive entry and exit events appear nearly identical for both Test Bearing 1 (TB1) and Test Bearing 2 (TB2), despite TB1 having a defect size of  $15.8^\circ$  and TB2 having a defect size of  $55.8^\circ$  (i.e.  $40^\circ$  larger). This is because the balls will enter and exit the defects in TB1 and TB2 with the same period as defects vary in size by exactly one angular ball spacing. Hence, current defect size estimation methods underestimate the size of a defect that is larger than, at least, one ball angular spacing.

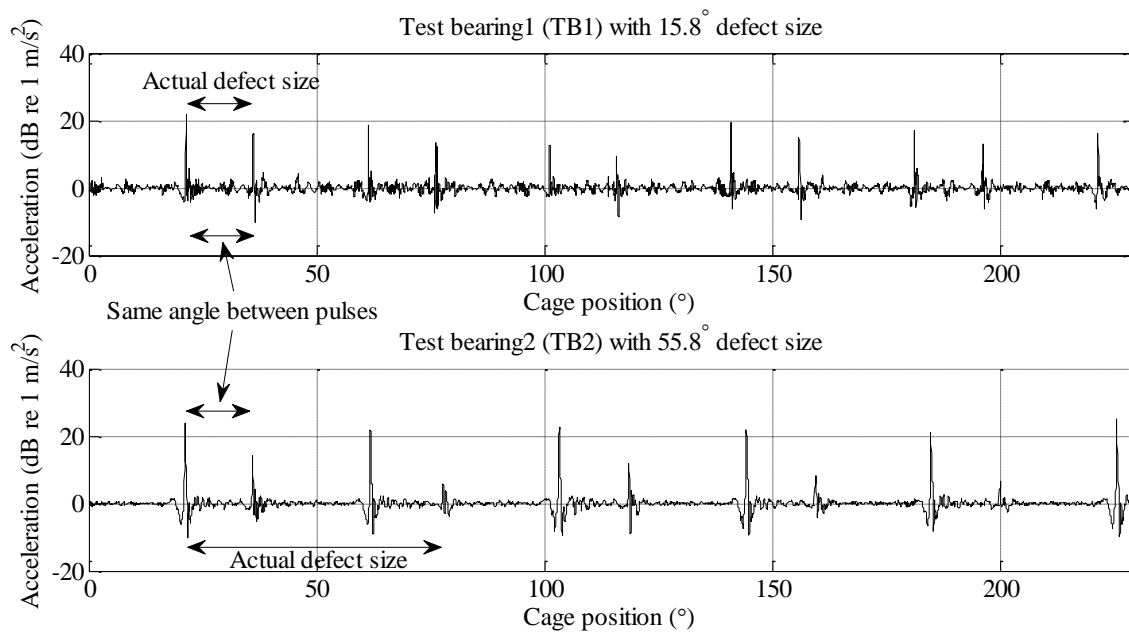


Figure 7: Experimentally measured acceleration in the horizontal direction of bearings TB1 ( $15.8^\circ$  defect size) and TB2 ( $55.8^\circ$  defect size) as a function of angular cage position at 500N of load and a shaft speed of 600 rpm. The corresponding sizes of the defects are indicated on the figures.

To resolve these issues, Petersen et al. (including the author Moazen-ahmadi) [2, 43] suggested the possibility of using stiffness variations in defective bearings as a measure to distinguish between extended defects and line-spall defects. They present an analytical formulation of the varying static stiffness and load distribution of a ball bearing assembly as a function of the cage angular position. Petersen et al. [2, 43] created a mathematical model to analyse the static stiffness variations in defective bearings with square shaped outer raceway defects of varying circumferential extents and similar depths, but did not validate their hypothesis with experimental test result.

#### **2.2.4. Effect of slippage**

Slippage in rolling element bearings causes variations in the time intervals associated with the defect-related impulses. Random variations occur due to slippage associated with the motion of the rolling elements within the loading zone and so the vibration signal is not periodic but rather it is termed non-stationary [44-46]. The contact angle between the rolling elements and the outer raceway and inner raceway varies with the position of each rolling element. The effect of this is that each rolling element has a different effective rolling diameter and tries to roll at different speeds. Since the cage limits the spacing of the rolling elements, some slippage occurs. The slippage phenomenon is a function of lubrication, ball cage clearance, angular alignment, as well as speed and load. Lubrication traction has a major effect on the rolling element slippage. Slippage happens when the moment due to the drag forces on the ball, which is created by the viscous shearing resistance of the grease, exceeds the traction moment at the raceway contacts [47]. The typical values for the maximum phase variation of the cage angular position suggested in the literature are of the order of 0.01–0.02 rad [48, 49]. In condition monitoring, the phenomenon of slippage makes fault identification a difficult task as the high phase variations lead to unclear results in conventional frequency analyses. This issue can be resolved by time-frequency analyses.

Alternatively, envelope analysis can be used to cope with the slippage phenomenon as it uses only the first few defect frequency harmonics, which generally remain discrete at the frequencies of interest.

### **2.2.5. Effect of clearance**

The effect of clearance on the vibration signal from a bearing has been investigated by Gurkan [50]. The maximum bearing force at the excitation frequency increases with increasing clearance. It is also observed that introducing clearance in a bearing causes a sudden jump in the bearing force around the resonance frequency of the bearing. While the magnitude of the sudden jump depends only on the amount of the clearance in the bearing, the frequency at which the jump occurs depends on the dynamic properties of the bearing assembly [50]. Gurkan [50] showed that as the clearance in the bearing increases, the frequency at which the jump occurs decreases. Hasanzadeh Ghafari [51] conducted a similar study to investigate the effect of clearance on the vibration signal in both vertical and horizontal directions, and confirmed the results by Gurkan [50]. They also found that by increasing the clearance in the bearing, the vibration in both the vertical and horizontal directions will increase and the resonance frequencies in both directions decreases. As the clearance increases, the average number of balls supporting the inner ring decreases, and therefore the effective stiffness decreases. This effect is more pronounced in the vertical direction rather than the horizontal direction.

Bearings with large clearances exhibit a higher degree of chaotic behaviour, especially at higher run speeds [51]. Although healthy ball and cylindrical roller bearings, which are installed with the factory recommended clearance, exhibit broadband chaotic vibration at various run speeds, the vibration signal of a faulty bearing manifests as quasi-periodic impulses. Therefore, the assumption of quasi-periodic vibration signals for impact type

bearing faults can be justified. However, since non-impact type bearing faults do not exhibit clear periodic or quasi-periodic impulses, the resultant signal cannot be considered as quasi-periodic. Large clearances add to this chaotic behaviour for non-impact type bearing faults as the bearing has more movement in the axial direction.

In summary, clearance is an important parameter that can change the vibration signature of a bearing. Therefore, it should be taken into account when studying the signature of non-impact type bearing faults.

#### **2.2.6. Stiffness of the bearing assembly**

The stiffness of a bearing assembly directly affects the vibration signature of rolling element bearings [2]. The stiffness of a bearing assembly in a particular direction can be calculated by dividing the applied load to the bearing in a particular direction by the deformation of the bearing in the same direction. This relationship is often studied using a load-deflection curve. The total deformation in rolling element bearings comprises the local deformation of rolling elements in the load zone and the global deformation of the inner and outer raceways [12]. The static stiffness behaviour of healthy ball bearings at various cage positions has been studied analytically [2, 52-58], numerically [59] and experimentally by measuring the force-displacement relationship [60-62]. However, the static stiffness of defective bearings as a function of the cage angular position has only been studied analytically and numerically [2], without experimental validation and analysis, and is covered in this thesis.

The load-deflection relationship in rolling element bearings was studied for the first time by Palmgren [63], Jones [64], and Harris [1], where they used a nonlinear stiffness coefficient. Later, Lim and Singh [55-58] introduced a more generalised formulation based on the Hertzian theory. In their method, the displacement vector of the bearing assembly is related to the applied load vector. The new theory led to the derivation of a time invariant bearing

stiffness matrix and early quasi-static formulation of the bearing assembly. Aktürk et al. [52] and Purohit and Purohit [54] used a time-invariant, two degree of freedom, dynamic model considering the horizontal and vertical motion of the inner ring and studied the effect of number of rolling elements and preload on the bearing stiffness. They concluded that the stiffness of the system increases as the number of rolling elements increases. Liew and Lim [53] extended the earlier linear time-invariant theory proposed by Lim and Singh [55-58] and suggested a new time-varying rolling element bearing stiffness formulation. The formulation takes into account the effect of the shaft rotational speed that causes the orbital motion of the rolling elements of the bearings, which in turn produces time-varying, periodic load and stiffness patterns. They showed that stiffness varies with the number of load carrying rolling elements in the load zone. Consequently, the stiffness in rolling elements is linked to the angular position of the cage, which changes the number of rolling elements in the load zone.

Guo and Parker [59] studied the quasi-static stiffness in healthy rolling element bearings for a wide range of bearing types and parameters. They used a combined surface integral and finite element method to solve for the contact mechanics between the rolling elements and races. Their model captured the time-dependent characteristics of the bearing contact due to the motion of the rolling elements. They analysed the bearing stiffness of healthy bearings and showed that it periodically varies. They validated their work using the published experimental results by Kraus et al. [61] and Royston and Basdogan [62].

Kraus et al. [61] measured the stiffness and damping, in the axial and radial directions, of healthy rolling element bearings for several speeds and preloads, and compared the results. They used modal analysis combined with a mathematical model of the system that was tested, and concluded that stiffness, in the radial and axial directions, increases by increasing the preload. However, this increase is more significant (by about three times) in the axial

direction. They showed that the damping in the radial direction decreases with the increase in preload, and increases in the axial direction. This variation is, however, more significant in the radial direction (by about seventeen times) when compared with the variation in the axial direction. Royston and Basdogan [62] measured the radial, axial and translational cross-coupling stiffnesses between the axial and radial directions on double row self-aligning rolling element bearings for several preload conditions, where moment stiffnesses are negligible. They showed that cross-coupling stiffness coefficients are negligible with simple radial or axial preloads. However, under the combined radial and axial preload conditions the cross-coupling stiffness coefficients become significant.

The only study found in the literature on the quasi-static stiffness in defective bearings is the work by Petersen et al. [43]. They present an analytical formulation of the load distribution and varying effective stiffness of a defective ball bearing assembly as a function of the cage angular position of varying size, when subjected to static loading in the radial, axial and rotational degrees of freedom, without experimental validation. Further analysis of the stiffness variations shows that as the defect size increases, the mean radial stiffness decreases in the loaded radial and axial directions and increases in the unloaded radial direction. Experimental measurements and analysis of the varying static stiffness as a function of defect length and applied load in defective bearings have not been found.

### **2.3. Models of defective bearings**

Bearing models based on physical laws and mathematical formulations can be used to develop effective and accurate condition monitoring algorithms [65, 66]. Physical models can also be used, together with other methods, i.e. data-driven approaches or symbolic modelling, to obtain a hybrid model that aims to overcome the limitations of each method in condition monitoring [67]. Dynamic models of rolling element bearings based on finite



element modelling, which are beyond the scope of this research, are also available, such as those reviewed by Singh et al. [68]. Chapter 3 of this thesis contains a comprehensive dynamic model of a defective bearing and Chapter 6 contains a hybrid defect size estimation algorithm that was developed using the aforementioned bearing model.

Numerous vibration generation mechanisms in rolling element bearings have been investigated and suggested by researchers. Several models have been developed for predicting the vibration response due to these mechanisms. These mechanisms include varying compliance due to the existence of different numbers of rolling elements in the load zone, distributed defects such as waviness due to manufacturing errors, and localised defects such as cracks, pits, line spalls and extended spalls caused by fatigue [6, 69-72]. In particular, single-row deep-groove ball bearings are the most studied [28, 38, 46, 48, 49, 53, 73-81]. There are other adjusted versions of the previously mentioned models to account for other configurations of the deep-groove ball bearings, such as angular contact ball bearings [82, 83]. A few models have also been developed for double-row rolling element bearings within the literature [84, 85].

Simplified bearing models have been developed which model the raceways as circular rings whose resonance modes are excited by a train of force impulses [31, 44, 46]. In these models the vibration signature is predicted by considering the applied load, the exponential decay of a resonant mode and the characteristic defect frequency. Rafsanjani et al. [86] reproduced the transient force that occurs when there is contact with a defective surface by means of a series of impulses repeated with the characteristic frequencies of the elements of the bearing. These models do not take the shape and size of localised defects into account and are limited to bearing defects that produce only impulsive vibration signals. Hence, these simple models cannot be employed to analyse the vibration responses of bearings with defects of varying shapes and sizes, which are important to study in order to develop new and improved defect

size estimation methods. Patil et al. [47] introduced defects in the raceways using circumferential half sinusoidal waves and cubic Hermite splines and studied the dynamic response of a bearing in that condition. Su et al. [4], Sunnersjö [5], Yhland [7] and Tandon and Choudhury [87] developed mathematical models to study the frequency characteristics of defective bearings due to distributed defect geometries, such as waviness and surface roughness.

Qiu et al. [80] use one degree of freedom to represent the dynamics of bearings in which both the stiffness and damping parameters are defined as the sum of the stiffness and damping parameters for damaged and undamaged cases. Harsha et al. [78], Aktürk [88] and Changqing and Qingyu [73] developed dynamic models to simulate the time domain vibration response of defective bearings with waviness geometric errors. Purohit and Purohit [54] used a two degree of freedom model considering the horizontal and vertical motions of the inner ring and studied the effect of the number of rolling elements and preload on the frequency response of the bearing. In these models, bearing contact forces are related to the displacement of bearing components using Hertzian contact theory. Harsha and Sandeep improved their earlier model to include the mass of the rolling elements in order to predict the nonlinear dynamic behaviour of a rolling element bearing due to waviness and unbalanced rotor support [75-77, 79]. The improved version of the model was further modified by Tadina [89] to predict the vibration response of bearings with localised spall defects on raceways. This model was designed for defects with curvatures larger than the curvature of the rolling element which maintains the contact between the raceways in the load zone, which makes it unsuitable for modelling rectangular shaped, sharp-edged defects that are large compared with the size of the rolling elements. Furthermore, Harsha's model and subsequent improved versions of it do not include mass-spring-dampers to represent a measured high frequency resonant response of the bearing, as included in the model

proposed by Sawalhi & Randall [48]. None of these models consider damping between the rolling elements and the raceways due to lubrication, as was undertaken by Sopenen & Mikkola [74, 81]. These models are suitable for prediction of the vibration response in defective bearings in which the rolling elements in the load zone are always in contact with both raceways, but they do not allow for inclusion of localised spalls in modelling. Therefore, these models cannot be used for predicting the vibration response of localised defects where rolling elements may become unloaded when traversing the defect zone.

Numerous multi-body dynamic models have been developed for modelling line spall defects [28, 48, 74, 81, 85, 89, 90], some of which do not consider the mass of rolling elements and none of which consider the finite size of the rolling element. The author was unable to find numerical models that included the finite size of the rolling element. In these models, the path of a rolling element is modelled such that its centre follows the geometry of the defect. For the case of rectangular shaped, sharp edged defects, this produces very large impulsive forces at the entry point into the defect, which results in large amplitude, high frequency accelerations that are not observed in experimental results. In order to avoid such incorrectly predicted large impulsive forces at the defect entrance point, Sawalhi and Randall [48] modified the shape of the modelled defect to resemble an assumed path travelled by rolling elements in the defect zone. They only modelled and experimentally investigated line spall defects for which it was assumed that the exit impact occurs mid-way through the defect. In their model, the path of the rolling element is assumed to be such that the high frequency event observed in measurements occurs when the centre of the rolling element is halfway through the line spall [37, 48]. However, they have not suggested any modifications for extended defects in which the high frequency event would not occur when the rolling element is half way through the defect. Extended defects that are sufficiently deep so that a rolling element could become unloaded momentarily could be simulated using these models

by increasing the length of the modelled defect. However, the path of the rolling elements and consequently the forces that are generated as the unloaded rolling elements strike the bottom of extended defects cannot be predicted, as these models do not consider the mass and finite size of the rolling elements. Further, since rolling element impacts on the bottom of extended defects have not previously been modelled or experimentally investigated, the assumed path of the rolling elements means that these models are incapable of predicting such impact events. In this thesis, a model is described that does not assume the path for the rolling elements, includes both the finite size and mass of the rolling elements, and is used to predict the vibration response when rollers strike the bottom of an extended defect.

Table 1 lists and compares the features of the models discussed above with those of the model proposed in this thesis. This table shows information regarding the following features of the models:

- **Inertia.RE.:** inclusion of the inertia of each rolling element. This feature is particularly important when the path of a rolling element is studied in the defect zone where the rolling element is not in contact with both raceways.
- **H.Fr.Res.:** inclusion of the high-frequency resonant mode.
- **Fin.S.RE:** finite size of rolling elements. This feature is important in studying the effect of the defect's profile on the relative distance between the features appearing on the vibration response. Study of these features is essential for developing defect size estimation methods based on the vibration characteristics of defective bearings.
- **Con.Damp.:** inclusion of contact damping due to lubricant film.
- **Roller Path Simulation:** ability of the model to simulate the path of the rolling elements in the defect zone.

- **Ind.Sys:** independent coordinate system for all bearing components. This feature is important for correctly estimating the contact force vectors acting on any bearing component. Accurate calculation of the force vectors in the dynamic model is essential for simulation of the path of a rolling element.
- **Slip.:** inclusion of slippage.
- **Defect Type.:** defect Type.
- **2Load.def.:** distinguish between the inner and outer load-deflection constants. Note that the contact curvatures between the inner raceway and rolling elements are different to the outer raceway and rolling elements. According to Hertzian contact theory the load-deflection constants, and consequently the contact stiffness, depends on the curvature of the contacting surfaces.
- **Housing:** Including the bearing housing in the model.

Table 1: Summary of the features of previously developed and proposed bearing models.

Feature	Reference													
	Randall & Sawalhi [48]	Harsha [75]	Soppanen & Mikkola [74]	Tandon and Choudhury [44]	Tadina and Boltežar [89]	Aktürk [88]	Rafsanjani et al. [86]	Su et al. [4],	Sunnersjö [5]	Patil et al. [47]	Purohit and Purohit [54]	Yhland [7]	Changqing and Qingyu [72]	Proposed model
<b>Inertia.RE.</b>	×	✓	×	×	✓	×	×	×	×	×	×	×	×	✓
<b>H.Fr.Res</b>	✓	×	×	✓	✓	×	✓	×	×	✓	✓	×	×	✓
<b>Fin.S.RE.</b>	×	×	×	×	×	×	×	×	×	×	×	×	×	✓
<b>Con.Damp.</b>	×	×	✓	×	×	×	×	×	✓	×	×	×	×	✓
<b>Roller Path Simulation</b>	Assumed	×	Assumed	×	×	×	×	×	×	×	×	×	×	Simulated
<b>Ind.Sys.</b>	×	×	×	×	×	×	×	×	×	×	×	×	×	✓
<b>Slip.</b>	✓	×	×	×	✓	×	×	×	×	×	×	×	×	✓
<b>Defect Type</b>	Line spall. Localised	Generalised waviness	Localised and distributed	Localised with only impulse response	Localised, only impressed ellipsoid shapes	Generalised waviness	Localised with only impulse response	Generalised waviness and roughness	Generalised waviness and roughness	Localised circumferential half sinusoidal wave	No defect	Generalised waviness	Generalised waviness	Potentially any (validated for outer raceway defects)
<b>Housing</b>	✓	×	✓	✓	✓	×	×	×	✓	×	×	✓	×	✓
<b>2Load.def.</b>	×	×	✓	×	✓	✓	×	×	×	×	✓	×	✓	✓

## **2.4. Conclusion of literature review and objectives**

The literature review presented in this chapter shows that there are discrepancies in previous theories describing the relationship between the characteristics of measured vibration responses and outer raceway defect entry and exit events that have led to poor results both when simulating the vibration response and when evaluating the existing defect size estimation methods. Therefore, extensive experiments and accurate models are necessary to study the dynamic behaviour and the vibration response in defective bearings.

Various dynamic models are reviewed in this chapter. The current research literature does not have a suitable physical model for studying the effects of the outer raceway defect shape and size on the vibration response, which could be used for developing an accurate defect size estimation algorithm. The main limitation of all the previous dynamic models is that the path of the rolling elements cannot be predicted, neither for a wide range of defects nor without including restricting assumptions. Prediction of the path of the rolling element in the defect zone (at the entry, mid-way through and at the exit from the defect) is essential to overcome the limitations of the previous models and will allow for the development of a more generally applicable dynamic model that is not limited to certain types of defects. Generally speaking, models that are adaptable to represent the dynamics of different bearing configurations and capable of predicting the path of rolling elements in the defect zone have not been found. Thus the objective of this thesis is to present a general approach for physical, multi-body modelling of rolling element bearings. A physical model suitable for studying the effect of the defect shape and size on the vibration response, which can be used for developing an accurate defect size estimation algorithm, including all the features listed in

Table 1, is proposed in this thesis. In the model developed in this research, the path of a rolling element is predicted by taking into account its mass and finite size. The actual defect geometry is used in the model. The proposed model does not make assumptions about the path of the rolling elements nor does it artificially modify the simulated defect geometry in order to obtain a more accurate prediction of the measured vibration response(s).

The literature review presented in this chapter also showed the inaccuracy of the previous hypothesis in describing the path of rolling elements and in the explanation for the analysis of the high-frequency event. This gap has been identified by showing the inaccuracy and dependency of the previous defect size estimation methods, based on these hypotheses. Studies to investigate the sources of inaccuracy and the speed-dependency in the existing hypotheses of the path of rolling elements and defect size estimation algorithms have not been found in the literature. The ultimate aim of this research is to develop accurate defect size estimation methods that are not dependent on the magnitude of the vibration response, but instead use features of the vibration signal that are generated when a rolling element enters and exits a defect. This has been achieved by identifying the gaps in the associated literature and addressing them in order to propose a novel defect size estimation method for localised defects on the outer raceway of bearings. In this thesis, the new hypothesis is validated through experimental tests.

One of the identified gaps is that previous defect size estimation methods underestimate the size of a defect that is larger than at least one roller angular spacing. The previous theory, which relied on the use of the stiffness variation in defective bearings to resolve the problem, is experimentally both validated (the theory has not been validated previously) and improved in this thesis. This research shows how knowledge of dynamic stiffness and measurement of the resonance frequency of the bearing assembly can be used to differentiate the size of the defects. The effects of the applied load on the static stiffness in defective bearings, which



were ignored previously, are investigated and included in the new method. Experimental measurements and analysis of the varying static stiffness in defective bearings with various defect lengths and applied loads, highlight the importance of the load on the varying static stiffnesses in bearings with extended defects. A time-frequency technique to detect the variation in the frequency response of the vibration signal due to stiffness variations of the bearing assembly is suggested, and the importance of including the effect of load in developing a reliable and accurate defect size estimation method is demonstrated in this thesis.

## Appendix 2A

Each component in rolling element bearings has a characteristic frequency at which a defect on that particular component increases the vibration energy. Bearing defect frequencies are widely used in vibration condition monitoring. These frequencies can be calculated from the rotational frequency and bearing dimensions. The following equations apply for a bearing in which the outer ring is fixed [1].

The rotational frequency of the cage:

$$FTF = \frac{f_r}{2} \left( 1 - \frac{D_p}{D_b} \cos\phi \right) \quad (\text{A.1})$$

The inner ring defect frequency:

$$BPFI = \frac{N_b f_r}{2} \left( 1 + \frac{D_p}{D_b} \cos\phi \right) \quad (\text{A.2})$$

The outer ring defect frequency:

$$BPFO = \frac{N_b f_r}{2} \left( 1 - \frac{D_p}{D_b} \cos\phi \right) \quad (\text{A.3})$$

The rolling element defect frequency:

$$BSF = \frac{f_r D_b}{2D_p} \left\{ 1 - \left( \frac{D_p}{D_b} \cos\phi \right)^2 \right\} \quad (\text{A.4})$$

The waviness characteristic frequencies:

$$WF = N_b \times FTF \quad (\text{A.5})$$

$N_b$     Number of rolling elements

$f_r$     Rotational speed of the inner ring or shaft (Hz)

$D_b$  Rolling element diameter (mm)

$D_p$  Pitch diameter of the bearing (mm)

$\emptyset$  Contact angle (degrees)

## References

1. T.A. Harris, *Rolling Bearing Analysis*. 2001, USA: Wiley.
2. D. Petersen, C.Q. Howard, N. Sawalhi, A. Moazen Ahmadi, and S. Singh, *Analysis of bearing stiffness variations, contact forces and vibrations in radially loaded double row rolling element bearings with raceway defects*. Mechanical Systems and Signal Processing, 2015. **50-51**: p. 139-160.
3. T. Nisbet, *ROLLING BEARINGS IN SERVICE*. 1978, London: Century Benham.
4. Y.T. Su, M.H. Lin, and M.S. Lee, *The effects of surface irregularities on roller bearing vibrations*. Journal of Sound and Vibration, 1993. **165**(3): p. 455-466.
5. C. Sunnersjö, *Rolling bearing vibrations-the effects of geometrical imperfections and wear*. Journal of Sound and Vibration, 1985. **98**(4): p. 455- 474.
6. F. Wardle, *Vibration forces produced by waviness of the rolling surfaces of thrust loaded ball bearings Part 2: experimental validation*. Proceedings of the Institution of Mechanical Engineers, Part C: Journal of Mechanical Engineering Science, 1988. **202**(5): p. 313-319.
7. E. Yhland, *A linear theory of vibrations caused by ball bearings with form errors operating at moderate speed*. Journal of Tribology, 1992. **114**(2): p. 348-359.
8. B.T. Kuhnell, *Wear in rolling element bearings and gears- How age and contamination affect them*. Machinery Lubrication, 2004: p. 62-64.
9. R.S. Beebe, *Machine Condition Monitoring: How to Predict Maintenance Requirements for Rotating and Stationary Plant*. 2009, MCM Consultants.
10. C.W. De Silva, *Vibration monitoring, testing, and instrumentation*. 2007: CRC.
11. J. Rao, *Vibratory condition monitoring of machines*. 2000: Narosa.
12. J.E. Shigley, *Mechanical engineering design*. 1972.
13. G. Lundberg and A. Palmgren, *Dynamic capacity of rolling bearings*. Journal of Applied Mechanics-Transactions of the ASME, 1949. **16**(2): p. 165-172.
14. W. Weibull, *A statistical theory of the strength of materials*. 1939: Generalstabens litografiska anstalts förlag.
15. E.V. Zaretsky, *STLE life factors for rolling bearings*. STLE Special Publication SP, 1992.

16. E. Bamberger, *Life Adjustment Factors for Ball and Roller Bearings: An Engineering Design Guide*. 1971: American Society of Mechanical Engineers.
17. E. Ioannides and T. Harris, *A new fatigue life model for rolling bearings*. Journal of Tribology, 1985. **107**(3): p. 367-377.
18. E.Y. Zaretsky, *Fatigue criterion to system design, life, and reliability*. Journal of Propulsion and Power, 1987. **3**(1): p. 76-83.
19. H. Takemura, Y. Matsumoto, and Y. Murakami, *Development of a new life equation for ball and roller bearings*. 2000, SAE Technical Paper.
20. J.E. Shigley, C.R. Mischke, R.G. Budynas, X. Liu, and Z. Gao, *Mechanical engineering design*. Vol. 89. 1989: McGraw-Hill New York.
21. A.K. Jardine, D. Lin, and D. Banjevic, *A review on machinery diagnostics and prognostics implementing condition-based maintenance*. Mechanical Systems and Signal Processing, 2006. **20**(7): p. 1483-1510.
22. M.S. Darlow, *Application of High-Frequency Resonance Techniques for Bearing Diagnostics in Helicopter Gearboxes*. 1974, DTIC Document.
23. J. Cusido, L. Romeral, J. Ortega, J. Rosero, and A.G. Espinosa, *Fault detection in induction machines using power spectral density in wavelet decomposition*. Industrial Electronics, IEEE Transactions on, 2008. **55**(2): p. 633-643.
24. R.B. Randall, J. Antoni, and S. Chobsaard, *The relationship between spectral correlation and envelope analysis in the diagnostics of bearing faults and other cyclostationary machine signals*. Mechanical Systems and Signal Processing, 2001. **15**(5): p. 945-962.
25. J. Antoni and R. Randall, *The spectral kurtosis: application to the vibratory surveillance and diagnostics of rotating machines*. Mechanical Systems and Signal Processing, 2006. **20**(2): p. 308-331.
26. F. Immovilli, M. Cocconcelli, A. Bellini, and R. Rubini, *Detection of generalized-roughness bearing fault by spectral-kurtosis energy of vibration or current signals*. Industrial Electronics, IEEE Transactions on, 2009. **56**(11): p. 4710-4717.
27. R. Randall, *Detection and diagnosis of incipient bearing failure in helicopter gearboxes*. Engineering Failure Analysis, 2004. **11**(2): p. 177-190.
28. N. Sawalhi and R. Randall, *Simulating gear and bearing interactions in the presence of faults: Part II: Simulation of the vibrations produced by extended bearing faults*. Mechanical Systems and Signal Processing, 2008. **22**(8): p. 1952-1966.

29. T. Igarashi and H. Hamada, *Studies on the vibration and sound of defective rolling bearings: First report: Vibration of ball bearings with one defect*. Bulletin of JSME, 1982. **25**(204): p. 994-1001.
30. R. Yan and R.X. Gao, *Approximate Entropy as a diagnostic tool for machine health monitoring*. Mechanical Systems and Signal Processing, 2007. **21**(2): p. 824-839.
31. P.D. McFadden and J.D. Smith, *The vibration produced by multiple point defects in a rolling element bearing*. Journal of Sound and Vibration, 1985. **98**(2): p. 263-273.
32. N.S. Swansson and S. Favaloro, *Applications of vibration analysis to the condition monitoring of rolling element bearings*. 1984, DTIC Document.
33. P. Boto, *Detection of bearing damage by shock pulse measurement*. Ball Bearing Journal, 1971(167): p. 1-8.
34. T. Williams, X. Ribadeneira, S. Billington, and T. Kurfess, *Rolling element bearing diagnostics in run-to-failure lifetime testing*. Mechanical Systems and Signal Processing, 2001. **15**(5): p. 979-993.
35. N. Gebraeel, M. Lawley, R. Liu, and V. Parmeshwaran, *Residual life predictions from vibration-based degradation signals: a neural network approach*. Industrial Electronics, IEEE Transactions on, 2004. **51**(3): p. 694-700.
36. N. Gebraeel, A. Elwany, and J. Pan, *Residual life predictions in the absence of prior degradation knowledge*. Reliability, IEEE Transactions on, 2009. **58**(1): p. 106-117.
37. N. Sawalhi and R.B. Randall, *Vibration response of spalled rolling element bearings: observations, simulations and signal processing techniques to track the spall size*. Mechanical Systems and Signal Processing, 2011. **25**(3): p. 846-870.
38. I. Epps and H. McCallion. *An investigation into the characteristics of vibration excited by discrete faults in rolling element bearings*. in *Annual Conference of the Vibration Association of New Zealand*. 1994. Christchurch.
39. A. Moazen Ahmadi, D. Petersen, and C.Q. Howard. *A nonlinear dynamic model of the vibration response of defective rolling element bearings*. in *Proc of Australian Acoustical Society*. 2013. Victor Harbor.
40. S. Singh, U. Köpke, C.Q. Howard, and D. Petersen, *Analyses of contact forces and vibration response for a defective rolling element bearing using an explicit dynamics finite element model*. Journal of Vibration and Control, 2014. **333**(21): p. 5356–5377.
41. S. Zhao, L. Liang, G. Xu, J. Wang, and W. Zhang, *Quantitative diagnosis of a spall-like fault of a rolling element bearing by empirical mode decomposition and the*

- approximate entropy method*. Mechanical Systems and Signal Processing, 2013. **40**(1): p. 154-177.
42. W.A. Smith, C. Hu, R.B. Randall, and Z. Peng. *Vibration-Based Spall Size Tracking in Rolling Element Bearings*. in *Proceedings of the 9th IFToMM International Conference on Rotor Dynamics*. 2015. Springer.
  43. D. Petersen, C. Howard, and Z. Prime, *Varying stiffness and load distributions in defective ball bearings: analytical formulation and application to defect size estimation*. Journal of Sound and Vibration, 2015. **337**(0): p. 284-300.
  44. N. Tandon and A. Choudhury, *An analytical model for the prediction of the vibration response of rolling element bearings due to a localized defect*. Journal of sound and vibration, 1997. **205**(3): p. 275-292.
  45. Z. Kiral and H. Karagülle, *Simulation and analysis of vibration signals generated by rolling element bearing with defects*. Tribology International, 2003. **36**(9): p. 667-678.
  46. P. McFadden and J. Smith, *Model for the vibration produced by a single point defect in a rolling element bearing*. Journal of Sound and Vibration, 1984. **96**(1): p. 69-82.
  47. M. Patil, J. Mathew, P. Rajendrakumar, and S. Desai, *A theoretical model to predict the effect of localized defect on vibrations associated with ball bearing*. International Journal of Mechanical Sciences, 2010. **52**(9): p. 1193-1201.
  48. N. Sawalhi and R. Randall, *Simulating gear and bearing interactions in the presence of faults: Part I. the combined gear bearing dynamic model and the simulation of localised bearing faults*. Mechanical Systems and Signal Processing, 2008. **22**(8): p. 1924-1951.
  49. H. Kanai, M. Abe, and K.i. Kido, *Detection of slight defects in ball bearings by nonperiodic analysis*. Journal of the Acoustical Society of Japan (E), 1986. **7**(4): p. 219-228.
  50. N. Gurkan, *Non-Linear Mathematical Modeling of Gear Rotor Bearing Systems Including Bearing Clearance*. 2005, Middle East Technical University.
  51. S. Hasanzadeh Ghafari, *A fault diagnosis system for rotary machinery supported by rolling element bearings*, in *Mechanical engineering*. 2008, University of Waterloo.
  52. N. Aktürk, M. Uneeb, and R. Gohar, *The effects of number of balls and preload on vibrations associated with ball bearings*. Journal of Tribology, 1997. **119**(4): p. 747-753.

53. H.-V. Liew and T.C. Lim, *Analysis of time-varying rolling element bearing characteristics*. Journal of Sound and Vibration, 2005. **283**(3): p. 1163-1179.
54. R. Purohit and K. Purohit, *Dynamic analysis of ball bearings with effect of preload and number of balls*. International Journal of Applied Mechanics and Engineering, 2006. **11**(1): p. 77-91.
55. T. Lim and R. Singh, *Vibration transmission through rolling element bearings, part I: bearing stiffness formulation*. Journal of Sound and Vibration, 1990. **139**(2): p. 179-199.
56. T. Lim and R. Singh, *Vibration transmission through rolling element bearings, part ii: system studies*. Journal of Sound and Vibration, 1990. **139**(2): p. 201-225.
57. T. Lim and R. Singh, *Vibration transmission through rolling element bearings. part iii: Geared rotor system studies*. Journal of Sound and Vibration, 1991. **151**(1): p. 31-54.
58. T. Lim and R. Singh, *Vibration transmission through rolling element bearings, part IV: statistical energy analysis*. Journal of Sound and Vibration, 1992. **153**(1): p. 37-50.
59. Y. Guo and R.G. Parker, *Stiffness matrix calculation of rolling element bearings using a finite element/contact mechanics model*. Mechanism and Machine Theory, 2012. **51**: p. 32-45.
60. M. Dougdag, N.E. Titouche, M. Djaoui, and M. Ouali, *The calculation of ball bearing nonlinear stiffness theoretical and experimental study with comparisons* Journal of Engineering and applied sciences, 2008. **3**(11): p. 872-883.
61. J. Kraus, J. Blech, and S. Braun, *In situ determination of rolling bearing stiffness and damping by modal analysis*. Journal of Vibration and Acoustics, 1987. **109**(3): p. 235-240.
62. T. Royston and I. Basdogan, *Vibration transmission through self-aligning (spherical) rolling element bearings: theory and experiment*. Journal of Sound and Vibration, 1998. **215**(5): p. 997-1014.
63. A. Palmgren, *Ball and roller bearing engineering*. Philadelphia: SKF Industries Inc., 1959, 1959. **1**.
64. A. Jones, *A general theory for elastically constrained ball and radial roller bearings under arbitrary load and speed conditions*. Journal of Fluids Engineering, 1960. **82**(2): p. 309-320.



65. J. Sikorska, M. Hodkiewicz, and L. Ma, *Prognostic modelling options for remaining useful life estimation by industry*. Mechanical Systems and Signal Processing, 2011. **25**(5): p. 1803-1836.
66. A. Heng, S. Zhang, A.C. Tan, and J. Mathew, *Rotating machinery prognostics: State of the art, challenges and opportunities*. Mechanical Systems and Signal Processing, 2009. **23**(3): p. 724-739.
67. D. Galar, A. Thaduri, M. Catelani, and L. Ciani, *Context awareness for maintenance decision making: a diagnosis and prognosis approach*. Measurement, 2015. **67**: p. 137-150.
68. S. Singh, C.Q. Howard, and C.H. Hansen, *An extensive review of vibration modelling of rolling element bearings with localised and extended defects*. Journal of Sound and Vibration, 2015. **357**: p. 300-330.
69. C.S. Sunnersjö, *Varying compliance vibrations of rolling bearings*. Journal of Sound and Vibration, 1978. **58**(3): p. 363-373.
70. R. Sayles and S. Poon, *Surface topography and rolling element vibration*. Precision Engineering, 1981. **3**(3): p. 137-144.
71. N. Tandon and A. Choudhury, *A review of vibration and acoustic measurement methods for the detection of defects in rolling element bearings*. Tribology International, 1999. **32**(8): p. 469-480.
72. G. Jang and S.W. Jeong, *Vibration analysis of a rotating system due to the effect of ball bearing waviness*. Journal of Sound and Vibration, 2004. **269**(3): p. 709-726.
73. B. Changqing and X. Qingyu, *Dynamic model of ball bearings with internal clearance and waviness*. Journal of Sound and Vibration, 2006. **294**(1): p. 23-48.
74. J. Sopianen and A. Mikkola, *Dynamic model of a deep-groove ball bearing including localized and distributed defects. Part 1: theory*. Proceedings of the Institution of Mechanical Engineers, Part K: Journal of Multi-body Dynamics, 2003. **217**(3): p. 201-211.
75. S.P. Harsha, *Nonlinear dynamic analysis of an unbalanced rotor supported by roller bearing*. Chaos, Solutions & Fractals, 2005. **26**(1): p. 47-66.
76. S.P. Harsha, *Nonlinear dynamic analysis of a high-speed rotor supported by rolling element bearings*. Journal of Sound and Vibration, 2006. **290**(1-2): p. 65-100.
77. S.P. Harsha and P.K. Kankar, *Stability analysis of a rotor bearing system due to surface waviness and number of balls*. International Journal of Mechanical Sciences, 2004. **46**(7): p. 1057-1081.

78. S.P. Harsha, K. Sandeep, and R. Prakash, *The effect of speed of balanced rotor on nonlinear vibrations associated with ball bearings*. International Journal of Mechanical Sciences, 2003. **45**(4): p. 725-740.
79. S.P. Harsha, K. Sandeep, and R. Prakash, *Non-linear dynamic behaviors of rolling element bearings due to surface waviness*. Journal of Sound and Vibration, 2004. **272**(3–5): p. 557-580.
80. J. Qiu, B.B. Seth, S.Y. Liang, and C. Zhang, *Damage mechanics approach for bearing lifetime prognostics*. Mechanical Systems and Signal Processing, 2002. **16**(5): p. 817-829.
81. J. Sopianen and A. Mikkola, *Dynamic model of a deep-groove ball bearing including localized and distributed defects. Part 2: implementation and results*. Proceedings of the Institution of Mechanical Engineers, Part K: Journal of Multi-body Dynamics, 2003. **217**(3): p. 213-223.
82. W.-Z. Wang, L. Hu, S.-G. Zhang, and L.-J. Kong, *Modeling high-speed angular contact ball bearing under the combined radial, axial and moment loads*. Proceedings of the Institution of Mechanical Engineers, Part C: Journal of Mechanical Engineering Science, 2013: p. 0954406213490874.
83. J. Jędrzejewski and W. Kwasny, *Modelling of angular contact ball bearings and axial displacements for high-speed spindles*. CIRP Annals-Manufacturing Technology, 2010. **59**(1): p. 377-382.
84. I. Bercea, S. Cretu, and D. Nelias, *Analysis of double-row tapered roller bearings, Part I-Model*. Tribology transactions, 2003. **46**(2): p. 228-239.
85. M. Cao and J. Xiao, *A comprehensive dynamic model of double-row spherical roller bearing—model development and case studies on surface defects, preloads, and radial clearance*. Mechanical Systems and Signal Processing, 2008. **22**(2): p. 467-489.
86. A. Rafsanjani, S. Abbasion, A. Farshidianfar, and H. Moeenfard, *Nonlinear dynamic modeling of surface defects in rolling element bearing systems*. Journal of Sound and Vibration, 2009. **319**(3): p. 1150-1174.
87. N. Tandon and A. Choudhury, *A theoretical model to predict the vibration response of rolling bearings in a rotor bearing system to distributed defects under radial load*. Journal of Tribology, 2000. **122**(3): p. 609-615.
88. N. Aktürk, *The effect of waviness on vibrations associated with ball bearings*. Journal of Tribology, 1999. **121**(4): p. 667-677.

89. M. Tadina and M. Boltežar, *Improved model of a ball bearing for the simulation of vibration signals due to faults during run-up*. Journal of Sound and Vibration, 2011. **330**(17): p. 4287-4301.
90. S. Sassi, B. Badri, and M. Thomas, *A numerical model to predict damaged bearing vibrations*. Journal of Vibration and Control, 2007. **13**(11): p. 1603-1628.

## Chapter 3

### **Nonlinear Dynamic Model of Defective Rolling Element Bearings**

This chapter has been published as

A. Moazen Ahmadi, D. Petersen, C.Q. Howard, A nonlinear dynamic vibration model of defective bearings – the importance of modelling the finite size of rolling elements, *Mechanical Systems and Signal Processing* 52–53 (2015) 309-326. published online (DOI: 10.1016/j.ymssp.2014.06.006).

This chapter is the first of four journal publications that has been published. In this chapter, an improved nonlinear dynamic model of the contact forces and vibration responses generated in rolling element bearings, with an outer raceway defect, is developed. The improvement comes about by considering the finite size of the rolling elements, which overcomes the limitations exhibited by previous models caused by the modelling of rolling elements as point masses. For line spall defects, a low frequency event occurs in the measured vibration response when a rolling element enters the defect. Previous models were not able to accurately predict this event without making the simulated and actual defect geometries significantly different. The chapter also presents comparisons between the proposed model, previous models and experimental results carried out to show that the low and high frequency events are more accurately predicted. This analysis identifies and explains the mechanisms leading to the inaccuracies of the previous models. The outcome of this chapter is a hypothesis to explain the path of rolling elements in the defect zone, which explains the discrepancies in the previous assumptions of the path of rolling elements in the defect zone and the corresponding features on the vibration response to the entry and exit events. The model presented in this chapter is used in subsequent analyses presented in this thesis.



# Statement of Authorship

Title of Paper	A nonlinear dynamic vibration model of defective bearings – The importance of modelling the finite size of rolling elements		
Publication Status	<input checked="" type="checkbox"/> Published	<input type="checkbox"/> Accepted for Publication	
	<input type="checkbox"/> Submitted for Publication	<input type="checkbox"/> Unpublished and Unsubmitted work written in manuscript style	
Publication Details	Mechanical Systems and Signal Processing		

## Principal Author

Name of Principal Author (Candidate)	Alireza Moazen-ahmadi		
Contribution to the Paper	Performed analytical work, interpreted data, wrote manuscript and acted as corresponding author.		
Overall percentage (%)	80%		
Certification:	This paper reports on original research I conducted during the period of my Higher Degree by Research candidature and is not subject to any obligations or contractual agreements with a third party that would constrain its inclusion in this thesis. I am the primary author of this paper.		
Signature		Date	27/9/2016

## Co-Author Contributions

By signing the Statement of Authorship, each author certifies that:

- i. the candidate's stated contribution to the publication is accurate (as detailed above);
- ii. permission is granted for the candidate to include the publication in the thesis; and
- iii. the sum of all co-author contributions is equal to 100% less the candidate's stated contribution.

Name of Co-Author	Dick Petersen		
Contribution to the Paper	Supervised the research and contributed in academic discussion and manuscript review.		
Signature	10%	Date	26/2/2016

Name of Co-Author	Carl Howard		
Contribution to the Paper	Supervised the research and contributed in academic discussion and manuscript review.		
Signature	10%	Date	27/9/2016

Please cut and paste additional co-author panels here as required.





ELSEVIER

Contents lists available at ScienceDirect

# Mechanical Systems and Signal Processing

journal homepage: [www.elsevier.com/locate/ymssp](http://www.elsevier.com/locate/ymssp)

## A nonlinear dynamic vibration model of defective bearings – The importance of modelling the finite size of rolling elements



Alireza Moazen Ahmadi\*, Dick Petersen, Carl Howard

School of Mechanical Engineering, The University of Adelaide, South Australia, Australia

### ARTICLE INFO

#### Article history:

Received 1 April 2014

Received in revised form

5 June 2014

Accepted 11 June 2014

Available online 22 August 2014

#### Keywords:

Rolling element bearing

Spall

Vibration model

Defect size

Contact forces

### ABSTRACT

This paper presents an improved nonlinear dynamic model of the contact forces and vibration response generated in defective rolling element bearings. The improvement comes about by considering the finite size of the rolling elements which overcomes the limitations exhibited by previous models caused by the modelling of rolling elements as point masses. For line spall defects, a low frequency event occurs in the measured vibration response when a rolling element enters the defect. Previous models were not able to accurately predict this event without making the simulated and actual defect geometries significantly different. Comparisons between the proposed model, previous models and experimental results are carried out to show that the low and high frequency events are more accurately predicted. This analysis identifies and explains the mechanisms leading to inaccuracy of the previous models. The model developed here can be used to aid in the development of new diagnostic algorithms.

© 2014 Elsevier Ltd. All rights reserved.

### 1. Introduction

Rolling element bearings are widely used in rotary machinery and the failure of bearings are the most common reason for machine breakdowns. Defects in bearings are commonly categorised into localised and distributed defects. Distributed defects, such as waviness, surface roughness, or off-size rolling elements, are usually the result of manufacturing errors [1,2]. Localised defects are often initiated by insufficient lubrication film between the surfaces in contact. This causes metal-to-metal contact between the rolling elements and the raceways which generates stress waves which in time form sub-surface cracks. The large forces in bearings cause the sub-surface cracks to grow into surface defects. This phenomenon is called pitting or spalling [3]. This paper considers the vibrations and contact forces generated in bearings with raceway spalls.

The study of the bearing vibration response generated by raceway spalls is useful for quality inspection and bearing condition monitoring. Numerical models are often used to develop and test diagnostic algorithms for condition monitoring purposes. Developing an understanding of the dynamic behaviour of defective bearings has received a great deal of attention and has led to the development of a number of numerical models. The previous models developed for distributed defects, such as raceway waviness, are not suitable for bearings with raceway spalls because they assume that the rolling elements are always under compression while in the load zone, which is not necessarily the case when a raceway defect is present. Numerous models have been developed that consider localised defects. The majority of these models [4–10] are

\* Corresponding author.

E-mail address: [alireza.moazenahmadi@adelaide.edu.au](mailto:alireza.moazenahmadi@adelaide.edu.au) (A. Moazen Ahmadi).



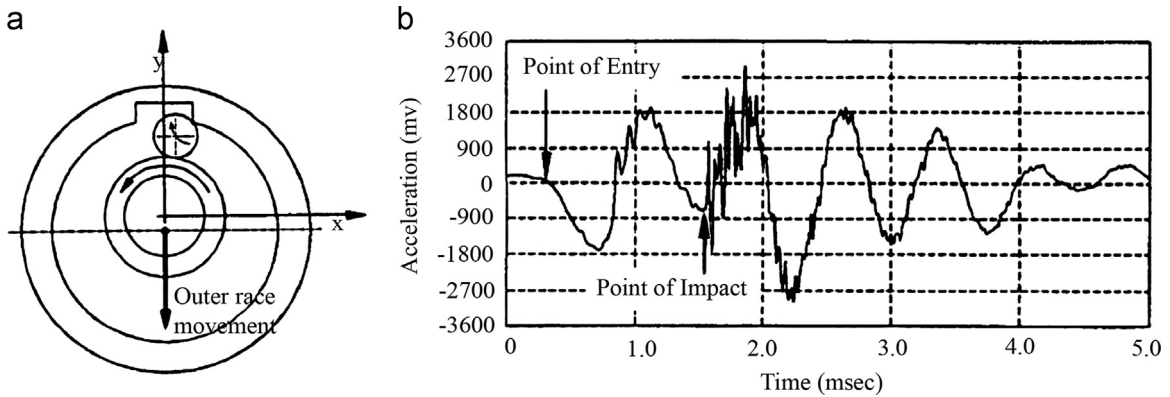


**Fig. 1.** (a) Diagram of a rolling element travelling into a rectangular shaped, sharp edged defect located on the outer raceway and (b) a typical measured vibration response [13].

designed to model bearings with line spall defects which occur at the early stages of bearing failure. The extended spall defects that occur at later stages due to successive rolling element passes over the defect have received very little attention [11]. In many models, the rolling elements are not included and hence the path of the rolling elements in the defect zone cannot be predicted [4–9]. In other models such as Ref. [10], the rolling elements are modelled as point masses, and although there is some improvement compared to models that do not consider rolling element inertia, the vibration response is not accurately predicted because the finite size of the rolling elements is neglected. In these models, the results from simulations involving a line spall defect were shown to be reasonably consistent with experimental observation but only if the shape of the defect was altered based on specific assumptions made for the path of the rolling elements while traversing the defect zone. In summary, no model is currently available that has the capability to accurately predict the vibration response of a bearing with a raceway defect without making specific assumptions on the paths taken by the rolling elements as they traverse the defect zone.

This paper presents a nonlinear multi-body dynamic model that can be used to predict the contact forces and time-domain vibration response of radially loaded rolling element bearings due to surface defects on a raceway. The presented model is based on the multi-body nonlinear dynamic models previously developed by Harsha [12] and Sawalhi and Randall [6,7]. Its main contribution is that it considers the finite size of the rolling elements. The advantages of this are that no rolling element path assumptions need to be made and, importantly, the vibration response is predicted more accurately compared to the previous models that modelled the rolling elements as point masses. Therefore, there is no need to assume a defect shape in the model that is different to the real defect geometry, as required in previous models [6,7].

A simulation and experimental study were conducted involving a double row rolling element bearing with an outer raceway spall. The size of the spall was such that the rolling elements strike the bottom of the defect on the raceway. This type of defect is specifically chosen here to demonstrate the capabilities of the proposed model in correctly predicting the characteristics of the vibration response of an experimentally tested defective bearing. The aim is to demonstrate that the proposed model is capable of predicting typical vibration characteristics of defective bearings with rectangular shaped, sharp edged raceway defects while previous models are either incapable of or limited use for this purpose. The proposed model is also compared with an improved version of the models developed previously by Harsha [12] and Sawalhi and Randall [6,7] in which the rolling elements are modelled as point masses. The characteristics of the resultant vibration signal are discussed and compared to the proposed model to highlight the benefits of considering the finite size of the rolling elements. Moreover, the mechanisms leading to inaccuracy or incapability of the previous models in predicting the time-domain vibration response of defective bearings are identified and explained. The proposed model can be used to simulate the vibration signal generated by bearings with different types of defects, understand the dynamic behaviour of bearings, and to develop new diagnostic algorithms including algorithms to determine the size of a defect.

## 2. Review of vibration characteristics and models of defective bearings

### 2.1. Vibration signature for a rectangular shaped, sharp edged raceway defect

Fig. 1(a) illustrates a diagram of a defective rolling element bearing with a rectangular shaped, sharp edged defect on the outer raceway. A typical measured vibration signal due to such a defect [13] is shown in Fig. 1(b). It has been shown by previous experimental studies that the entry of a rolling element into a sharp edged defect produces a vibration signal with low frequency content [13,14]. Moreover, the exit of the rolling element excites a much broader range of frequencies including the high frequency bearing resonances. These resonances are excited by the impact of the rolling element mass on the sharp edged defect exit, as well as the parametric excitations caused by rapid changes in the bearing stiffness which occur when the rolling element restresses between the raceways [11]. The high frequency event observed in experimental

results [13,15] often appears to have been caused by multiple impacts rather than a single impact. Simulation results of defective bearings presented by Singh [16] indicate that the multiple impacts occur when the rolling element successively impacts on the inner and outer raceways at it restresses at the exit point.

## 2.2. Vibration models of defective bearings

Numerous vibration generation mechanisms in rolling element bearings have been investigated by researchers and several models have been developed for predicting the vibration response due to these mechanisms [1,2,11,17–27]. These mechanisms include varying compliance due to the existence of different number of rolling elements in the load zone, distributed defects such as waviness due to manufacturing errors, and localised defects such as cracks, pits, line spalls and extended spalls caused by fatigue [28–32]. A limitation of all previous dynamic models is that the correct path of the rolling elements cannot be predicted for a wide range of defects. Prediction of the path of the rolling element in the defect zone (at the entry, mid-way through and exit from the defect) is essential to overcome the limitations of the previous models and makes developing a more generally applicable dynamic model that is not limited to certain types of defects possible. In the model developed here, the path of a rolling element is predicted by taking into account its mass and finite size, and the actual defect geometry is used in the model. The proposed model does not make assumptions about the path of the rolling elements or artificially modify the simulated defect geometry in order to obtain a more accurate prediction of the measured vibration response.

Simplified bearing models [17–20] have been developed which model the raceways as circular rings whose resonance modes are excited by a train of force impulses [33]. The vibration signature is predicted by considering the applied load, the exponential decay of a resonant mode and the characteristic defect frequency. These models do not take the shape and size of a localised defect into account and are limited to bearing defects that produce only impulsive vibration signals. Hence, these simple models cannot be employed to analyse the vibration response of bearings with defects of varying shape and size.

Dynamic models have been developed for distributed defect geometries such as waviness and surface roughness [1,2,21–27]. In these models, the bearing contact forces are related to the displacement of bearing components using Hertzian contact theory [6,34]. The vibration response prediction in these models is based on the assumption that the rolling elements in the load zone are always in contact with both raceways, and they do not allow for inclusion of localised spalls in modelling. Therefore, these models cannot be used for predicting the vibration response of localised defects for which rolling elements may become unloaded when traversing the defect zone.

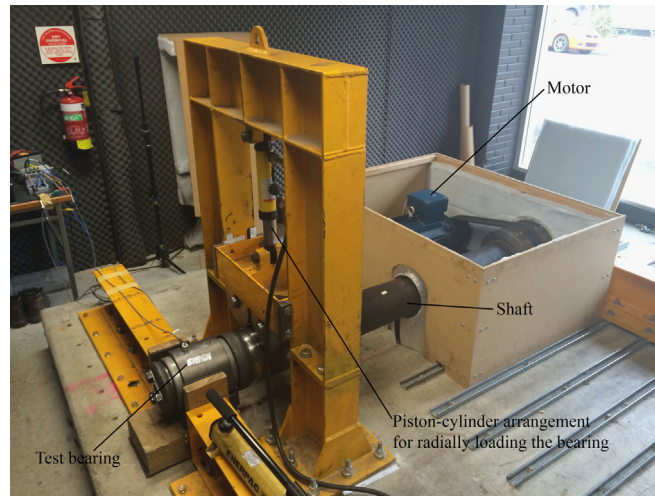
Numerous multi-body dynamic models have been developed for modelling line spall defects [4–10] which do not consider the mass and finite size of the rolling element. In these models, the path of a rolling element is modelled such that its centre follows the geometry of the defect. For the case of rectangular shaped, sharp edged defects, this produces very large impulsive forces at the entry point into the defect, which results in large amplitude, high frequency accelerations that are not observed in experimental results. In order to avoid such incorrectly predicted large impulsive forces at the defect entrance point, Sawalhi and Randall [6] modified the shape of the modelled defect to resemble an assumed path travelled by rolling elements in the defect zone. They only modelled and experimentally investigated line spall defects for which it was assumed that the exit impact occurs mid-way through the defect. In their model, the path of the rolling element is assumed such that the high frequency event observed in measurements occurs when the centre of the rolling element is halfway through the line spall [6,14]. However, they have not suggested any modifications for extended defects in which the high frequency event would not occur when the rolling element is half way through the defect. Extended defects that are sufficiently deep to make a rolling element unload momentarily could be modelled using these models by increasing the length of the modelled defect. However, the path of the rolling elements and, consequently, the force impacts that are generated as the unloaded rolling elements strike the bottom of extended defects cannot be predicted as these models do not consider the mass and finite size of the rolling elements. Moreover, since rolling element impacts on the bottom of extended defects have not been previously modelled or experimentally investigated, the assumption of the rolling element's path makes these models incapable of predicting such events.

Recently, a more comprehensive multi-body dynamic model was developed by Harsha [12,25,26,35]. This model was initially developed to predict the vibration response of defective bearings with distributed defects [34]. Later on the model was improved to include the mass of the rolling elements in order to predict the nonlinear dynamic behaviour of a rolling element bearing due to waviness and unbalanced rotor support [12,25,26,35]. The improved version of the model was further modified by Tadina [10] to predict the vibration response of bearings with localised spall defects on raceways. All of the aforementioned models are designed for defects with curvatures larger than the curvature of the rolling element which maintains the contact between the raceways in the load zone. Therefore, Harsha's model is not suitable for modelling rectangular shaped, sharp-edged defects that are large compared to the size of the rolling elements. Furthermore, Harsha's model and subsequent improved versions of it do not include mass-spring-dampers to represent a measured high frequency resonant response of the bearing, as included in the model proposed by Sawalhi and Randall [6]. None of these models consider damping between the rolling elements and the raceways due to lubrication, as was done by Sopenan and Mikkola [4,5]. Additionally, Harsha's model has never been compared or validated against experimental measurements. Table 1 lists and compares the features of the models developed by Sawalhi and Randall [6,7] and Harsha [12,25,26,35] to those of the model proposed in this paper.

**Table 1**

Summary of the features of previously developed and proposed bearing models.

Feature	Model name			
	Sawalhi and Randall [6,7]	Harsha [12,25,26,35]	Sopanen and Mikkola [4,5]	Proposed model
Mass of rolling elements	×	✓	×	✓
High-frequency resonant mode	✓	×	×	✓
Finite size of rolling elements	×	×	×	✓
Contact damping due to lubricant film	×	×	✓	✓
No assumption on path of rolling element centre	×	N/A	N/A	✓
Independent coordinate system for all bearing components	×	×	×	✓

**Fig. 2.** Photo of the test rig with a test bearing installed on the loading-end of the shaft, and a defect-free bearing on the drive-end.

The only model which considers the finite size of the rolling elements is the model developed by Epps [13]. Epps calculated the contact forces acting on the rolling elements but the results were only valid for a particular case of a rectangular shaped defect and with the inner raceway constraint to move only in the direction of the vertically applied static load. Therefore, the contact positions between a rolling element and the raceways for defect geometries other than rectangular shaped ones cannot be calculated using this method. In bearings with higher radial clearance, lower radial loads, or non-vertical radial loads in which the inner raceway have movements in both  $x$  and  $y$  directions, Epps' model cannot be used either [13]. The model proposed in this paper does not make the assumptions made by Epps [13] which makes it a more comprehensive model that can accept a wider range of defect geometries.

### 3. Bearing test rig and the test bearing

Fig. 2 shows a photo of the test rig used to conduct experiments on rolling element bearings. The test rig has a 15 kW three-phase induction motor, a steel structure and a hydraulic piston for applying a vertical load to the bearing under test, as well as a variable frequency drive to control the rotational speed of the motor. Four V-belts and pulleys couple the electric motor to the shaft. The test rig is capable of applying vertical loads up to 100 kN and run speeds up to 1200 rpm. The bearing to be tested is pressed onto the shaft and located at the loading-end of the shaft and away from the motor (drive-end). The bearing installed at the drive-end of the shaft is a defect-free bearing. The force from the hydraulic pistons is applied to the shaft using two rollers via the loading structural arrangement.

An accelerometer is mounted onto the outer shell of the bearing in order to measure the defect-induced vibrations. The accelerometer is screwed to an aluminium base and the bases are attached to the bearing using superglue. The bases are specifically made to match the curvature of the outer bearing shell. A tachometer is mounted near the shaft in order to measure its rotational speed. The data acquisition system consisted of a National Instruments (NI) CompactDAQ system with NI 9234 modules. Data was acquired using the NI Labview Sound and Vibration toolbox and post-processing was done using MATLAB. The vibration signals were acquired with a sampling frequency of 102.4 kHz. The test bearing is a double row tapered roller bearing which has a nominal pitch diameter  $D_p=180.2$  mm, a roller diameter  $D_b=17.9$  mm, clearance  $cl=0.015$  mm and  $N_b=24$  rolling elements on each row.

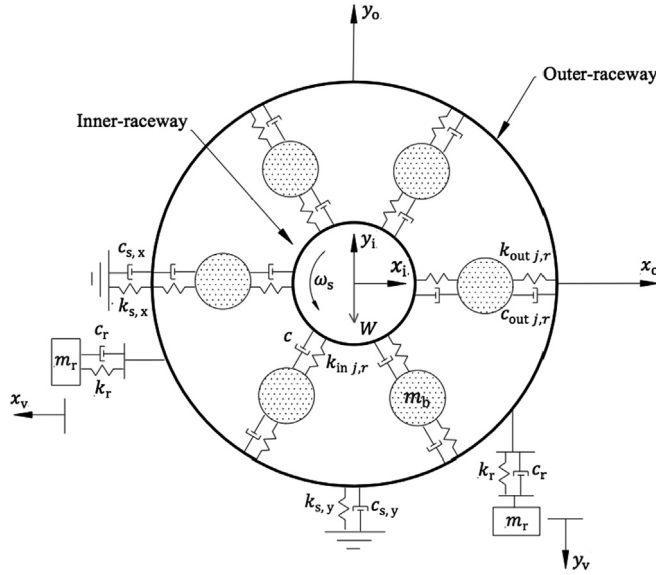


**Fig. 3.** Diagram of the proposed multi-body nonlinear dynamic model, with  $k_{in/out,j,r}$  nonlinear contact stiffness,  $c_{in/out,j,r}$  linear contact damping,  $k_s$  is the stiffness of the support,  $c_s$  is the damping of the support,  $\omega_s$  is the run speed,  $W$  is the static load,  $m_r$  is the mass of the high frequency bearing resonance,  $k_r$  is the stiffness of the high frequency bearing resonance,  $c_r$  is the damping of the high frequency bearing resonance,  $m_o$  is the mass of the outer raceway plus the support structure,  $m_b$  is the mass of a rolling element, and  $m_i$  is the mass of the inner raceways plus the shaft.

A rectangular shaped, sharp edged defect was machined into the surface of one of the outer raceways using an electric discharge method. The circumferential length of the bearing defect was chosen as 10 mm and the depth as 0.2 mm, so that a rolling element becomes unloaded as it traverses through the defect. The depth and circumferential length of the defect are chosen to match the typical size of defects in bearings pulled out from service by the industry partner on this research project. The test bearing was subjected to a static vertical load of  $W=50$  kN and the vibration measurements were recorded at a shaft rotational speed of 250 rpm. The test bearing was orientated such that the defect was located in the load zone.

#### 4. Nonlinear multi-body dynamic modelling of a defective bearing

##### 4.1. Diagram of the model

Fig. 3 shows a diagram of the multi-body nonlinear dynamic model used to simulate the vibration response of a defective rolling element bearing. The model includes the masses of the outer raceway plus the support structure ( $m_o$ ), inner raceways plus the shaft ( $m_i$ ), and rolling elements ( $m_b$ ). The static load  $W$  is applied to the shaft in the  $y$  direction.

In the proposed model, the rows  $r=1, 2$  of the double row bearing share the same outer bearing shell ( $m_o$ ). The inner raceways of the two rows are press-fitted onto a common shaft. Therefore,  $(x_i, y_i)$  and  $(x_o, y_o)$  represent the centre line of the two inner raceways (rows) and the two outer raceways, that encompasses the two rows, respectively. The model has  $2N_b+6$  degrees of freedom, where  $N_b$  is the number of rolling elements, but note that Fig. 3 only shows one of the rows. The additional six degrees of freedom are the displacement of the inner raceway ( $x_i, y_i$ ), displacement of outer raceway ( $x_o, y_o$ ), and the measured vibration response of the outer raceway ( $x_v, y_v$ ), which includes a high frequency bearing resonant mode.

The nonlinear contact stiffness and damping between the  $j$ th rolling element on row  $r$  and the raceways are represented by  $k_{out,j,r}, c_{out,j,r}, k_{in,j,r}$  and  $c_{in,j,r}$ . The stiffness and damping of the bearing support are represented by  $k_{s,x}, k_{s,y}, c_{s,x}$ , and  $c_{s,y}$ . Using the method explained in [11], these parameters can be adjusted to reasonably match the characteristics of the low frequency event observed in experimental results. A typical high frequency resonant response of the bearing is modelled by including the spring-mass-damping systems ( $k_r, m_r, c_r$ ) in both  $x$  and  $y$  directions, as shown in Fig. 3. These parameters are adjusted to match one of the high frequency resonant responses measured experimentally on the bearing casing. These high frequency resonant responses typically correspond to excitation of the bending modes of the casing which results in radial vibrations across the entire casing. The parameters  $m_r, k_r$  and  $c_r$  are therefore chosen to be similar for both  $x$  and  $y$  directions.

##### 4.2. Kinematics of the rolling elements

The role of the cage in rolling element bearings, which is not shown in Fig. 3, is to maintain constant distance and zero relative speed between the rolling elements. Assuming that there is no slippage between the shaft and the two inner

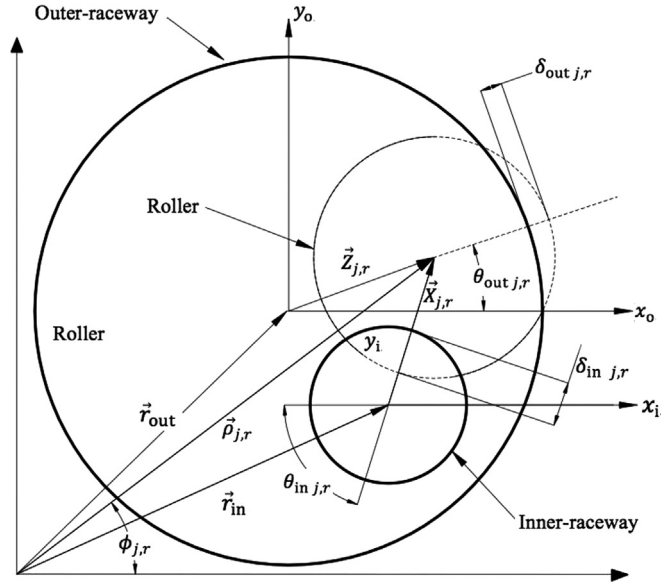


**Fig. 4.** Diagram of the relative position of the components of a rolling element bearing, with  $\delta_{out,j,r}$  the contact deformation between the  $j$ th rolling element and the outer raceway,  $\delta_{in,j,r}$  the contact deformation between the  $j$ th rolling element and the inner raceway,  $\vec{x}_{j,r}$  and  $\vec{z}_{j,r}$  are the location vectors of the  $j$ th rolling element with respect to the centre of the raceways,  $\vec{p}_{j,r}$  is the independent polar generalised coordinate for the  $j$ th rolling element,  $\theta_{out,j,r}$  is the angle of the vector  $\vec{z}_{j,r}$  with respect to the centre of the outer raceway,  $\theta_{in,j,r}$  is the angle of the vector  $\vec{x}_{j,r}$  with respect to the centre of the inner raceway and independent Cartesian coordinates for the inner raceway  $(x_{in}, y_{in})$ , the outer raceway  $(x_{out}, y_{out})$ .

raceways, the nominal rotational speed of the cage is given by

$$\omega_c = \omega_s \left( 1 - \frac{D_b \cos \alpha}{D_p} \right) \quad (1)$$

where  $\omega_s$  is the shaft run speed,  $D_b$  is the diameter of a rolling element,  $D_p$  is the pitch diameter, and  $\alpha$  is the contact angle. The angular position of the  $j$ th rolling element of the  $r$ th row is

$$\phi_{j,r}(t) = \phi_c(t) + \frac{2\pi(j-1)}{N_b} + \varphi_{rnd}(r-1); \quad j = 1, 2, \dots, N_b; \quad r = 1, 2 \quad (2)$$

with the cage position  $\phi_c(t)$  given by

$$\phi_c(t+dt) = \phi_c(t) + \omega_c dt + v(t) \quad (3)$$

where  $v(t)$  is a random process uniformly distributed between  $[-\varphi_{slip}, \varphi_{slip}]$  that accounts for slippage of the rolling elements. Typical values for the maximum phase variation  $\varphi_{slip}$  are of the order 0.01–0.02 rad [6]. In Eq. (2),  $\varphi_{rnd}$  is a random number between  $[0, \pi/N_b]$  and defines the relative positions of the two rows to take into account that they do not share the same cage. The simulated results presented in this paper are for one fixed angle  $\varphi_{rnd}$  since the effect of varying  $\varphi_{rnd}$  was found to be negligible when a defect is present on one of the rows.

#### 4.3. Contact deformation for defect-free bearings

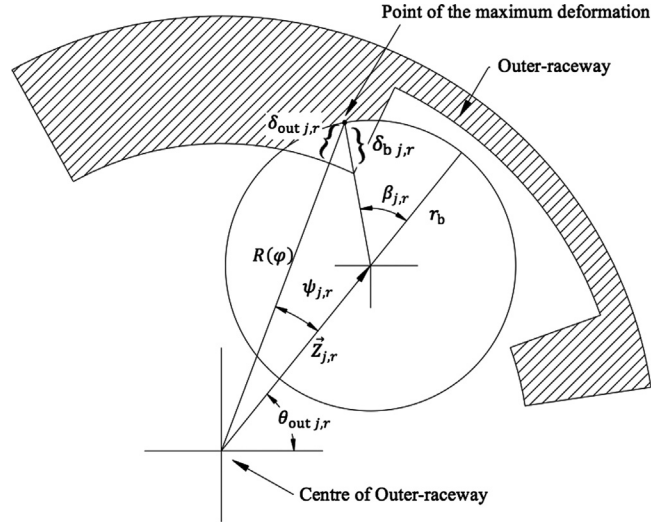
The contact deformations between a rolling element and the raceways are calculated from their relative positions described by the dynamic motion of the bearing components. Therefore, the nonlinear contact stiffness parameters are related to the dynamics of the system.

Fig. 4 presents a diagram of the relative positions of the components of a rolling element bearing. A set of independent generalised Cartesian coordinates for the inner raceway  $(x_{in}, y_{in})$ , the outer raceway  $(x_{out}, y_{out})$ , and an independent set of polar generalised coordinates for the rolling elements  $(\rho_{j,r}; j = 1, 2, 3, \dots, N_b; r = 1, 2)$  are defined. Compared with Harsha's model, in which the general coordinate  $\rho_j$  is placed on the general coordinate defined for the centre of the outer raceway [12,25,26,35], in the proposed model, the general coordinates defined for the centre of the outer raceway and the cage are independent.

The contact deformations  $\delta_{in,j,r}$  and  $\delta_{out,j,r}$  between the  $j$ th rolling element on row  $r$  and both raceways with no defect present are

$$\delta_{in,j,r} = \frac{d + D_b + cl}{2} - X_{j,r} \quad (4)$$





**Fig. 5.** Schematic diagram of the rolling element passing a rectangular shape defect on the outer raceway, with  $\lambda$  the defect depth,  $r_b$  the rolling element radius,  $\vec{Z}_{j,r}$  the distance of the rolling element from the centre of the outer raceway,  $\beta_{j,r}$  the angle of the deformation location on the rolling element,  $\delta_{b,j,r}$  deformation perpendicular to the  $j$ th rolling element,  $\delta_{out,j,r}$  deformation toward the centre of the outer raceway,  $\psi_{j,r}$  the angle between the point of the maximum deformation and the vector  $\vec{Z}_{j,r}$ ,  $\theta_{out,j,r}$  the angle of the vector  $\vec{Z}_{j,r}$  with respect to the centre of the outer raceway, and  $R(\varphi)$  the distance between the outer raceway and the centre of the outer raceway at angle  $\varphi = \theta_{out,j,r} + \psi_{j,r}$ .

$$\delta_{out,j,r} = \frac{-D + D_b - cl}{2} + Z_{j,r} \tag{5}$$

where  $d$ ,  $D$  and  $D_b$  are the diameters of the inner raceway, outer raceway and a rolling element respectively, and  $cl$  is the radial clearance of the bearing. The displacement vectors  $\vec{x}_{j,r}$  and  $\vec{z}_{j,r}$ , which specify the location of the  $j$ th rolling element on row  $r$  with respect to the centre of the inner and outer raceways, can be related to the parameter  $\rho_{j,r}$  by solving the following relations:

$$\vec{X}_{j,r} = \begin{bmatrix} \rho_{j,r} \cos \phi_{j,r} - x_{in} \\ \rho_{j,r} \sin \phi_{j,r} - y_{in} \end{bmatrix} \tag{6}$$

$$\vec{Z}_{j,r} = \begin{bmatrix} \rho_{j,r} \cos \phi_{j,r} - x_{out} \\ \rho_{j,r} \sin \phi_{j,r} - y_{out} \end{bmatrix} \tag{7}$$

where  $\phi_{j,r}$  is the angular position of the  $j$ th rolling element with respect to the polar generalised coordinates of the row  $r$  illustrated in Fig. 4 and defined by Eq. (2). The amplitudes of the vectors  $\vec{x}_{j,r}$ ,  $\vec{z}_{j,r}$  and  $\vec{p}_{j,r}$  are denoted by  $X_{j,r}$ ,  $Z_{j,r}$  and  $\rho_{j,r}$ , respectively, in this document.

#### 4.4. Contact deformation for defective bearings including finite size of rolling elements

In order to model the geometry of a defect on one of the raceways,  $r=1$ , the defect shape function  $\gamma(\phi)$  is introduced, which is a function of the angle  $\phi$ . This function can be adapted to include defects of any geometry as explained in [7,11]. A rectangular shaped, sharp edged bearing defect on the outer raceway can be modelled as

$$\gamma(\phi) = \begin{cases} \lambda, & \phi_{en} < \phi_{j,r} < \phi_{ex} \\ 0, & \text{otherwise} \end{cases}, \quad r = 1 \tag{8}$$

where  $\phi_{en}$  and  $\phi_{ex}$  are the angular positions of the defect entry and exit, and  $\lambda$  is the depth of the defect. Therefore, the geometry function of the outer raceway for a given angle  $\varphi$  with reference to the centre of the outer raceway is given by

$$R(\varphi) = \frac{(D + cl)}{2} + \gamma(\varphi) \tag{9}$$

In contrast to the previous models [6,12], where the rolling element is considered as a point mass to calculate the contact deformation between each rolling element and the raceways, the model proposed in this paper takes into account a finite number of points on the circumference of a rolling element. In other words, the dimensions of the rolling element are taking into account rather than modelling it as point mass.

Fig. 5 shows a diagram of a rolling element in the defect zone. On the outer raceway, as a rolling element at a given angular position  $\phi_{j,r}$  contacts the edges of the defect, the deformation  $\delta_{b,j,r}$  occurs at the angle  $\beta_{j,r}$  perpendicular to the  $j$ th rolling element, as illustrated in Fig. 5.

For the example used in this paper to demonstrate the capabilities of the proposed model, the defect is modelled on the outer raceway. The deformations between the rolling elements and the inner raceway always happen at a point perpendicular to the inner raceway. However, the deformation between a rolling element and the outer raceway in the defect zone happens at a point which is not necessarily at the angular position  $\beta_{j,r} = 0$  as assumed in previous models [12]. This limitation is overcome by considering a finite number of points on each rolling element to calculate the angular position of the maximum contact deformation between a rolling element and the defect on the outer raceway at a given angular position  $\theta_{out,j,r}$ . This angle can be related to the angular position  $\phi_{j,r}$  of the rolling element using Eq. (6), such that

$$\theta_{out,j,r} = \cos^{-1} \left( \frac{\rho_{j,r} \cos \phi_{j,r} - x_{out}}{Z_{j,r}} \right) \quad (10)$$

The contact deformation  $\delta_{out,j,r,\beta}$  perpendicular to the outer raceway with a defect profile  $\gamma(\phi)$  for every point at an angle  $\beta_j$  on the rolling element is given by

$$\delta_{out,j,r,\beta} = \frac{2Z_{j,r} + D_b \cos \beta_{j,r}}{2 \cos \psi_{j,r}} R(\theta_{out,j,r} + \psi_{j,r}) \quad (11)$$

where  $R(\theta_{out,j,r} \pm \psi_{j,r})$  is the polar function of the outer raceway defined by Eq. (9). The angle  $\psi_{j,r}$ , illustrated in Fig. 5, is the angle between the point of the maximum deformation on a rolling element and the displacement vector  $\vec{Z}_{j,r}$  of the rolling element and is given by

$$\psi_{j,r} = \tan^{-1} \left( \frac{D_b \sin \beta_{j,r}}{2Z_{j,r} + D_b \cos \beta_{j,r}} \right) \quad (12)$$

Therefore, the contact deformation  $\delta_{out,j,r}$  perpendicular to the outer raceway with a defect profile  $\gamma(\phi)$  is

$$\delta_{out,j,r} = \max [\delta_{out,j,r,\beta}]; \quad -\frac{\pi}{2} < \beta_{j,r} < \frac{\pi}{2} \quad (13)$$

Considering the finite size of a rolling element provides a more realistic prediction of its path as it traverses a defect, especially when the defect has a sharp edged entry and exit. This improves the accuracy of the simulated vibration response compared to previous models which include the rolling elements as point masses.

#### 4.5. Hertzian contact model

The contact forces are related to the elastic contact deformations, defined in the previous section, using the Hertzian elastic contact theory [36]. Since the Hertzian contact force arises only when there is contact between a rolling element and a raceway, the respective contact force is set to zero when the contact deformation is equal or smaller than zero. This is indicated by subscript “+” throughout this paper. The radial contact forces  $Q_{in,j,r}$  and  $Q_{out,j,r}$  between rolling element  $j$  on row  $r$  and the inner and outer raceways are calculated using the load–deflection relationship

$$\begin{bmatrix} Q_{in,j,r} \\ Q_{out,j,r} \end{bmatrix} = \begin{bmatrix} K_{in} [\delta_{in,j,r}]_+^n \\ K_{out} [\delta_{out,j,r}]_+^n \end{bmatrix} \quad (14)$$

where  $\delta_{in,j,r}$  and  $\delta_{out,j,r}$  are calculated using Eqs. (4) and (5). The load–deflection factors  $K_{in}$  and  $K_{out}$  depend on the curvature of the rolling elements and raceways, and  $n = 10/9$  for cylindrical roller bearings and  $3/2$  for spherical roller bearings [3]. Using Eq. (14), the nonlinear stiffnesses  $k_{in,j,r}$  and  $k_{out,j,r}$  of the springs shown in Fig. 3 are defined as

$$\begin{bmatrix} k_{in,j,r} \\ k_{out,j,r} \end{bmatrix} = \begin{bmatrix} \partial Q_{in,j,r} / \partial \delta_{in,j,r} \\ \partial Q_{out,j,r} / \partial \delta_{out,j,r} \end{bmatrix}_+ = \begin{bmatrix} K_{in} \delta_{in,j,r}^{n-1} \\ K_{out} \delta_{out,j,r}^{n-1} \end{bmatrix}_+ \quad (15)$$

which shows that the nonlinear contact stiffnesses are functions of the contact deformations  $\delta_{in,j,r}$  and  $\delta_{out,j,r}$ . Previous analysis of the time-varying characteristics of the bearing stiffness [37] shows that for roller bearings, significant parametric excitations occur due to stiffness variations even though the load–deflection relationship is almost linear. Using Eqs. (6), (7) and (14), the total contact forces in the  $x$  and  $y$  directions acting on the inner raceway are obtained by summing over the  $N_b$  rolling elements on each row, such that

$$\begin{bmatrix} F_{in,x} \\ F_{in,y} \end{bmatrix} = \sum_{r=1}^2 \sum_{j=1}^{N_b} K_{in} [\delta_{in,j,r}]_+^n \begin{bmatrix} \cos(\theta_{in,j,r}) \\ \sin(\theta_{in,j,r}) \end{bmatrix} \quad (16)$$

with

$$\theta_{in,j,r} = \cos^{-1} \left( \frac{\rho_{j,r} \cos \phi_{j,r} - x_{in}}{X_{j,r}} \right) \quad (17)$$

Similarly, the total contact forces acting on the outer raceway are defined as

$$\begin{bmatrix} F_{\text{out},x} \\ F_{\text{out},y} \end{bmatrix} = - \sum_{r=1}^2 \sum_{j=1}^{N_b} K_{\text{out}} [\delta_{\text{out},j,r}]^n \begin{bmatrix} \cos(\theta_{\text{out},j,r}) \\ \sin(\theta_{\text{out},j,r}) \end{bmatrix} \quad (18)$$

where  $\theta_{\text{out},j,r}$  is defined in Eq. (10).

#### 4.6. Contact damping

Damping in the contacts due to the lubricant film between the rolling elements and raceways is taken into account by including linear dampers  $c_{\text{in},j,r}$  and  $c_{\text{out},j,r}$  as shown in Fig. 3. The radial contact damping forces associated with the rolling element  $j$  on row  $r$  are given by

$$\begin{bmatrix} Q_{\text{d in},j,r} \\ Q_{\text{d out},j,r} \end{bmatrix} = c \begin{bmatrix} \dot{\delta}_{\text{in},j,r} \\ \dot{\delta}_{\text{out},j,r} \end{bmatrix} \quad (19)$$

where  $c$  is the viscous damping constant. The total contact damping forces acting on the inner and outer raceways in the  $x$  and  $y$  directions are now given by

$$\begin{bmatrix} F_{\text{d in},x} \\ F_{\text{d in},y} \end{bmatrix} = \sum_{r=1}^2 \sum_{j=1}^{N_b} Q_{\text{d in},j,r} \begin{bmatrix} \cos(\theta_{\text{in},j,r}) \\ \sin(\theta_{\text{in},j,r}) \end{bmatrix} \quad (20)$$

$$\begin{bmatrix} F_{\text{d out},x} \\ F_{\text{d out},y} \end{bmatrix} = - \sum_{r=1}^2 \sum_{j=1}^{N_b} Q_{\text{d out},j,r} \begin{bmatrix} \cos(\theta_{\text{out},j,r}) \\ \sin(\theta_{\text{out},j,r}) \end{bmatrix} \quad (21)$$

The damping in a bearing assembly (normalised by 1 N s/m) is typically in the order of  $0.25\text{--}25 \times 10^{-5}$  times the linearised stiffness (normalised by 1 N/m) of the bearing assembly [4,5]. The viscous damping constant  $c$  in Eq. (19) is adjusted to achieve damping within this range [11].

#### 4.7. Nonlinear equations of motion

The equations of motion for the inner raceway, outer raceway and the measured response which includes the high-frequency resonant mode are now given by

$$m_{\text{in}} \begin{bmatrix} \ddot{x}_{\text{in}} \\ \ddot{y}_{\text{in}} - g \end{bmatrix} + \begin{bmatrix} F_{\text{in},x} + F_{\text{d in},x} \\ F_{\text{in},y} + F_{\text{d in},y} \end{bmatrix} = \begin{bmatrix} 0 \\ -W \end{bmatrix} \quad (22)$$

$$m_{\text{out}} \begin{bmatrix} \ddot{x}_{\text{out}} \\ \ddot{y}_{\text{out}} - g \end{bmatrix} + \begin{bmatrix} c_{s,x} \dot{x}_{\text{out}} \\ c_{s,y} \dot{y}_{\text{out}} \end{bmatrix} + \begin{bmatrix} k_{s,x} x_{\text{out}} \\ k_{s,y} y_{\text{out}} \end{bmatrix} + \begin{bmatrix} F_{\text{out},x} + F_{\text{d out},x} \\ F_{\text{out},y} + F_{\text{d out},y} \end{bmatrix} = \begin{bmatrix} 0 \\ 0 \end{bmatrix} \quad (23)$$

$$\begin{aligned} m_r \ddot{y}_v + k_r (y_v - y_{\text{out}}) + c_r (\dot{y}_v - \dot{y}_{\text{out}}) &= 0 \\ m_r \ddot{x}_v + k_r (x_v - x_{\text{out}}) + c_r (\dot{x}_v - \dot{x}_{\text{out}}) &= 0 \end{aligned} \quad (24)$$

where  $g = 9.81 \text{ m/s}^2$ , and the contact forces are calculated as described in Section 4.5 and 4.6. In order to derive the equations of motion for the rolling elements on row  $r$ , Lagrange's equation for the set of generalised coordinates  $\rho_{j,r}$  are used

$$\frac{d}{dt} \frac{\partial T_r}{\partial \dot{\rho}_{j,r}} - \frac{\partial T_r}{\partial \rho_{j,r}} + \frac{\partial V_r}{\partial \rho_{j,r}} = \{f_r\} \quad (25)$$

where  $T_r$  is the kinetic energy,  $V_r$  is the potential energy,  $\{\rho_{j,r}\}$  is a vector of the generalised coordinates defined for the rolling elements, and  $\{f_r\}$  is the vector with generalised contact forces. The total kinetic and potential energy of the rolling elements on row  $r$  is

$$V_r = \sum_{j=1}^{N_b} m_b g \rho_{j,r} \sin \phi_{j,r} \quad (26)$$

$$T_r = \sum_{j=1}^{N_b} 0.5 m_b (\dot{\vec{\rho}}_{j,r} \cdot \dot{\vec{\rho}}_{j,r}) + 0.5 I \omega_b^2 \quad (27)$$

where  $I$  is the moment of inertia about the centre of a rolling element,  $\omega_b$  is the rotational speed of the rolling element, and  $\vec{\rho}_{j,r}$  is given by

$$\vec{\rho}_{j,r} = (\rho_{j,r} \cos \phi_{j,r}) \hat{i} + (\rho_{j,r} \sin \phi_{j,r}) \hat{j} \quad (28)$$

The term  $\dot{\vec{\rho}}_{j,r} \cdot \dot{\vec{\rho}}_{j,r}$  in Eq. (27) can be re-arranged to



$$\dot{\rho}_{j,r} \cdot \dot{\rho}_{j,r} = \dot{\rho}_{j,r}^2 + \rho_{j,r}^2 \dot{\phi}_{j,r}^2 = \dot{\rho}_{j,r}^2 + \rho_{j,r}^2 \omega_c^2 \quad (29)$$

since  $\dot{\phi}_{j,r} = \omega_c$ . By substituting equation Eq. (29) into (27) the total kinetic energy of each row is

$$T_r = \sum_{j=1}^{N_b} 0.5 m_b (\dot{\rho}_{j,r}^2 + \rho_{j,r}^2 \omega_c^2) + 0.5 I \omega_c^2 \left( \frac{D_p}{D_b} + \cos \alpha \right)^2 \quad (30)$$

The terms in Eq. (25) can be evaluated individually as

$$\frac{\partial V_r}{\partial \{\rho_{j,r}\}} = m_b g \sin \phi_{j,r} \quad (31)$$

$$\frac{d}{dt} \frac{\partial T_r}{\partial \{\dot{\rho}_{j,r}\}} - \frac{\partial T_r}{\partial \{\rho_{j,r}\}} = m_b \ddot{\rho}_{j,r} - m_b \rho_{j,r} \omega_c^2 \quad (32)$$

The vector of generalised contact forces  $\{f_r\}$  in Eq. (25) is the sum of the radial contact and damping forces acting on each rolling element with respect to the generalised coordinates  $\rho_{j,r}$  which can be calculated by differentiating Eqs. (14) and (19) with respect to the generalised coordinates  $\rho_{j,r}$ , such that

$$\{f_r\} = \frac{\partial (Q_{in\ j,r} + Q_{out\ j,r} + Q_{d\ in\ j,r} + Q_{d\ out\ j,r})}{\partial \{\rho_{j,r}\}} = \left( K_{in} [\delta_{in\ j,r}]_+^n + c [\dot{\delta}_{in\ j,r}]_+ \right) \frac{\partial X_{j,r}}{\partial \rho_{j,r}} + \left( K_{out} [\delta_{out\ j,r}]_+^n + c [\dot{\delta}_{out\ j,r}]_+ \right) \frac{\partial Z_{j,r}}{\partial \rho_{j,r}} \quad (33)$$

where the partial derivatives of  $X_{j,r}$  and  $Z_{j,r}$  with respect to  $\rho_{j,r}$  are defined as

$$\frac{\partial X_{j,r}}{\partial \rho_{j,r}} = \frac{\rho_{j,r} - x_{in} \cos \phi_{j,r} - y_{in} \sin \phi_{j,r}}{X_{j,r}} \quad (34)$$

$$\frac{\partial Z_{j,r}}{\partial \rho_{j,r}} = \frac{\rho_{j,r} - x_{out} \cos \phi_{j,r} - y_{out} \sin \phi_{j,r}}{Z_{j,r}} \quad (35)$$

Substituting Eqs. (31)–(33) into Eq. (25) gives the following equations of motion for the rolling elements on row  $r$ :

$$m_b \ddot{\rho}_{j,r} - m_b \rho_{j,r} \omega_c^2 + m_b g \sin \phi_{j,r} - \{f_r\} = 0 \quad (36)$$

Eqs. (22)–(24) and (36) form a system of coupled, second order, nonlinear, ordinary differential equations. The dynamic system is excited by variations in the stiffnesses of the nonlinear contact springs (parametric excitations [11]) as well as the impacts that occur when a rolling element mass traverses through a defect.

## 5. Simulation and experimental results

### 5.1. Simulation and model parameters

This section presents a comparison between simulated and experimental vibration results, as well as a validation of the static load distribution predicted by the model. The test bearing described in Section 3 was modelled using the proposed model presented in Section 4. The simulations were undertaken using Matlab<sup>®</sup> and Simulink<sup>®</sup> and the equations of motion were solved using the ordinary differential equation solver (ode45). The high frequency resonant mode was modelled to have a resonance frequency of 10 kHz and damping ratio of 3%, which corresponds to one of the dominant experimentally measured bearing resonant modes. The model parameter values used in the simulations are given in Table 2.

The aim of the simulations is to show that the developed model can predict characteristics observed in the measured vibration response, whilst modelling the actual shape of the defect. This is in contrast with previous models in which the modelled defect shape was altered from the actual shape in order to achieve better agreement between modelled and measured results.

**Table 2**

Model parameter values used for simulation.

Hertzian contacts	Mass	Stiffness	Damping
$K_{in} = 4576 \text{ MN/m}^{1.11}$	$m_o = 200 \text{ kg}$	$k_r = 19,739 \text{ MN/m}$	$c_r = 18,850 \text{ N s/m}$
$K_{out} = 4576 \text{ MN/m}^{1.11}$	$m_i = 480 \text{ kg}$	$k_{s,x} = 457.6 \text{ MN/m}$	$c_{s,x} = 1.46 \text{ MN s/m}$
$c = 9000 \text{ N s/m}$	$m_r = 5 \text{ kg}$	$k_{s,y} = 457.6 \text{ MN/m}$	$c_{s,y} = 1.46 \text{ MN s/m}$

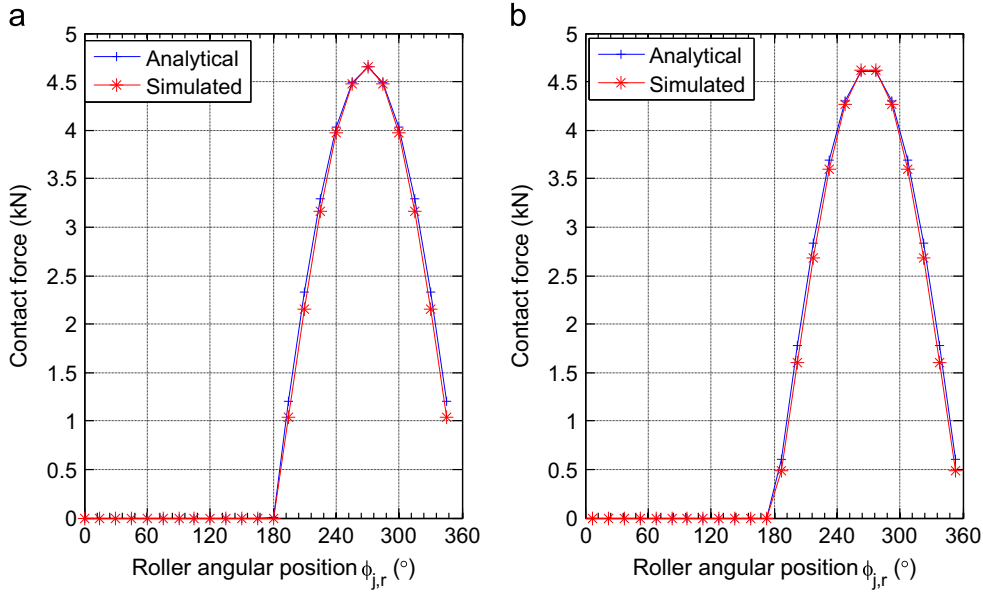


Fig. 6. Static load distribution validation for cage angular positions of 0° and 7.5.

5.2. Load distribution validation

This section compares the static load distribution results of the proposed model and the well-known Stribeck results [3,11]. The static load distribution for a defect-free bearing is defined by [3]

$$Q_{j,r} = F_{max} \left( 1 - \frac{1 + \cos \phi_{j,r}}{2\epsilon} \right)^n \tag{37}$$

where  $n = 10/9$  for roller bearings and  $\epsilon = 0.5$  for zero clearance. The maximum load  $F_{max}$  for a double row roller bearing with zero clearance is given by Harris [3]

$$F_{max} = \frac{4.37W}{2N_b \cos \alpha} \tag{38}$$

The static load distribution as a function of the cage position is obtained by modelling a defect-free double row roller bearing using the proposed model while the cage is stationary. Fig. 6 compares the simulated and analytical static load distribution for roller’s angular positions  $\phi_{j,r}$  of 0° and 7.5°. The results show that the simulated load distribution accurately matches the analytical solution.

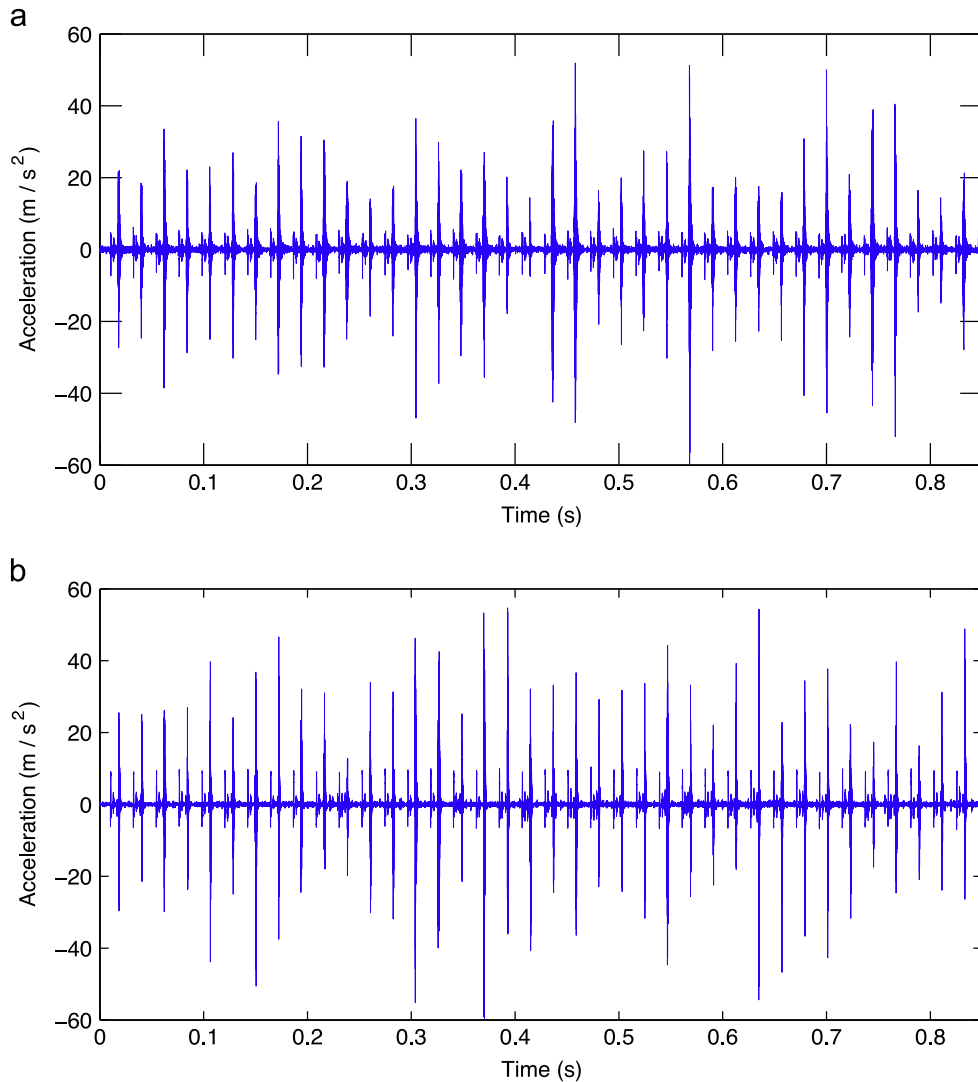
5.3. Comparison of simulated and measured results

Fig. 7(a) shows 0.85 s of the acceleration that was experimentally measured on the test bearing at a speed of 250 rpm and 50 kN radial load. The simulated acceleration response  $\ddot{y}_r$ , obtained with the proposed model is included in Fig. 7(b). The experimental data was low-pass filtered at 12 kHz as the bearing resonances at higher frequencies are not considered in the model.

Fig. 7 shows that the amplitude of the high frequency events is fluctuating in time, and that these fluctuations are predicted by the proposed model. This is not the case for the previous models [1,2,11,17–27] which predict near-constant amplitudes. In order to compare the simulated and measured fluctuations in the amplitude of the high-frequency events, the variances of the envelopes were calculated after band-pass filtering both signals between 9.6 and 10.8 kHz. This resulted in variances of 17.1 and 17.8 for the simulated and measured vibration responses, which shows that the proposed model accurately predicts the fluctuations in amplitude of the high-frequency event.

Fig. 8 compares the acceleration squared envelope spectra of the measured and simulated vibration response. The envelope spectra were calculated after band-pass filtering the acceleration signals between 9.6 and 10.8 kHz. The defect frequency components at  $f_{bpo} = 45.4$  Hz and its harmonics are clearly visible, and very good agreement is achieved between the measured and simulated results.

Fig. 9(a) and (b) shows zoomed-in sections of the signals presented in Fig. 7, where the zoomed-in section corresponds to the period of time in which roller  $j=5$  on the defective raceway  $r=1$  approaches and leaves the defect. Fig. 9(c) shows the path of the radial position of the 5th rolling element on row  $r=1$  ( $Z_{j,1}$ ). In Fig. 9(c), the small difference between the roller path and the defect geometry, outside the defect zone, is the roller contact deformation. Fig. 9(a) and (b) shows that at



**Fig. 7.** 0.85 s of bearing vibration response at 252 rpm and under 50 kN vertical static load: (a) measurement vibration response of the test bearing and (b) simulated vibration response.

approximately 0.0394 s, when the roller enters the defect, low frequency vibration is generated in both the experimentally measured and predicted vibration. Similarly experimentally measured and predicted vibration signals indicate that impacts occur when the rolling element hits the bottom of the defect and upon exiting the defect. The key vibration characteristics observed in the simulated and measured results are analysed as follows.

### 5.3.1. Rolling element entry

The entry of the rolling element into the defect generates predominantly low frequency content in the vibration response. This low frequency vibration is due to the gradual de-stressing of the rolling element, which starts when it is positioned at an angle of  $\phi_{en}$  and ends when it loses its load carrying capacity. The gradual de-stressing of the rolling element as it enters the defect can be seen in the gradual decay in the contact force in Fig. 9(d). During this stage, the load has to be redistributed amongst the other rolling elements in the load zone. Therefore, the contact forces of the leading and lagging rolling elements in the load zone gradually increase. Consequently, as the number of the load carrying rolling elements decreases, the bearing assembly stiffness decreases. As this reduction is gradual, only low frequency modes of the system will be excited which results in the low frequency event in the vibration signal. The low frequency event can also be explained by examining the rolling element path in Fig. 9(c). The change of the acceleration at the entry is due to the trace of the rolling element following an arc path and gradually losing contact with both raceways.

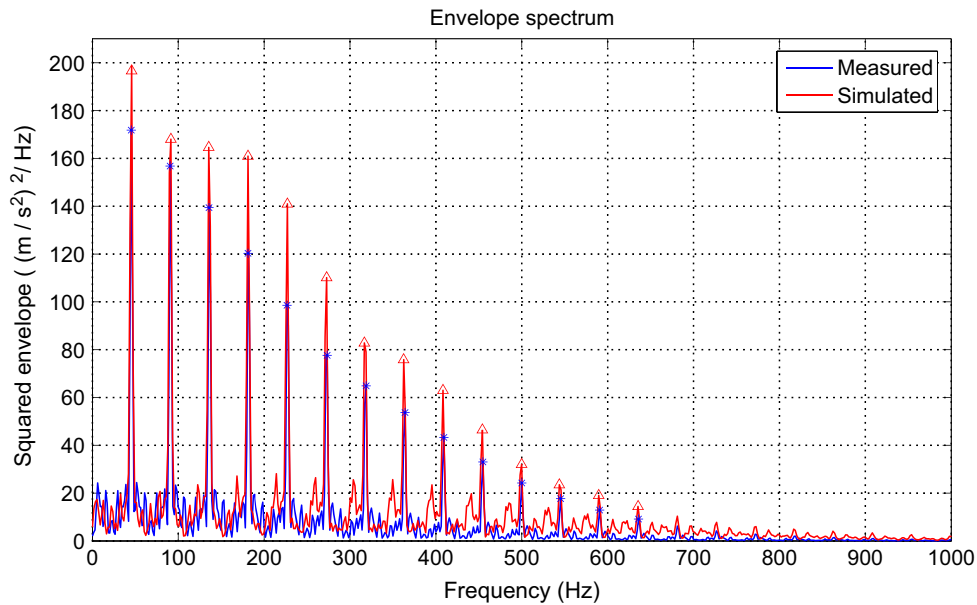


**Fig. 8.** Comparison of the measured and modelled acceleration squared envelope spectra. The signals were band-pass filtered between 9.6 and 10.8 kHz before calculating the envelope spectra. The markers indicate the defect frequency  $f_{bpo} = 45.4$  Hz and its harmonics.

### 5.3.2. Impact of the rolling element and outer raceway

After losing contact with the raceways, the rolling element travels through the defect and impacts the bottom of the outer raceway defect, as shown in Fig. 9(b)–(d) at approximately 0.043 s. It follows a curved path, the exact pattern of which depends on the centrifugal and inertia forces of the rolling element, until it hits the bottom of the defect. Depending on the dynamics of the system, the rolling element bounces a couple of times between the raceways before it hits the exit point of the defect. The time from when the 5<sup>th</sup> rolling element is at the defect entry to the time that it strikes the bottom of the outer raceway, matches the timing when a high frequency excitation of relatively low amplitude is observable at time 0.043 s in the experimental results, see Fig. 9(a). This event is predicted by the proposed model as shown in Fig. 9(b) whereas previous models do not correctly predict this event.

### 5.3.3. Rolling element exit

The high frequency event in the vibration response observed in Fig. 9(b) at approximately 0.048 s is associated with the rolling element exiting the defect. The rolling element has to change direction suddenly and restress back to its normal load carrying capacity [23]. This abrupt change in the direction of movement causes a step change in velocity and generates an impulse in the acceleration signal, which excites the high frequency resonance mode of the bearing assembly that is included in the proposed model. As the rolling element restresses between the raceways at the defect exit, multiple impacts occur as it alternatively strikes the outer and inner raceway. The multiple impacts at the defect exit can be seen in the experimental results in Fig. 9(a) at approximately 0.048 s, and have also been observed in experiments presented in previous studies [16]. The proposed model is able to predict and explain the mechanism of multiple impact events at the exit which cannot be predicted by the previous models [4–7].

## 6. Comparing results to the previous models and discussion

This section demonstrates the importance of considering the finite size of the rolling elements. This is achieved by comparing the simulated results of the previous section against those predicted when not including the finite size algorithm introduced in Section 4 into the proposed model. The resulting model will be referred to as the “point mass model” and is representative of the previous models which included the rolling elements as point masses. The mechanisms that lead to inaccurate vibration response predictions in these previous models are identified and explained.

Fig. 10 shows a comparison of the simulated vibration responses of the test bearing using the point mass and proposed models. Fig. 11 shows a comparison of the path of the rolling element in the defect zone and the corresponding dynamic contact forces calculated using the proposed model and the point mass model. The following sections describe observations of these simulation results by studying the significant events in the responses.

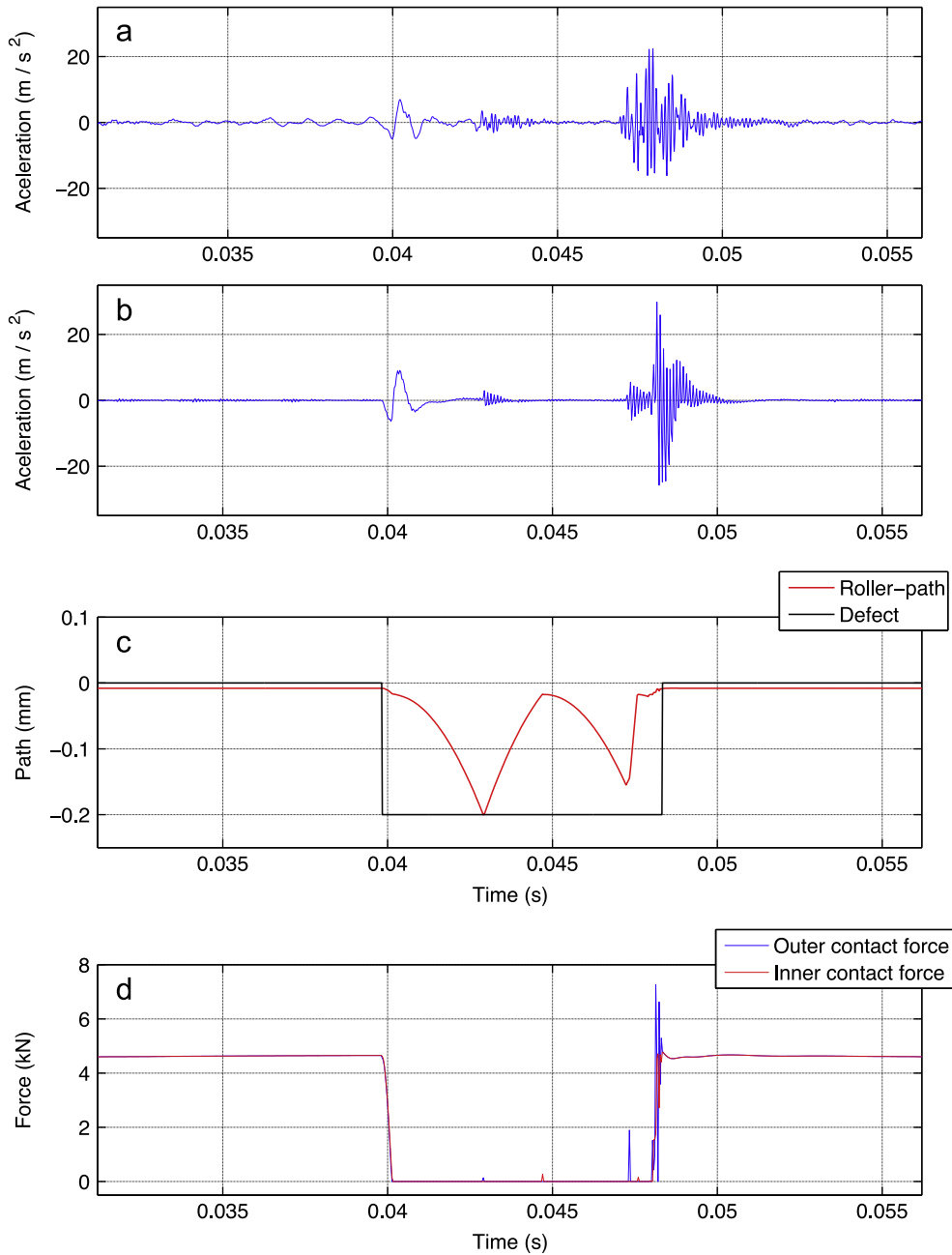


**Fig. 9.** (a) Measurement vibration response of the test bearing at 252 rpm and under 50 kN vertical static load, (b) simulated vibration response, (c) simulated path ( $Z_{5,1} - D_p - D_b + \delta_{out\ 5,1}$ ) of the rolling element  $j=5$ th as it travels through the defect zone and (d) simulated inner and outer contact forces acting on the 5th rolling element.

### 6.1. Entry event

Fig. 10(c) shows that as the rolling element enters the defect zone at time  $t_1$  (marked on the graph), the low frequency event is observable in the vibration response. The frequency characteristics of this event match closely with the experimentally measured response shown in Fig. 9(a). In contrast to the proposed model, the simulation result of the point mass model exhibits a high frequency event superimposed on the low frequency event at time  $t_1$  that is not consistent with the experimental results shown in Fig. 9(a). The high frequency event modelled by the point mass model is the result of a near step change in contact forces, as shown in Fig. 11(e) and (f) at time  $t_1$ . Contact forces in the previous models are predicted for only one point on the rolling element and any step change in the defect profile results in a step change in the contact forces. By modelling rectangular shaped defects using the previous models, as the rolling element reaches the entry

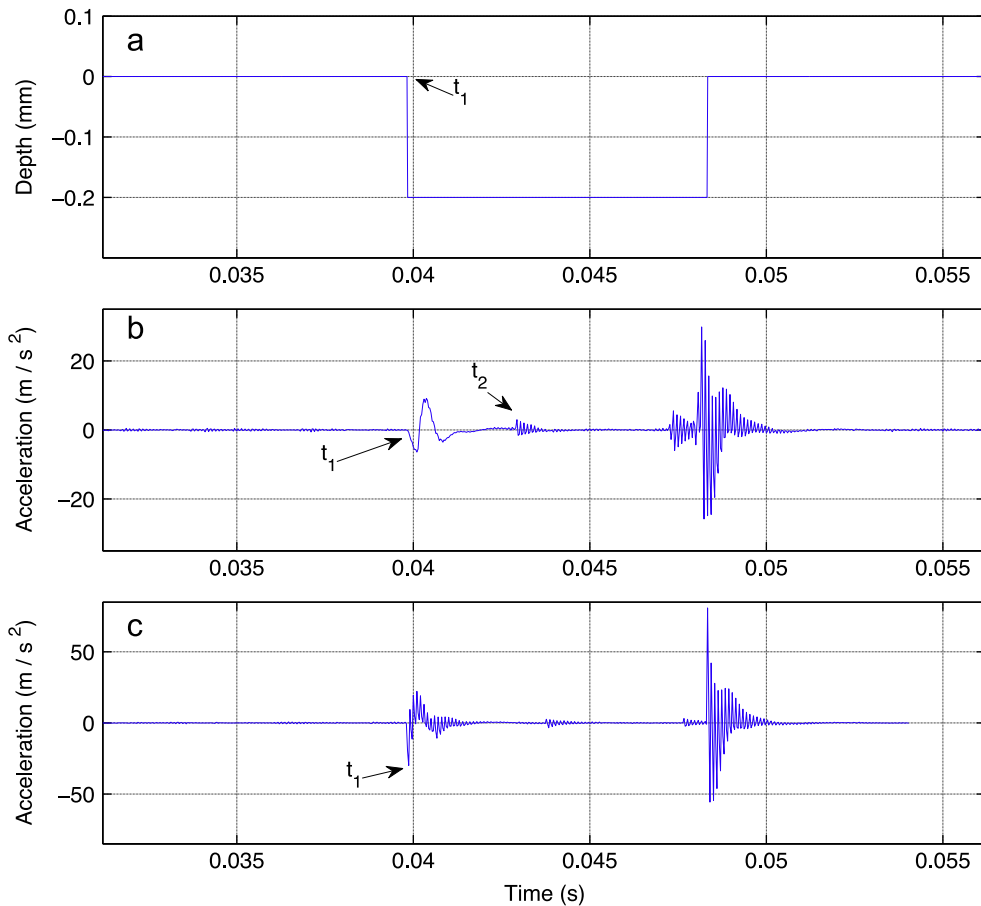


**Fig. 10.** The effect of including the finite size of rolling elements: (a) defect profile; (b) simulated vibration response using the proposed model and (c) simulated vibration response using the point mass model.

point of the defect (the time when the radius of the outer raceway is  $D/2$ ), both inner and outer contact forces are non-zero. The value of these contact forces suddenly changes to zero when the radius of the outer raceway changes to  $D/2 + \lambda$ , as is shown in Fig. 11(e). However, the proposed model considers the finite size of the rolling elements, which results in a gradual decay of the contact forces, as opposed to a step change, as seen in Fig. 11(c).

## 6.2. Mid-events

The next major event is the rolling element striking the bottom of the defect at time  $t_2$ , shown in Fig. 11(a), which excites the high-frequency natural mode of the system (shown in Fig. 10(b) at time  $t_2$ ), and matches the timing of the high frequency event of the measured response shown in Fig. 9(a) at time  $t_2$ . Fig. 11(a) shows the path of the rolling element in the defect zone ( $Z_{5,1} - D_p - D_b + \delta_{out\ 5,1}$ ) and the corresponding contact forces are shown in Fig. 11(b). The rolling element falls into the defect once both the inner and outer raceway contact forces acting on the rolling element have gradually decayed to zero. This results in the rolling element falling and striking the bottom of the defect at time  $t_2$ , which matches the vibration signal at time  $t_2$  in the experimental results shown in Fig. 9(a). The point mass model incorrectly predicts a faster drop of the rolling element to the bottom of the defect, which in turn results in a higher contact force estimation than the proposed model, shown in Fig. 11(d)–(f). The prediction of the sudden fall of the rolling element into the defect by point mass models [12,25,26,35] is due to the step change of the defect profile. In these point mass models, the contact forces do not gradually decay to zero before losing contact with the entry point as predicted by the proposed model. Rather, the outer raceway contact force suddenly becomes zero when the inner raceway contact force still has a non-zero value, which results in an unrealistic rapid fall of the rolling element into the defect. It can be seen from the path of the rolling element in the point mass simulation, illustrated in Fig. 11(d), that the first strike to the bottom of the defect occurs at time  $t_4$ . This is earlier than the more accurate prediction provided by the proposed model, as shown in Fig. 11(a) at time  $t_2$ . Further, the point mass model predicts that the roller strikes the bottom of the defect three times as it traverses through the defect, whereas the proposed model predicts only a single strike. The experimental results in Fig. 9(a) suggest that there is only a single strike, demonstrating the improvements provided by considering the finite size of the rolling element.

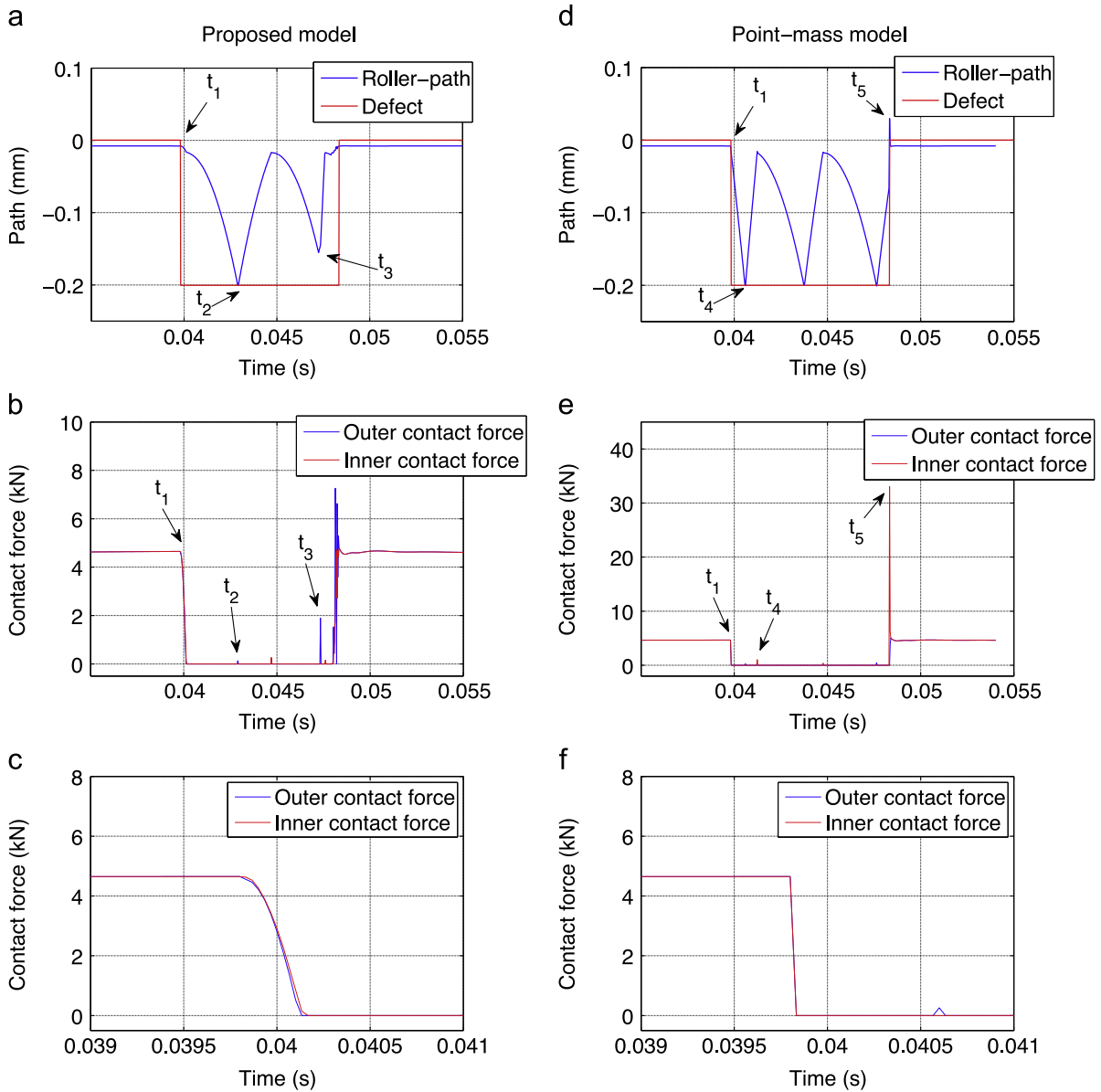


**Fig. 11.** Comparison of simulated roller path and contact forces using the point mass and proposed model. (a) and (c) The path of the 5th rolling element in the defect zone ( $Z_{5,1} - D_p - D_b + \delta_{out\ 5,1}$ ) simulated by the proposed and point mass models, respectively. (b) and (e) The inner and outer contact forces of the 5th rolling element simulated by the proposed and point mass models, respectively. (c) and (f) The zoomed section of the entry point to the defect.

### 6.3. Exit events

The point mass model incorrectly predicts only one impact at the exit point as shown in Figs. 10(c) and 11(d) and (e). In contrast, the proposed model has the capacity to predict the multiple impacts observed in the experimental results, as seen in Figs. 10(b) and 11(a) and (b). The simulation results for the point mass model show that the impact at the exit point occurs at time  $t_5$  in Fig. 11(c) and (d), whereas the first exit event (of the multiple exit events) predicted by the proposed model occurs at time  $t_3$  in Fig. 11(a) and (b), which is similar to the measured response shown in Fig. 9(a). The proposed model is able to correctly predict the timing of this event because the finite size of the rolling elements is included in the model. In the proposed model, the circumference of the rolling element can strike the defect at any point before the centre of the rolling element reaches the exit point (i.e. before  $\phi_{j,1} = \phi_{en}$ ). However, in the point mass model, the exit impact event incorrectly occurs when the rolling element centre is positioned at the exit point ( $\phi_{j,1} = \phi_{en}$ ). Moreover, the step changes in the contact forces at the exit predicted by the point mass model result in unrealistically large contact forces and accelerations. Therefore, the exit event will be predicted incorrectly both in timing and magnitude when not considering the finite size of the rolling elements.



In summary it has been demonstrated that dynamic models of defective bearings that employ point masses to simulate rolling elements cannot accurately predict the characteristics typically observed in the vibration response measured for sharp edged defects. This limitation is overcome in the proposed model by including the finite size of the rolling elements, with results showing that this leads to accurate predictions that compare favourably with experimental findings.

## 7. Conclusion

This paper has demonstrated the importance of including the finite size of rolling elements into nonlinear multi-body dynamic models of defective rolling element bearings. A method for accounting for the finite rolling element size was presented and included into a nonlinear multi-body dynamic model of a defective bearing, which has the capacity to model a wide range of defect geometries. The vibration response predicted by the proposed model was compared with experimental results for the case of a rectangular shaped, sharp edged defect. This showed that the time–frequency characteristics of the significant events observed in the experimentally measured vibration response were more accurately predicted in comparison to previous models that do not account for the finite rolling element size. These significant events include the low-frequency event that occurs when a rolling element enters the defect entry, the multiple high-frequency events that occur when it exits the defect, and the events that occur when the rolling element strikes the raceway mid-way through the defect. Unlike the previous models, the actual defect geometry does not need to be artificially modified in the simulations to obtain a reasonable agreement with experimental results, and no assumptions on the rolling element path at the defect entry and exit need to be made. The mechanisms that cause inaccuracies in the predicted vibration response when including the rolling elements as point masses instead of finite size objects, as done in previous models, were identified and explained. The proposed model can be used to investigate the dynamic behaviour of defective bearings for a wide range of defect geometries. This will facilitate the development of new diagnostics algorithms, such as defect size estimation techniques for a wider range of defect sizes and geometries.

## Acknowledgements

This research is supported and funded in part by ARC Linkage grant LP110100529.

## References

- [1] Y.-T. Su, M.-H. Lin, M.-S. Lee, The effects of surface irregularities on roller bearing vibrations, *J. Sound Vib.* 165 (1993) 455–466.
- [2] C. Sunnersjö, Rolling bearing vibrations – the effects of geometrical imperfections and wear, *J. Sound Vib.* 98 (1985) 455–474.
- [3] T.A. Harris, *Rolling Bearing Analysis*, Wiley, New York, USA, 2001.
- [4] J. Sopanen, A. Mikkola, Dynamic model of a deep-groove ball bearing including localized and distributed defects. Part 1: theory, *Proc. Inst. Mech. Eng. Part K: J. Multi-body Dyn.* 217 (2003) 201–211.
- [5] J. Sopanen, A. Mikkola, Dynamic model of a deep-groove ball bearing including localized and distributed defects. Part 2: Implementation and results, *Proc. Inst. Mech. Eng. Part K: J. Multi-body Dyn.* 217 (2003) 213–223.
- [6] N. Sawalhi, R. Randall, Simulating gear and bearing interactions in the presence of faults: Part I. The combined gear bearing dynamic model and the simulation of localised bearing faults, *Mech. Syst. Signal Process.* 22 (2008) 1924–1951.
- [7] N. Sawalhi, R. Randall, Simulating gear and bearing interactions in the presence of faults: Part II. Simulation of the vibrations produced by extended bearing faults, *Mech. Syst. Signal Process.* 22 (2008) 1952–1966.
- [8] M. Cao, J. Xiao, A comprehensive dynamic model of double-row spherical roller bearing – model development and case studies on surface defects, preloads, and radial clearance, *Mech. Syst. Signal Process.* 22 (2008) 467–489.
- [9] S. Sassi, B. Badri, M. Thomas, A numerical model to predict damaged bearing vibrations, *J. Vib. Control* 13 (2007) 1603–1628.
- [10] M. Tadina, M. Boltežar, Improved model of a ball bearing for the simulation of vibration signals due to faults during run-up, *J. Sound Vib.* 330 (2011) 4287–4301.
- [11] D. Petersen, C. Howard, N. Sawalhi, A. Moazen Ahmadi, S. Singh, Analysis of bearing stiffness variations, contact forces and vibrations in radially loaded double row rolling element bearings with raceway defects, *Mech. Syst. Signal Process.* 50–51 (2015) 139–160, <http://dx.doi.org/10.1016/j.ymssp.2014.04.014>.
- [12] S.P. Harsha, Nonlinear dynamic analysis of an unbalanced rotor supported by roller bearing, *Chaos, Solut. Fractals* 26 (2005) 47–66.
- [13] I. Epps, H. McCallion, An investigation into the characteristics of vibration excited by discrete faults in rolling element bearings, in: *Proceedings of the Annual Conference of the Vibration Association of New Zealand*, Christchurch, 1994.
- [14] N. Sawalhi, R.B. Randall, Vibration response of spalled rolling element bearings: observations, simulations and signal processing techniques to track the spall size, *Mech. Syst. Signal Process.* 25 (2011) 846–870.
- [15] A. Moazenahmadi, D. Petersen, C. Howard, A nonlinear dynamic model of the vibration response of defective rolling element bearings, in: *Proceedings of Australian Acoustics*, Victor Harbor, 2013.
- [16] S. Singh, U.G. Köpke, C.Q. Howard, D. Petersen, Analyses of contact forces and vibration response for a defective rolling element bearing using an explicit dynamics finite element model, *J. Sound Vib.* 333 (2014) 5356–5377.
- [17] P. McFadden, J. Smith, Model for the vibration produced by a single point defect in a rolling element bearing, *J. Sound Vib.* 96 (1984) 69–82.
- [18] P.D. McFadden, J.D. Smith, The vibration produced by multiple point defects in a rolling element bearing, *J. Sound Vib.* 98 (1985) 263–273.
- [19] Y.-T. Su, S.-J. Lin, On initial fault detection of a tapered roller bearing: frequency domain analysis, *J. Sound Vib.* 155 (1992) 75–84.
- [20] N. Tandon, A. Choudhury, An analytical model for the prediction of the vibration response of rolling element bearings due to a localized defect, *J. Sound Vib.* 205 (1997) 275–292.
- [21] F. Wardle, Vibration forces produced by waviness of the rolling surfaces of thrust loaded ball bearings Part 2: experimental validation, *Proc. Inst. Mech. Eng. Part C: J. Mech. Eng. Sci.* 202 (1988) 313–319.
- [22] E. Yhland, A linear theory of vibrations caused by ball bearings with form errors operating at moderate speed, *J. Tribol.* 114 (1992) 348–359.
- [23] N. Tandon, A. Choudhury, A theoretical model to predict the vibration response of rolling bearings in a rotor bearing system to distributed defects under radial load, *J. Tribol.* 122 (2000) 609–615.
- [24] N. Aktürk, The effect of waviness on vibrations associated with ball bearings, *J. Tribol.* 121 (1999) 667–677.



- [25] S.P. Harsha, K. Sandeep, R. Prakash, Non-linear dynamic behaviors of rolling element bearings due to surface waviness, *J. Sound Vib.* 272 (2004) 557–580.
- [26] S.P. Harsha, P.K. Kankar, Stability analysis of a rotor bearing system due to surface waviness and number of balls, *Int. J. Mech. Sci.* 46 (2004) 1057–1081.
- [27] B. Changqing, X. Qingyu, Dynamic model of ball bearings with internal clearance and waviness, *J. Sound Vib.* 294 (2006) 23–48.
- [28] C.S. Sunnersjö, Varying compliance vibrations of rolling bearings, *J. Sound Vib.* 58 (1978) 363–373.
- [29] R. Sayles, S. Poon, Surface topography and rolling element vibration, *Precis. Eng.* 3 (1981) 137–144.
- [30] F. Wardle, Vibration forces produced by waviness of the rolling surfaces of thrust loaded ball bearings Part 2: experimental validation, *J. Mech. Eng. Sci.* 202 (1988) 313–319.
- [31] N. Tandon, A. Choudhury, A review of vibration and acoustic measurement methods for the detection of defects in rolling element bearings, *Tribol. Int.* 32 (1999) 469–480.
- [32] G. Jang, S.W. Jeong, Vibration analysis of a rotating system due to the effect of ball bearing waviness, *J. Sound Vib.* 269 (2004) 709–726.
- [33] W. Soedel, *Vibrations of Shells and Plates*, CRC Press, 2004.
- [34] S.P. Harsha, K. Sandeep, R. Prakash, The effect of speed of balanced rotor on nonlinear vibrations associated with ball bearings, *Int. J. Mech. Sci.* 45 (2003) 725–740.
- [35] S.P. Harsha, Nonlinear dynamic analysis of a high-speed rotor supported by rolling element bearings, *J. Sound Vib.* 290 (2006) 65–100.
- [36] G. Stachowiak, A.W. Batchelor, *Engineering Tribology*, Butterworth-Heinemann, 2011.
- [37] H.-V. Liew, T.C. Lim, Analysis of time-varying rolling element bearing characteristics, *J. Sound Vib.* 283 (2005) 1163–1179.

## Chapter 4

### Parametric Studies

This chapter has been published as

A. Moazen Ahmadi, C.Q. Howard, D. Petersen, The path of rolling elements in defective bearings: Observations, analysis and methods to estimate spall size, *Journal of Sound and Vibration* 336 (2016) 277-292. published online (DOI: 10.1016/j.jsv.2015.12.011).

This chapter is the second of four journal publications that has been published. This chapter presents an experimental investigation of the vibration signature generated by rolling elements entering and exiting a notch defect in the outer raceway of a bearing. The hypothesis of the path of rolling elements in the defect zone and the corresponding features on the vibration response to the entry and exit events, developed in Chapter 3, is tested experimentally by simultaneously measuring the vibration generated by a defective bearing on a bearing housing, and the shaft displacement. These key features can be used to estimate the size of a defect and are demonstrated in this paper for a range of shaft speeds and bearing loads. It is shown that existing defect size estimation methods include assumptions that describe the path of the rolling elements in the defect zone, leading to poor estimates of the size of a defect. A new method is proposed to estimate the size of a defect, and is shown to be accurate for estimating a range of notch defect geometries over a range of shaft speeds and applied loads.



# Statement of Authorship

Title of Paper	The path of rolling elements in defective bearings: Observations, analysis and methods to estimate spall size
Publication Status	<input checked="" type="checkbox"/> Published <input type="checkbox"/> Accepted for Publication <input type="checkbox"/> Submitted for Publication <input type="checkbox"/> Unpublished and Unsubmitted work written in manuscript style
Publication Details	Journal of Sound and Vibration

## Principal Author

Name of Principal Author (Candidate)	Alireza Moazen-ahmadi		
Contribution to the Paper	Performed analytical work, interpreted data, wrote manuscript and acted as corresponding author.		
Overall percentage (%)	80%		
Certification:	This paper reports on original research I conducted during the period of my Higher Degree by Research candidature and is not subject to any obligations or contractual agreements with a third party that would constrain its inclusion in this thesis. I am the primary author of this paper.		
Signature		Date	27/9/2016

## Co-Author Contributions

By signing the Statement of Authorship, each author certifies that:

- i. the candidate's stated contribution to the publication is accurate (as detailed above);
- ii. permission is granted for the candidate to include the publication in the thesis; and
- iii. the sum of all co-author contributions is equal to 100% less the candidate's stated contribution.

Name of Co-Author	Carl Howard		
Contribution to the Paper	Supervised the research and contributed in academic discussion and manuscript review.		
Signature	10%	Date	27/9/2016

Name of Co-Author	Dick Petersen		
Contribution to the Paper	Supervised the research and contributed in academic discussion and manuscript review.		
Signature	10%	Date	26/2/2016

Please cut and paste additional co-author panels here as required.





# The path of rolling elements in defective bearings: Observations, analysis and methods to estimate spall size



Alireza Moazen Ahmadi <sup>a,\*</sup>, Carl Q. Howard <sup>a</sup>, Dick Petersen <sup>b</sup>

<sup>a</sup> School of Mechanical Engineering, The University of Adelaide, Australia

<sup>b</sup> Trakside Intelligence Pty Ltd., 17–19 King William Street, Kent Town, South Australia 5067, Australia

## ARTICLE INFO

### Article history:

Received 14 September 2015

Received in revised form

2 December 2015

Accepted 4 December 2015

Handling Editor: L.G. Tham

Available online 24 December 2015

## ABSTRACT

This paper describes the experimental investigation of the vibration signature generated by rolling elements entering and exiting a notch defect in the outer raceway of a bearing. The vibration responses of the bearing housing and the displacement between the raceways were measured and analyzed. These key features can be used to estimate the size of the defect and is demonstrated in this paper for a range of shaft speeds and bearing loads. It is shown that existing defect size estimation methods include assumptions that describe the path of the rolling elements in the defect zone leading to poor estimates of defect size. A new defect size estimation method is proposed and is shown to be accurate for estimating a range of notch defect geometries over a range of shaft speeds and applied loads.

© 2015 Elsevier Ltd. All rights reserved.

## 1. Introduction

Rolling element bearings are widely used in rotating machinery and bearing failure is one of the common reasons for machinery breakdowns. Effective bearing condition monitoring systems should be able to detect and estimate the size of defects in bearings at early stages of a defect development to either enable remedial action to be taken, or schedule the replacement of the bearing at a convenient time. The typical vibration condition monitoring process involves the measuring vibration level on a bearing housing and trending the level over time. When the level exceeds a nominated threshold, the bearing is flagged for replacement. Alternatively, the philosophy used in this paper is to determine the geometric arc length of a bearing defect from the vibration signal, without using historical data.

Defects in bearings are commonly categorized into localized and distributed defects. Distributed defects, such as waviness, surface roughness or off-size rolling elements, are usually the result of manufacturing errors [1,2]. Localized defects are often initiated by insufficient lubrication film between the contact surfaces. This causes metal-to-metal contact between the rolling elements and the raceways. This in turn generates stress waves, leading over time to the formation of sub-surface cracks. The large forces between bearing parts cause sub-surface cracks to grow into surface defects, a phenomenon called pitting or spalling [3]. This paper considers vibrations and displacements between raceways generated in bearings with an outer raceway line-spall of various dimensions.

Previous studies on the vibration signature of defective bearings with raceway spalls show that the passage of a rolling element over the spall generates two main components [4–7]. The first component, which has low frequency content, results from the entry of a rolling element into the spall. The second component, which has higher frequency content,

\* Corresponding author. Tel.: +61 4254 9 4666.

E-mail address: [alireza.moazenahmadi@adelaide.edu.au](mailto:alireza.moazenahmadi@adelaide.edu.au) (A. Moazen Ahmadi).

results from the impact of a rolling element into the trailing edge of the spall [6,8–10]. Several defect size estimation methods have been previously suggested based on the time separation between these two components from the vibration signal [6,11]. These algorithms are based on assumptions of the path of a rolling element as it traverses a defect, and led to less accurate estimates of the defect size, as shown in Section 5.2.

In the work conducted here, a bearing test rig was used to measure the vibration of a “floating” bearing housing, and eddy current proximity probes were used to measure the relative displacement between the inner and outer raceways. Deep-groove ball bearings with electro-discharged-machined (EDM) notches with various dimensions were installed on the test rig and the vibration signals were measured for a range of speeds and loads. The design of the test rig made it possible to investigate the hypotheses proposed in previous studies and findings from previous simulation results. There are several studies on the effect of the high frequency vibration responses of defective bearings in the literature [12,13]. Epps and McCallion [14] have investigated the effect of speed and load on the amplitude of the low frequency entry and exit events. However, investigation of the effect of speed and load on the angular extent of the low frequency entry and exit transient events has not been done previously. Based on the findings in this study, a defect size estimation method is proposed. The proposed method is compared with previous defect size estimation methods for various defect sizes, speeds and loads. The proposed method is shown to be more accurate and reliable than previous methods in estimating the defect size in bearings.

The main contributions of this paper are (1) an improved method of estimating the size of a line spall defect based on vibration signals on the bearing housing, (2) comparing and highlighting the relationship between the vibration signature and the shaft displacement signal as a rolling element passes through a line spall defect, and (3) the effect of speed and load on the duration of the low frequency entry and exit transient vibration signals.

This paper is structured as follows: Section 2 reviews the previous experimental and modeling studies of the vibration response of defective bearings in regards to the path of rolling elements in the defect zone. Section 3 describes the test rig used in the experiments. Section 4 presents the experimental outcomes and the detailed analysis of the vibration and displacements between raceways to indirectly study and explain the probable path of the rolling element in the defect zone for various speeds and loads. Section 5 presents a reliable defect size estimation method resulting from the analysis presented in the previous sections. The method is tested on three bearings with various defect sizes, for a range of speeds and loads. The estimated bearing defect size using the method proposed in this paper is compared with previously proposed estimation methods. Section 6 summarizes the findings of this work.

## 2. Previous work

Fig. 1(a) illustrates a typical defective rolling element bearing with a localized line-spall defect on the outer raceway. A typical measured vibration response generated by the defect is shown in Fig. 1(b). Previous experimental studies show that the entry of a rolling element into a line-spall defect produces a vibration signal with low frequency content, while the exit of the rolling element excites a much broader range of frequencies, including the high frequency bearing resonances [4,6,14]. These resonances are excited by the impact of the rolling element on the exit point of a defect. Furthermore,

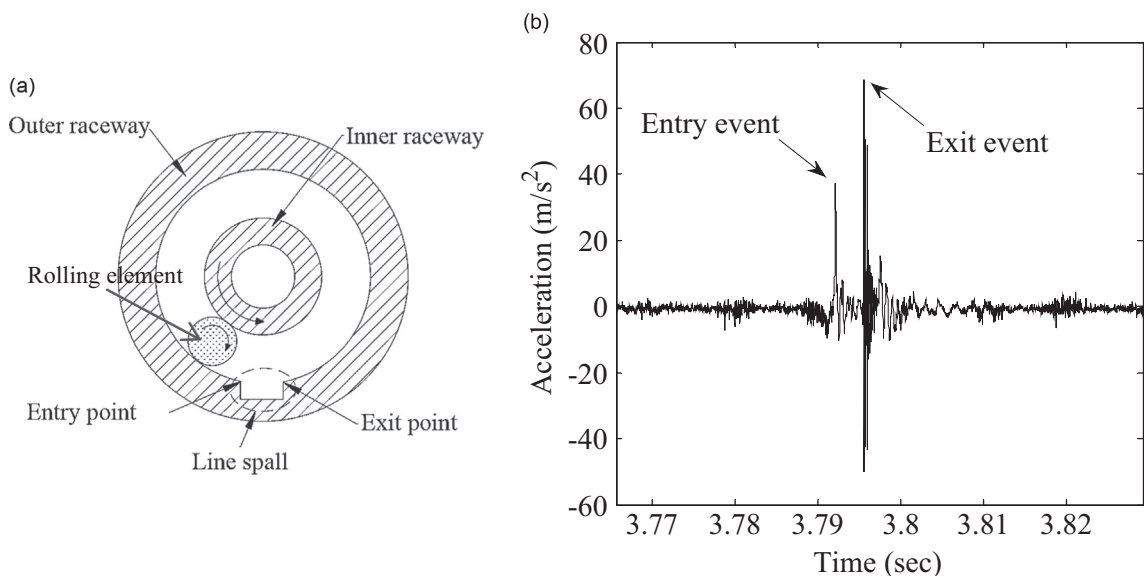


**Fig. 1.** (a) Diagram of a rolling element traveling into a line-spall defect located on the outer raceway. (b) A typical measured vibration response. Typical entry and exit points as suggested by previous studies [6,11], are shown as entry and exit points.

parametric excitations are caused by rapid changes in the bearing stiffness which occur when the rolling element re-stresses between the raceways [8]. The high frequency event observed in the experimental results [10,14] often appears to have been caused by multiple impacts rather than a single impact. Numerical simulation results of defective bearings presented by Singh et al. [9] and the analytical simulation results presented by Moazen Ahmadi et al. [4] indicate that multiple impacts occur when the rolling element re-stresses at the exit point.

Limited experimental studies have examined the relationship between the path of a rolling element and the characteristics appearing in the vibration signal. Sawalhi and Randall [6] measured the vibration of several defective ball bearings and observed the appearance of low and high frequency vibration signatures and related these events to the entry and exit points of the defect. Those authors suggested that when the low frequency vibration event is at its maximum local amplitude (see point entry event point in Fig. 1(b)), the center of a rolling element passes the entry point. Furthermore, these authors assumed that the high frequency exit event is associated with the time that the center of a rolling element is in the middle of the defect. These hypotheses were examined indirectly in an experiment which aimed to estimate the defect size in a bearing using a method based on these hypotheses. However, the estimation results of different bearings often showed large errors and standard deviations [6]. Their assumption that the exit-impact event occurs when the center of a rolling element is in the middle of the defect zone might be valid for very small defects. However the authors did not specify the size limit of the defect for which their suggested method is valid.

Numerous multi-body dynamic models have been developed to understand the relationship between the vibration characteristics and the path of the rolling elements in the defect zone for line-spall defects [15–21]. Although some of these models include the mass of the rolling element, they do not include both, the mass and the finite size of the rolling element. In these models, the path of a rolling element is modeled such that its center follows the geometry of the modeled defect. Harsha [22–25] considered the mass and centrifugal forces acting on a rolling element but not the finite size of the rolling element in a multi-body dynamic model. This model was initially developed to predict the vibration response of defective bearings with distributed defects [26]. The model was subsequently improved to include the mass of the rolling elements to predict the nonlinear dynamic behavior of a rolling element bearing, due to waviness and unbalanced rotor support [22–25]. The improved version of the model was further modified by Tadina [21] to predict the vibration response of bearings with localized spall defects on raceways. All of the aforementioned models were designed for defects with curvatures larger than the curvature of the rolling element, which maintains the contact between the raceways in the load zone. Therefore, none of the above mentioned multi-body dynamic models are suitable for modeling the path of a rolling element in the defect zone or determining the effect of the entry and exit points on the vibration signal of a defective bearing with a line-spall defect.

A more comprehensive multi-body dynamic model, developed by Moazen Ahmadi et al. [4,10], considers the mass and centrifugal forces acting on rolling elements and the finite size of the rolling elements. These authors show that in order to predict the path of a rolling element and the corresponding features in the vibration response correctly, it is crucial to include the finite size of rolling elements when modeling localized defects. Their analytical simulation revealed that the local maximum of the low frequency signature in the vibration response corresponds to the instant that a rolling element completely de-stresses between the two raceways upon entering the defect. Moreover, the process of de-stressing starts well before the entry point. Therefore, based on the analytical simulation of Moazen Ahmadi et al. [4,10], it can be concluded that the entry event, shown as the entry point in Fig. 1(b), does not correspond to the time that the center of the rolling element is at the entry point of the defect. This conclusion contradicts the observations and analyzes of an earlier study [6].

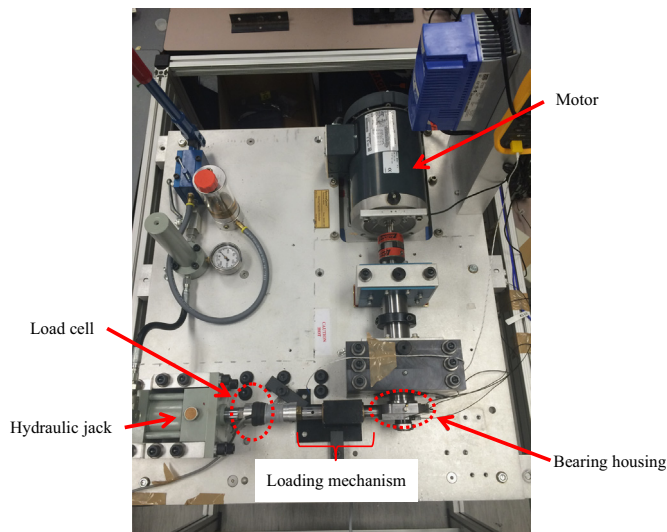


Fig. 2. Top view of the test rig used in this study.



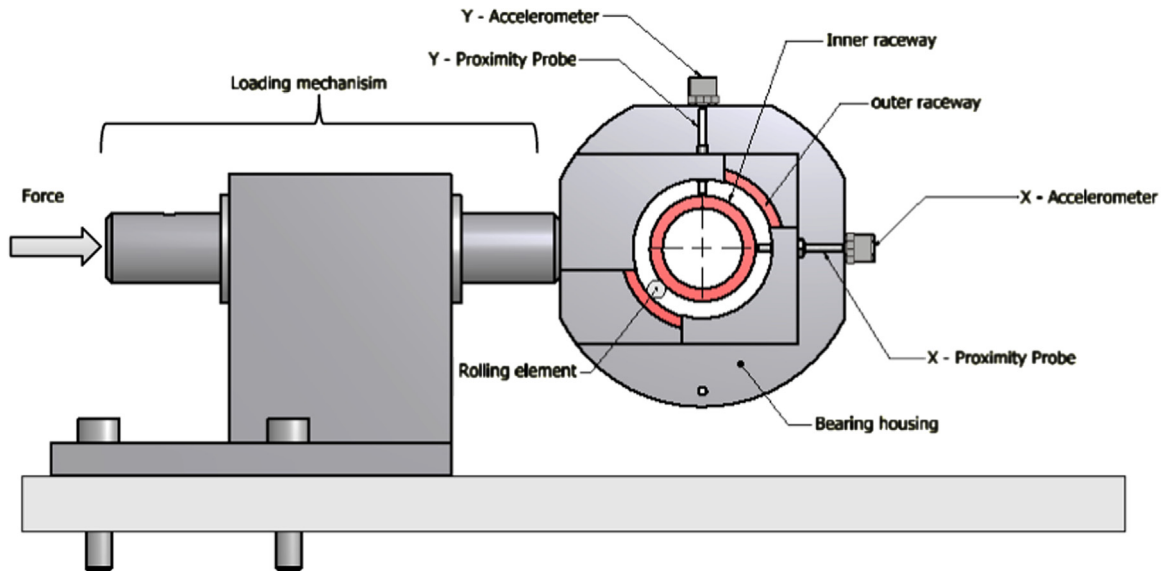


Fig. 3. Schematic view of the test bearing housing and the method of load application.

In this paper, the relationship between the characteristics of the vibration response and the relative displacement between the raceways to study and explain the probable interactions of a rolling element with raceways in the load zone of defective bearings is explored. Eddy current proximity probes were used to measure the relative displacement between the inner and outer raceways. Experimental measurements show the relationship between entry and exit events and vibration response in defective bearings. The effects of the rotational speed and the applied load on the magnitude of the entry and exit events on the acceleration signal are investigated. These findings are used to propose an accurate defect size estimation method.

This study investigated the assumptions used in previously described defect size estimation methods and identifies discrepancies of the assumed path of a rolling element into a defect and the corresponding features on the vibration response to the entry and exit events. These discrepancies contribute to inaccuracies found in the defect size estimation algorithms proposed previously. This paper demonstrates that impacts at the exit do not necessarily occur midway through a defect and previous assumptions made regarding the relationship between the vibration response and the entry and exit events are not accurate. The defect size estimation method proposed in this paper is based on numerical modeling [4] and supported by the experimental findings presented in this paper.

### 3. Test equipment

The test rig used in this study was manufactured by Spectra Quest, Inc., as shown in Fig. 2. The bearing housing supplied with the test-rig was replaced with a custom-made housing to enable testing of the hypotheses proposed in this study. The test rig includes an electric motor controlled by a variable frequency drive. The motor was fitted onto a shaft via a coupling and supported by two back-to-back tapered roller bearings. Test bearings were fitted into a custom-made bearing housing at the end shaft that has a radial load applied by a hydraulic jack.

Fig. 3 shows the custom-made bearing housing that was designed to accommodate accelerometers to measure the vibration of the housing, and eddy current proximity probes to measure the relative displacement between the inner and outer raceways of the test bearing.

Two stud mounted accelerometers (Bruel & Kjaer type 4393) were attached to the bearing housing to measure vibrations. Eddy current proximity probes (Micro-Epsilon type EPU05-C3) were mounted on the bearing housing to measure the relative displacement between the inner and outer raceways. A tachometer was used to measure the shaft speed and a load cell measured the force applied to the bearing housing. The data acquisition system consisted of a National Instruments (NI) CompactDAQ system with two NI 9234 modules. Data was acquired and post-processed using MATLAB software. All signals were acquired with a sampling frequency of 102.4 kHz.

The test bearings used in this study were ball bearings manufactured by Rexnord (ER16K), incorporating 9 balls, ball diameter of 7.94 mm, pitch diameter of 39.32 mm, and a contact angle of 0°. Line spall defects with various circumferential lengths, which were less than the angular separation of the rolling elements, and across the full axial extent of the outer raceway, were machined using electro-discharge machining (EDM) on the outer raceway of the bearings. Fig. 4 shows microscopic images of the three test bearings that were tested. Table 1 lists the geometry of the defects tested in this study that was measured using an Olympus model BX60M microscope fitted with a digital camera and software for obtaining

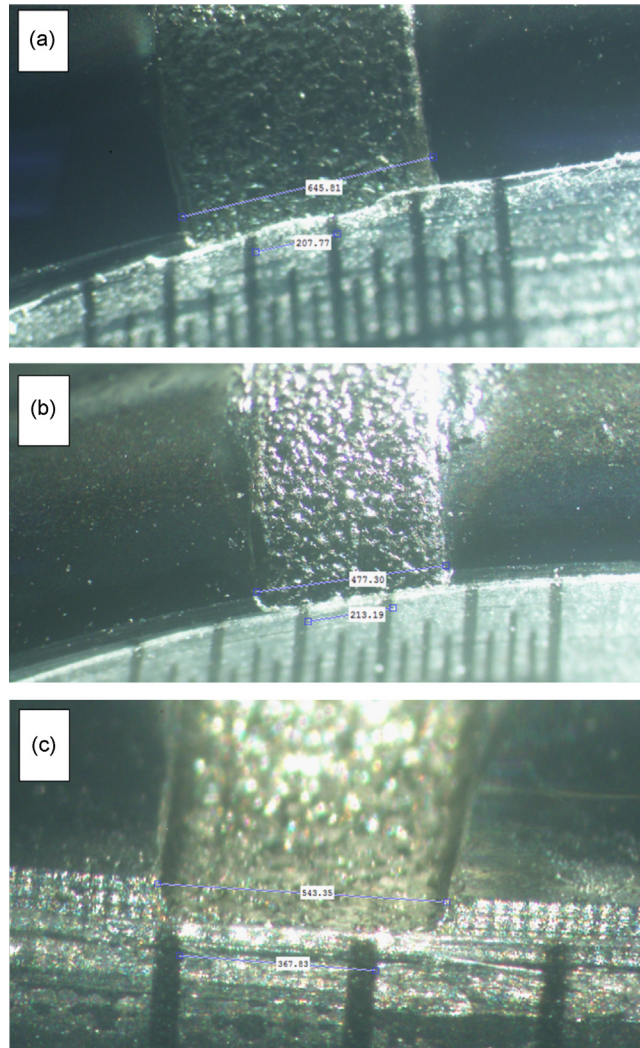


**Fig. 4.** Microscopic images of three defective bearings tested in this study. Pictures show the width of the defect and the scale in pixels measured on the digital photo: (a) 3.11 mm; (b) 2.24 mm and (c) 1.48 mm.

**Table 1**

Geometry of the defects in the three test bearings.

Measured defect circumferential length (mm)	Nominal angular extent (rad)	Radial depth ( $\mu\text{m}$ )
3.11	0.138	100
2.24	0.103	100
1.48	0.068	100

calibrated geometry measurements. The defective bearing was installed into the bearing house such that the center of the defect was aligned with the radial load.

#### 4. Measurements

This section presents an analysis of the measured signals using the test rig described in the previous section. Measurements were conducted at rotational speeds of 5 Hz, 10 Hz and 15 Hz and at radial loads of 2.5 kN and 5 kN. The aim of the analysis was to provide insights into the relationships of the vibration and displacement responses to indirectly study

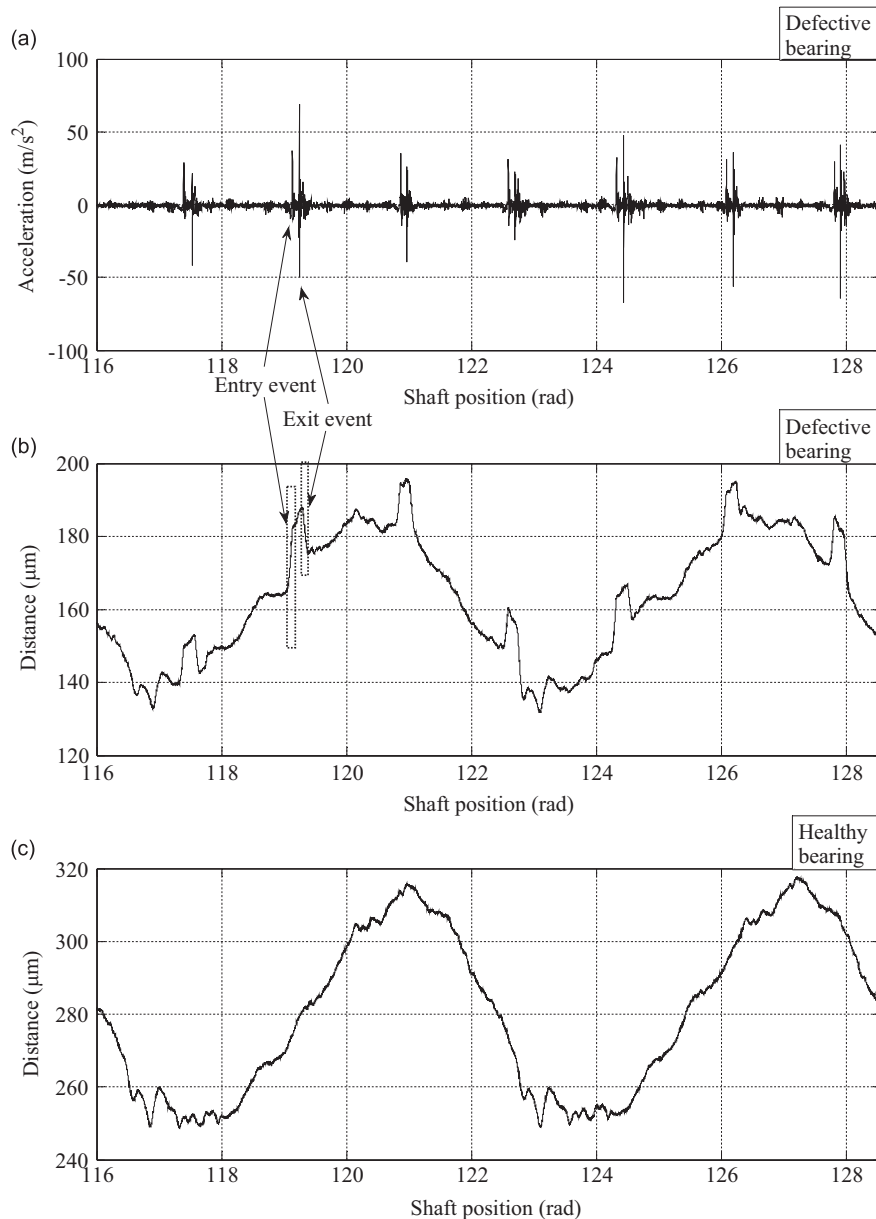


**Fig. 5.** Vibration signals generated by a defective bearing with a 0.103 rad angular extent defect at a rotational speed of 5 Hz with a 2.5 kN load showing (a) acceleration of the bearing housing, (b) relative displacement between the outer raceway to inner raceway for the defective bearing, and (c) relative displacement of the outer raceway to inner raceway for an undamaged bearing.

the probable path of the rolling element in the load zone and use the results as a basis for developing a method to estimate the size of a defect. This study distinguishes the low frequency entry and exit transient events and the low frequency response of the pedestal after the transient events. There are several studies on the effect of the high frequency vibration responses of defective bearings exists in the literature [12,13]. However, investigation of the effect of speed and load on the duration of the low frequency entry and exit transient events has not been done previously. The effects of load and speed on the characteristics of the entry and exit acceleration signal are also investigated in this section. These analyses are important to develop a reliable and accurate defect size estimation method.

#### 4.1. Analysis of entry and exit points

Fig. 5(a) and (b) presents two revolutions of the measured vibration and outer-to-inner race relative displacement measured on the bearing with a 0.103 rad angular extend defect at a rotational speed of 5 Hz and 2500 N load. The

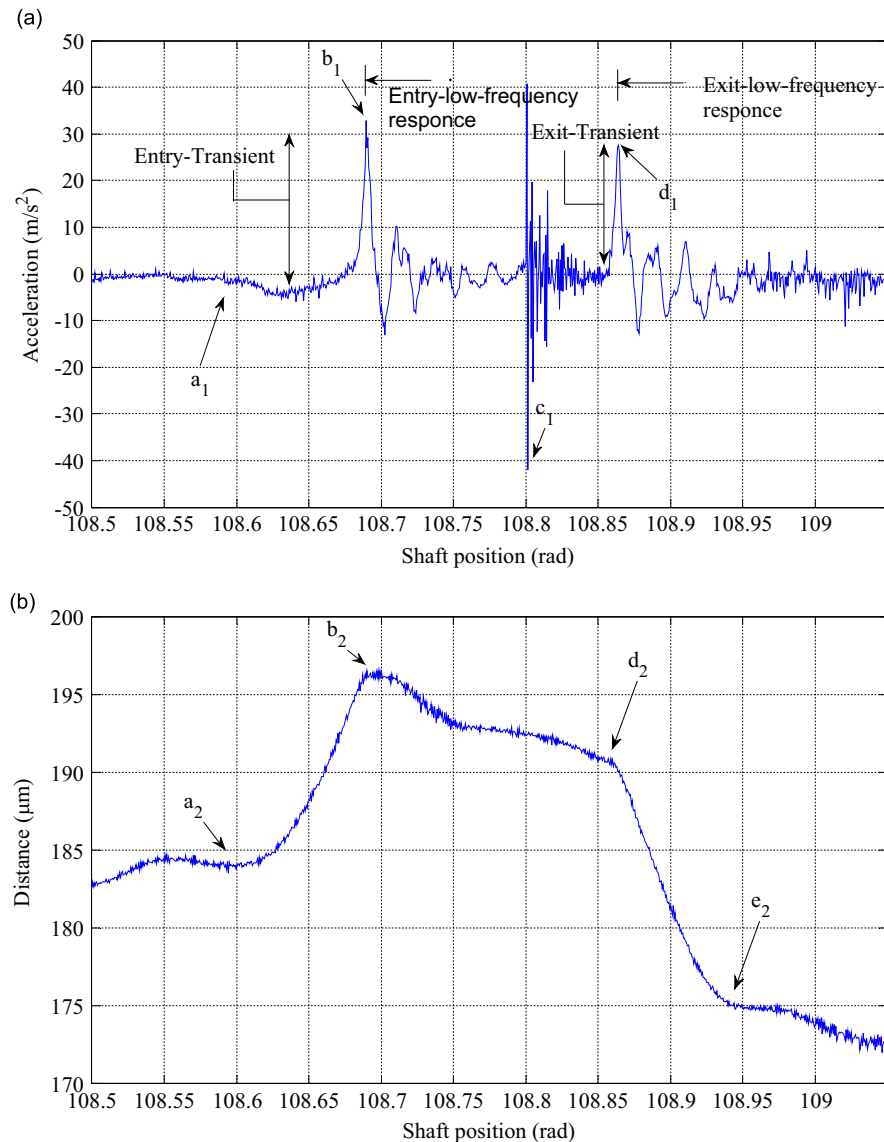


**Fig. 6.** (a) Zoomed measured signals at a 5 kN load and rotational speeds of 5 Hz: (a) vibration response and (b) relative displacement of the outer raceway to inner raceway signal.

measured relative displacement between the two raceways for a new (undamaged) bearing is presented in Fig. 5(c) for comparison.

Compared with the undamaged bearing, the relative displacement of the faulty bearing clearly shows sharp and large magnitude impulses each time an event is occurs on the acceleration signal, as shown in Fig. 5(a) and (b). These vibration impulses are caused when a ball bearing enters and exits the defect zone. Note that the oscillation of the displacement signal at the run speed frequency is the result of the small out-of-roundness measured on the inner raceway, which could be the result of quenching the inner raceway.

Fig. 6 shows a zoomed-in section of the acceleration signal and the corresponding relative displacement signal. This zoomed-in section corresponds to the period when a roller approaches and leaves the defect. The key characteristics observed in Fig. 6 are described below.

#### 4.1.1. Rolling element entry event

The entry of the rolling element into the defect generates predominantly low frequency content in the vibration response. Observations of the relationship between the relative displacement signal and the acceleration signal reveal that the entry event is composed of two components which are summarized in Table 2.

**Table 2**

Description of the entry event components and the related schematic view of the location of the rolling element.

Schematic view of the location of the rolling element in the defect zone	Description of the entry event
	<p><b>Entry-transient phase:</b> In this phase, the acceleration amplitude displayed a small decrease followed by a sharp increase due to the gradual de-stressing of the rolling element in the defect zone. This phase started at entry point <math>a_1</math> on the acceleration and <math>a_2</math> on the relative displacement signals. This phase ended when the rolling element loses contact with both raceways at point <math>b_1</math> on the acceleration and <math>b_2</math> on the relative displacement signals, as shown in Fig. 6. In this phase, the center of the rolling element traveled from the entry point of the defect to a point through the defect at which the contact forces acting on the rolling element become zero.</p> <p><b>Entry-low-frequency response:</b> Low frequency modes of the system were excited when the rolling element in the defect zone completely unloaded. At this stage, the number of the load carrying rolling elements decreases from 9 to 8 balls and consequently the bearing assembly stiffness decreases. Therefore, the low frequency modes of the system are excited as suggested by Petersen et al. [8].</p>

#### 4.1.2. Rolling element exit event

The rolling element exit event is generally associated with the excitation of high and low frequency modes of the bearing assembly. Observation of the relationship between the relative displacement signal and the acceleration signal suggest that the exit event exhibits a transient phase similar to the entry transient which has previously received little attention in the literature. The exit events consist of the components summarized in Table 3.

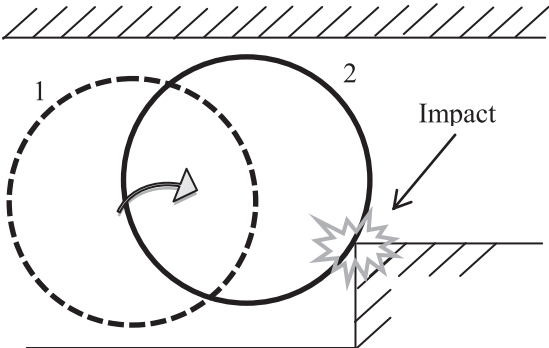
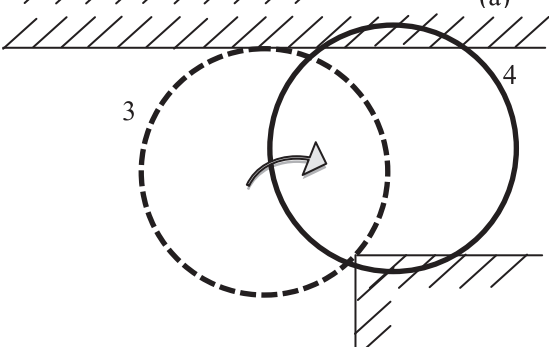
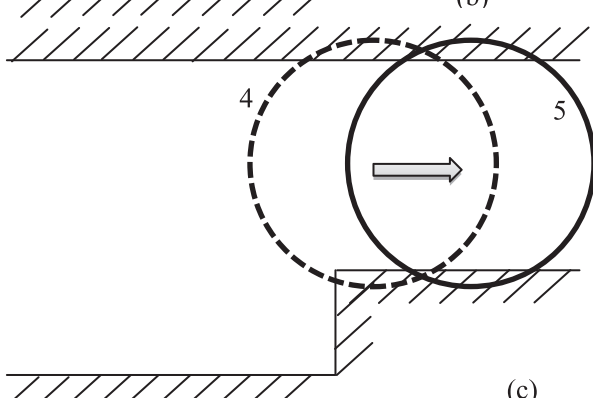
When a rolling element re-stresses between the raceways at the exit point of the defect, the rolling element may alternately strike both raceways as it re-stresses back to its normal load carrying capacity [27]. Multiple impacts at the exit of the defect have been observed in previous studies [9,10]. Maximum local amplitude of the high frequency response can be either the result of the summation of several different excited natural frequencies or a superposition of the excited high frequency modes and the low frequency component excited in turn by the exit-transient event. Depending on dynamics of a bearing assembly and its pedestal, the two events, namely the high-frequency impact response and the low-frequency response, could be separated or superimposed. Therefore, detection of the maximum local amplitude of the high frequency response cannot be used as a reliable marker to indicate the exit point of the defect.

#### 4.2. The effect of load

In this section, the effect of varying the applied load on a defective bearing is investigated in regards to the change in the amplitude and the angular extent of the low-frequency acceleration response. Fig. 7 shows a comparison of the acceleration response and the relative displacement signal of the bearing with 0.103rad angular extent defect at a rotational speed of 10Hz for two radial loads. The angular positions of two signals were adjusted to match the entry point of the defect at which the entry-transient event starts, shown as point A in Fig. 7. The constant offset of the relative displacement signal was also adjusted to coincide with the entry point.

**Table 3**

Discerption of the exit event components and the related schematic view of the location of the rolling element.

Schematic view of the location of rolling element in the defect zone	Description of the exit event component
 <p>(a)</p>	<p><b>High-frequency response:</b> The rolling element strikes the exit point of a defect and excites the high frequency resonance modes of the bearing assembly. The high-frequency event in the acceleration response observed at point <math>c_1</math> at angle 108.8 rad as shown in Fig. 6(a), is associated with this event. Note that there is no corresponding event in the relative displacement response at time 108.8 rad in Fig. 6(b). Further, the impact to the outer raceway is well before points <math>d_1</math> and <math>d_2</math>, where the re-stressing phase between the raceways starts.</p>
 <p>(b)</p>	<p><b>Exit-transient phase:</b> When the rolling element re-stresses between the raceways at the exit point of the defect, it re-stresses back to its normal load carrying capacity. The starting point of re-stressing is marked as points <math>d_1</math> and <math>d_2</math> in Fig. 6(a) and (b) respectively, and is associated with the beginning of when the magnitude of the relative displacement signal decreases sharply.</p>
 <p>(c)</p>	<p><b>Exit-low-frequency response:</b> the exit-transient phase ends at points <math>e_1</math> and <math>e_2</math>. Between points <math>d_1</math> to <math>e_1</math> and <math>d_2</math> to <math>e_2</math>, low frequency oscillations occur during this re-stressing phase. Depending on the damping characteristics of the bearing assembly, the exit low frequency response continues after point <math>e_2</math>.</p>

The increase in the relative displacement magnitude  $\Delta$  shown in Fig. 7(b) is the result of the increased relative contact deformation between the rolling elements and both raceways in the load zone due to the increase in the applied load. The maximum total elastic contact deformation on a rolling element can be calculated using the load–deflection relation [3]:

$$\delta_{max} = \left( \frac{Q_{max}}{k_n} \right)^{1/n} \tag{1}$$

where  $n$  is the load–deflection exponent ( $n = 1.5$  for point contact),  $Q_{max}$  is the maximum radial distributed load in the direction of the applied load and  $k_n$  is the total load–deflection factor of a bearing which depends on the curvature of rolling elements and raceways. Detailed descriptions and formulae for  $Q_{max}$  and  $k_n$  for ball bearings can be found in Harris [3]. For small defects which are smaller than angular separation of the rolling elements (with only one rolling element in the load zone), it can be assumed that the relative contact deformation between a rolling element and both raceways at the entry and exit points of the defect is equal to  $\delta_{max}$ . The average increase of the relative displacement magnitude,  $\Delta$ , is 14.5  $\mu\text{m}$  and the calculated increase of the elastic contact deformation due to the load increasing, using Eq. (1), is 12.1  $\mu\text{m}$ . The agreement

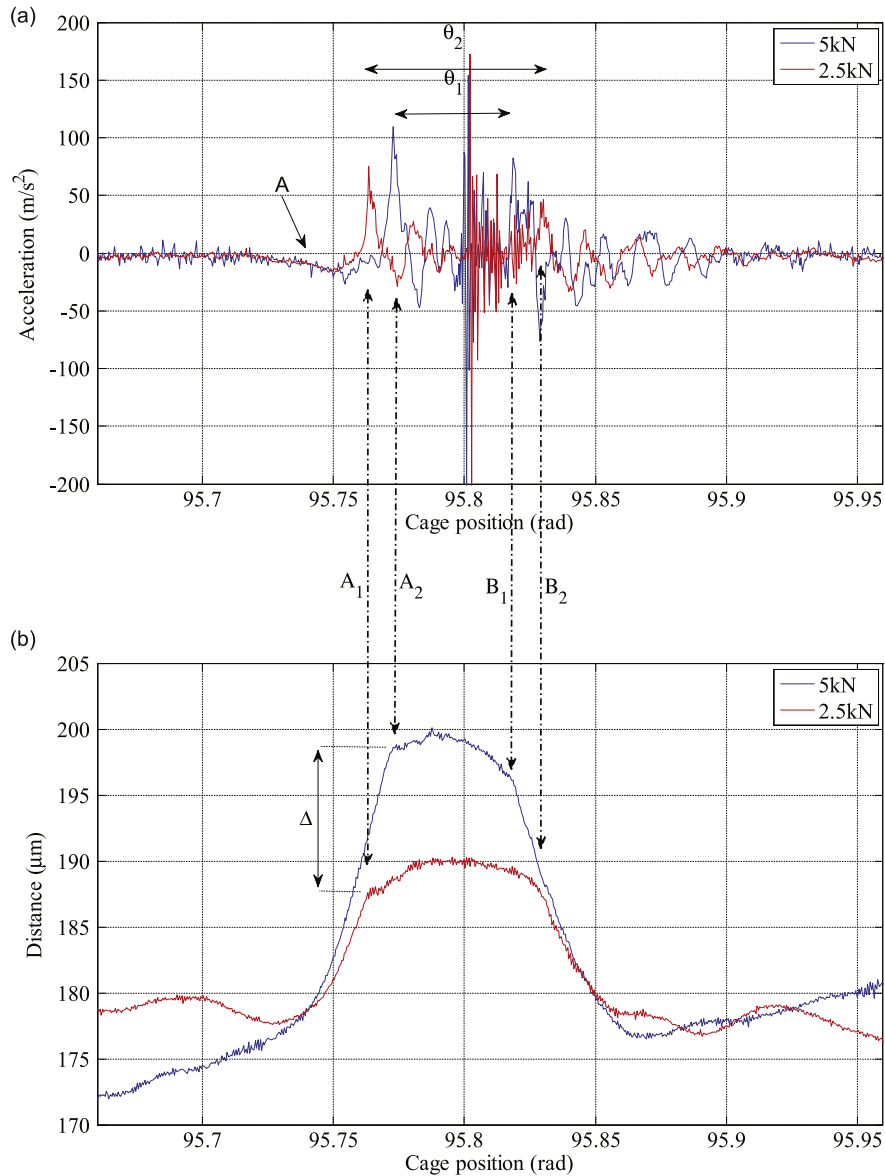


**Fig. 7.** Comparison of the measured signals for the defective bearing with 0.103 rad angular extent defect at a rotational speed of 10 Hz and two different loads, 5 kN and 2.5 kN: (a) acceleration signal and (b) the relative inner-to-outer raceway displacement signal.

between the measured and calculated relative displacement justifies the adjustments made to plot the signals shown in Fig. 7.

Relatively flat sections in the displacement signals,  $\theta_1$  and  $\theta_2$ , are the angular extents where a rolling element is unloaded and travels through the defect before the start of the exit-transient phase. Fig. 7(b) shows that the angular extent  $\theta$  decreases with increasing applied load, which may seem counter-intuitive as the defect size is identical for both tests. This is due to the additional angular extent that a rolling element requires to travel in order to lose contact between the raceways, as the elastic contact deformations are greater in bearings with a larger load. Points  $A_1$  and  $A_2$  show the end of the entry transient phases on Fig. 7(b). Similarly, the period of time for the rolling element to re-stress between the raceways and raceways is also greater in the bearing with higher load. Since the elastic contact deformations between the load-carrying rolling elements and raceways are also greater in the bearing with higher load, the rolling element in the defect zone engages the raceways at the exit points ( $B_1$  and  $B_2$ ) of the defect earlier, as shown in Fig. 7(b).

The presented analysis highlights the importance of including the effect of the applied load when attempting to develop a defect size estimation algorithm for rolling element bearings. The proposed defect size estimation method in this study



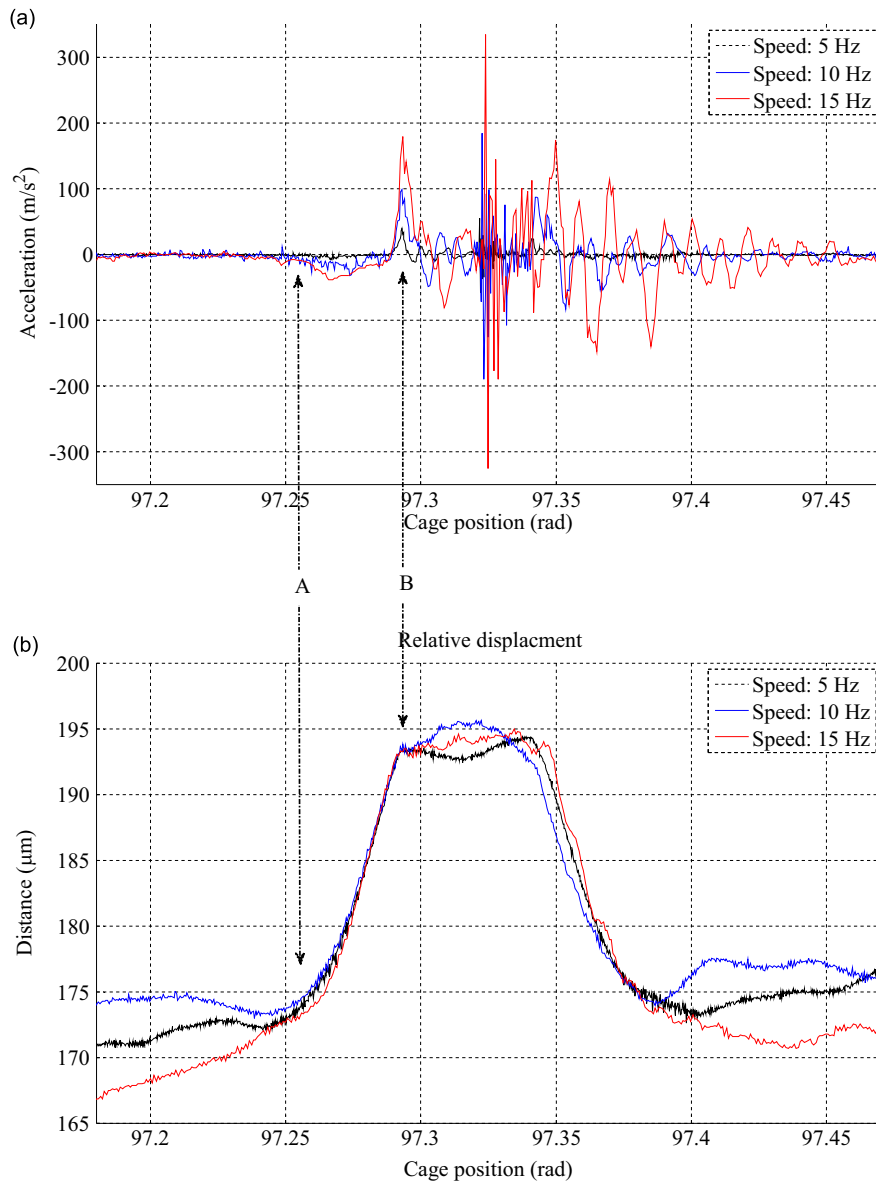


**Fig. 8.** Comparison of the measured signals for the bearing with a 0.103 rad angular extent defect at a 5 kN load and rotational speeds of 5 Hz, 10 Hz and 15 Hz: (a) acceleration signal, and (b) relative displacement signal between the inner and outer raceways.

includes the effect of the applied load on the duration of the entry and exit transient events to achieve accurate estimation of the defect size.

#### 4.3. The effect of speed

In this section, the effect of varying the rotational speed is investigated in regards to the change in the angular extent of the low-frequency entry transient response. Fig. 8 shows a comparison of the acceleration and the relative displacement signals of the bearing with a 0.103 rad angular extent defect under 5 kN load, at three rotational speeds. The angular positions of the signals were adjusted to match at the local maxima of the entry event. The relative displacement signals were also adjusted to coincide at the matched cage angular position as shown at point B in Fig. 8(a) and (b).

Fig. 8(b) shows that the magnitude of the relative displacement does not change significantly in the entry transient phase (A–B in Fig. 8) with increasing rotational speed. This is because the relative contact deformation between a rolling element and both raceways in the load zone depends only on the applied load at the considered speed [3], as is shown in Fig. 7(b). Therefore, the angular extent that the center of a rolling element travels from the entry point of the defect until it de-stresses completely is not dependent on the rotational speed. The increase in the acceleration response due to the



increasing rotational speed can be explained by the fact that the rolling element has to de-stress and re-stress faster in the transient phases at the entry and exit points of the defect when rotational speed increases.

Investigation of the effect of speed and load on the angular extents of the low frequency entry and exit transient events has not been done previously. The experimental results show strong dependency of the angular extent of the low frequency entry and exit transient events on the applied load. It is evident that changes in the speed have almost no effect on angular extents of the low frequency entry and exit transient events.

## 5. Proposed defect size estimation method

### 5.1. Formulation

In this section, a method is proposed to estimate the size of a defect in a bearing based on measured acceleration signals. The observations presented in the previous section revealed the following discrepancies in the assumptions used in defect size estimation algorithms in previous studies:

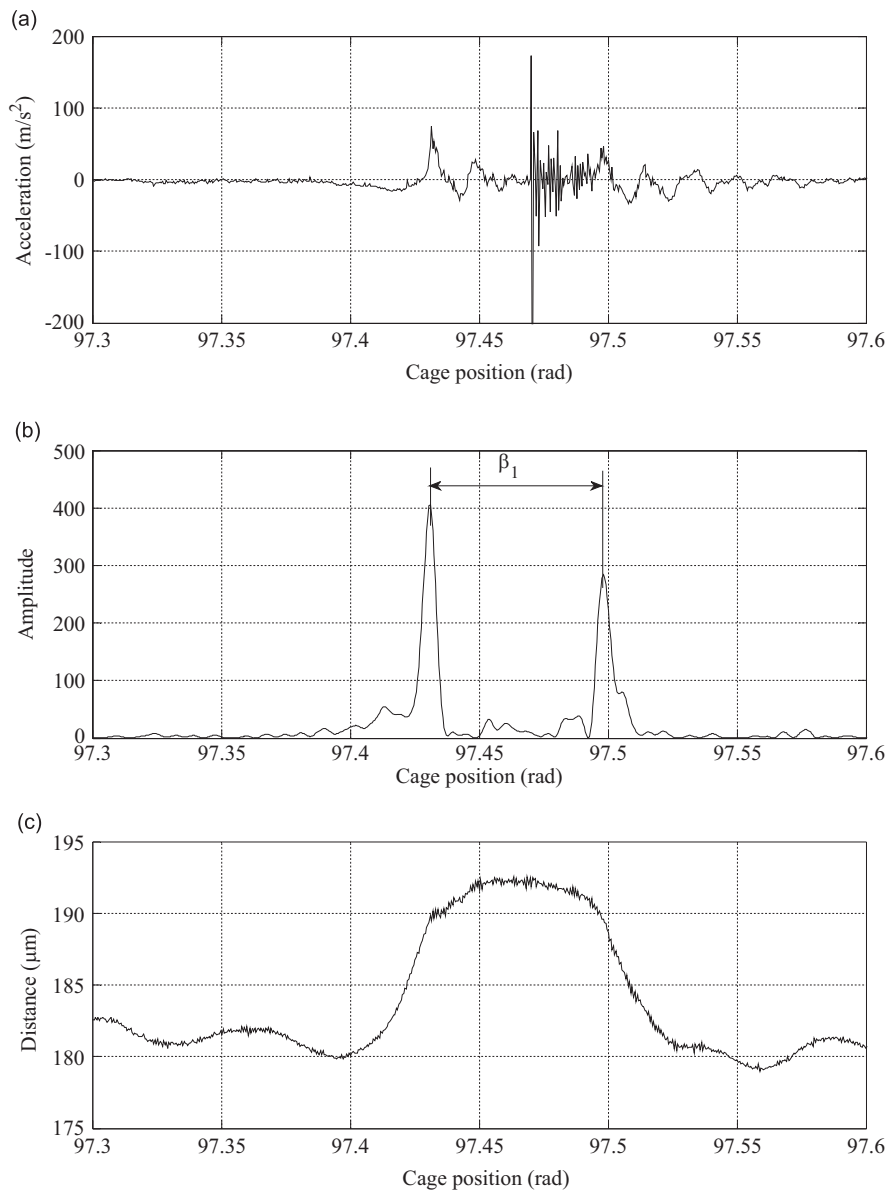


**Fig. 9.** Experimentally measured response of a bearing with a 0.103 rad extent defect at 5 kN load and a rotational speed of 10 Hz: (a) acceleration signal; (b) enhanced acceleration signal and (c) the relative displacement between the inner and outer raceways.

- It was generally accepted that the first peak of the low frequency oscillation on the vibration response corresponds to the time when a rolling element strikes the entry point of the defect. Thus, the peak of the low frequency oscillation was used in previous defect size estimation methods. However, this study shows that the corresponding point on the vibration response to the entry point of the defect is the rising point of the first low frequency event in the vibration response.

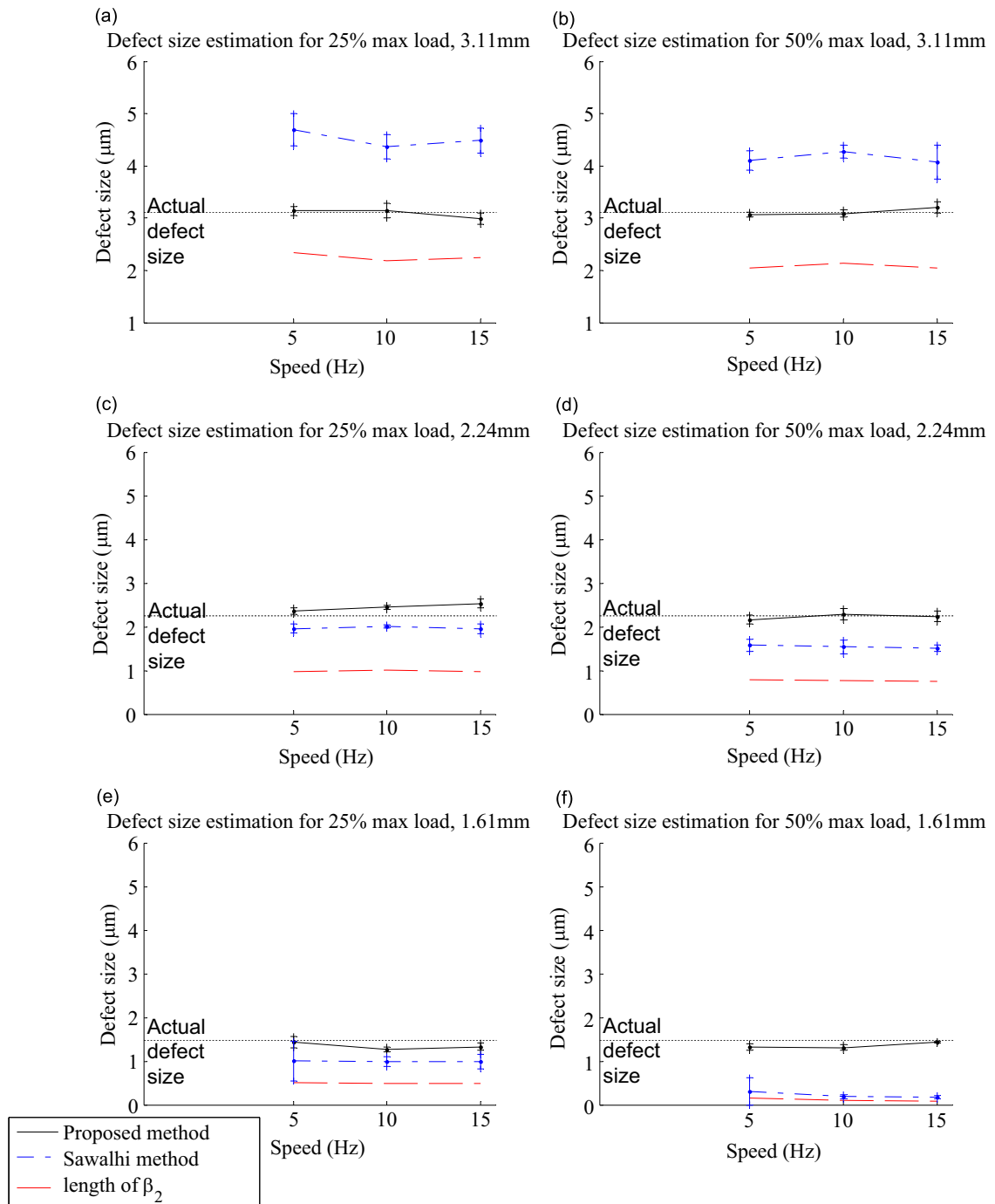


**Fig. 10.** Comparison between the estimated mean and standard deviation of outer race defects using the method suggested by Sawalhi and Randall [6], the method proposed in this paper, and the angular extent between the two maxima points  $\beta_1$  using the enhanced acceleration signal described in Section 5.1 for (a) actual defect size of 3.11 mm and load of 2.5 kN, (b) actual defect size of 3.11 mm and load of 5 kN, (c) actual defect size of 2.24 mm and load of 2.5 kN, (d) actual defect size of 2.24 mm and load of 5 kN, (e) actual defect size of 1.48 mm and load of 2.5 kN, and (f) actual defect size of 1.48 mm and load of 5 kN.

- It was assumed that the rolling element strikes the exit point when the center of a rolling element is mid-way through the defect. This assumption requires the rolling element to maintain contact with both raceways, where the center of the rolling element is in the middle of the defect. However, this study has revealed that the rolling element de-stresses long before it reaches the exit point. Although the previously held assumption might be valid for extremely small defects (smaller than the contact deformation patch), application of the assumption produces increasing errors in defect size estimation as the defect grows.
- It was assumed that the highest peak amongst the high frequency responses in the multiple impact region corresponds to the time that the rolling element is at the exit point of the defect. However, our results suggest that this assumption is not necessarily valid, as the highest high frequency event may happen at the time when the rolling element is not at the transient phase.

The above findings explain the origin of inaccuracies of previous algorithms and are instrumental for the development of an improved algorithm to accurately estimate the size of a defect. Rather than the high-frequency event used by others in previous works, the low-frequency event at the exit to estimate defect size is used in the proposed defect size estimation method in this study.

Fig. 9(a) and (c) shows the acceleration response and the relative inner-to-outer raceway displacement of the defective bearing with a 0.103 rad angular extent, respectively. To enhance the entry and exit events, the acceleration signal was pre-whitened and then low-pass filtered at 5 kHz to remove high frequency resonances excited by the impact event. Finally, the squared enveloped signal was calculated using the Hilbert transform, as shown in Fig. 9(b).

Locating the exact starting point of the entry transient phase on the acceleration signal, and locating the exact ending point of the exit transient phase, is often not possible due to the presence of background noise or the vibrations of other components. Therefore, it may not be practical to use these points to estimate the defect size in situation where there is significant signal noise. Thus, we propose the following algorithm to estimate the defect size accurately by detection of the local maxima in the acceleration signal.

The angular extent between the two maxima points of the first and second rising events on the enhanced acceleration signal was measured as shown as  $\beta_1$  in Fig. 9(c). This distance corresponds to the angular travel of the center of the rolling element between the time that it completely de-stresses at the entry of the defect and the time when it starts the re-stressing phase.

The de-stressing and re-stressing angular travel of the center of a rolling element  $\beta_2$ , depends on the maximum total elastic contact deformation that a rolling element requires to lose in the transient phase at the entry and exit. The angular travel  $\beta_2$ , can either be simulated using the mathematical model presented in Moazen Ahmadi et al. [4,10] or estimated by geometrically relating the relative elastic contact deformation to the geometry of the bearing using the following equation:

$$\beta_2 = \sqrt{\frac{2r_b\delta_{\max} - \delta_{\max}^2}{(r_b + R)^2}} \quad (2)$$

where  $R$  is the radius of the outer raceway,  $r_b$  is the radius of the rolling element and  $\delta_{\max}$  can be calculated using Eq. (1). Therefore, the total length of a defect can be estimated by

$$L = \sin(2\beta_2 + \beta_1) \times R \quad (3)$$

## 5.2. Validation

The method described in Section 5.1 was used to measure the angle  $\beta_2$ , and then estimate the defect size in three bearings with nominal angular extents of 0.138, 0.103 and 0.068 (measured circumferential lengths of 3.11 mm, 2.24 mm and 1.48 mm defects respectively), as described in Section 3. The enhanced vibration response, described in Section 5.1, was used to measure the angle  $\beta_1$ . The angle  $\beta_2$  is calculated using Eq. (2). The size of the defect is calculated using Eq. (3). Mean and standard deviations for a number of events on the vibration response of the three defective bearings for various speeds and loads were estimated as shown in Fig. 10. The same events were used to estimate the size of defects using the method suggested by Sawalhi and Randall [6] for comparison. In addition, the average distance (rad) between the low and high frequency local maximum levels measured on the vibration response ( $\beta_2$ ), for each case, is shown for reference in Fig. 10.

The defect size estimates based on the method presented in this paper are more accurate (closer to the actual defect size as shown in Fig. 10) and have smaller standard deviations when compared with the previous methods. The importance of including the applied load in the estimation algorithms is evident by comparing the estimations of the two methods and the length of  $\beta_2$  in the higher applied load cases. Since the angular extent between the end of the entry-transient phase and the start of the exit-transient phase depends on the applied load for a defective bearing, estimation algorithms that do not consider the applied load exhibit greater errors when applied load increases.

Comparison of estimation results for the three defective bearings demonstrates that the effect of omitting the angular extents of the entry and exit transients is greatest for larger defects. In larger defects these angular extents are less significant than the angular extent between the end of the entry-transient phase and the start of the exit-transient phase. For extremely small defects, of an order smaller than the patch of the relative deformation between a rolling element and the

raceways, where the rolling element does not completely de-stress before hitting the exit point, the method suggested by Sawalhi and Randall [6] could be used. The method of using only the measured time between the low and high frequency local maximums on the vibration response for the estimation and ignoring the entry and exit transient times could be sufficient for larger defects. The method proposed in this study is found to be more accurate for both small and large defects.

## 6. Conclusions

This paper describes the experimental measurements of acceleration and relative displacement between the raceways of rolling element bearings with machined defects of various sizes that are tested at various speeds and loads. The effects of entry and exit events on the vibration response were explained. The probable path of a rolling element in the defect zone was studied indirectly by experimental investigation of the vibration and displacement responses. The experimental results showed that:

- Exit impacts do not necessarily occur at the moment that the rolling element in the defect zone is midway through a defect. The exit impact events shown by acceleration impulses can occur before the center of a rolling element reaches the end of a defect and are not apparent in the relative displacement measurements.
- The relative displacement measurements indicate that the entry transient event to the defect starts before the local maxima of the low frequency response.
- The angular extent for a rolling element to de-stress or re-stress between the raceways increases with increasing applied load. These angular extents are not speed dependent. Therefore the relative angular extents between the low frequency entry and exit transient events decrease with increasing load.
- The assumption used in previous defect size estimation methods is only valid for very small defects, of an order smaller than the patch of the relative deformation between a rolling element and the raceways. Ignoring the effect of the applied load, which is done in other defect sizes estimation methods, causes errors in the estimate of larger defect sizes.

Based on the experimental results, the characteristics of the vibration response in defective bearings are categorized into different events which are related to different stages of the probable travel path of a rolling element in the defect zone. A method for defect size estimation based on an explanation of the path of a rolling element was presented. It was shown that the proposed method estimates the bearing's defect size more accurately compared to previously proposed methods.

## References

- [1] Y.T. Su, M.H. Lin, M.S. Lee, The effects of surface irregularities on roller bearing vibrations, *Journal of Sound and Vibration* 165 (1993) 455–466.
- [2] C. Sunnersjö, Rolling bearing vibrations—the effects of geometrical imperfections and wear, *Journal of Sound and Vibration* 98 (1985) 455–474.
- [3] T.A. Harris, *Rolling Bearing Analysis*, Wiley, USA, 2001.
- [4] A. Moazen Ahmadi, D. Petersen, C.Q. Howard, A nonlinear dynamic vibration model of defective bearings – the importance of modelling the finite size of rolling elements, *Mechanical Systems and Signal Processing* (2015) 52–53.
- [5] D. Petersen, C. Howard, Z. Prime, Varying stiffness and load distributions in defective ball bearings: analytical formulation and application to defect size estimation, *Journal of Sound and Vibration* 337 (2015) 284–300.
- [6] N. Sawalhi, R.B. Randall, Vibration response of spalled rolling element bearings: observations, simulations and signal processing techniques to track the spall size, *Mechanical Systems and Signal Processing* 25 (2011) 846–870.
- [7] S. Singh, U.G. Köpke, C.Q. Howard, D. Petersen, Analyses of contact forces and vibration response for a defective rolling element bearing using an explicit dynamics finite element model, *Journal of Sound and Vibration* 333 (2014) 5356–5377.
- [8] D. Petersen, C.Q. Howard, N. Sawalhi, A. Moazen Ahmadi, S. Singh, Analysis of bearing stiffness variations, contact forces and vibrations in radially loaded double row rolling element bearings with raceway defects, *Mechanical Systems and Signal Processing* 50–51 (2015) 139–160.
- [9] S. Singh, U. Köpke, C.Q. Howard, D. Petersen, Analyses of contact forces and vibration response for a defective rolling element bearing using an explicit dynamics finite element model, *Journal of Vibration and Control* 333 (2014) 5356–5377.
- [10] A. Moazen Ahmadi, D. Petersen, C.Q. Howard, A nonlinear dynamic model of the vibration response of defective rolling element bearings, *Proceedings of the Australian Acoustics*, Victor Harbor, 2013.
- [11] S. Zhao, L. Liang, G. Xu, J. Wang, W. Zhang, Quantitative diagnosis of a spall-like fault of a rolling element bearing by empirical mode decomposition and the approximate entropy method, *Mechanical Systems and Signal Processing* 40 (2013) 154–177.
- [12] Z. Bin, C. Sconyers, C. Byington, R. Patrick, M. Orchard, G. Vachtsevanos, A probabilistic fault detection approach: application to bearing fault detection, *IEEE Transactions on Industrial Electronics* 58 (2011) 2011–2018.
- [13] N. Lybeck, S. Marble, B. Morton, Validating prognostic algorithms: a case study using comprehensive bearing fault data, *Proceedings of the IEEE Aerospace Conference*, 2007.
- [14] I. Epps, H. McCallion, An investigation into the characteristics of vibration excited by discrete faults in rolling element bearings, *Proceedings of the Annual Conference of the Vibration Association of New Zealand*, Christchurch, 1994.
- [15] J. Sopenan, A. Mikkola, Dynamic model of a deep-groove ball bearing including localized and distributed defects. Part 1: theory, *Proceedings of the Institution of Mechanical Engineers, Part K: Journal of Multi-body Dynamics* 217 (2003) 201–211.
- [16] J. Sopenan, A. Mikkola, Dynamic model of a deep-groove ball bearing including localized and distributed defects. Part 2: implementation and results, *Proceedings of the Institution of Mechanical Engineers, Part K: Journal of Multi-body Dynamics* 217 (2003) 213–223.
- [17] N. Sawalhi, R. Randall, Simulating gear and bearing interactions in the presence of faults: Part I. The combined gear bearing dynamic model and the simulation of localised bearing faults, *Mechanical Systems and Signal Processing* 22 (2008) 1924–1951.
- [18] N. Sawalhi, R. Randall, Simulating gear and bearing interactions in the presence of faults: Part II: simulation of the vibrations produced by extended bearing faults, *Mechanical Systems and Signal Processing* 22 (2008) 1952–1966.
- [19] M. Cao, J. Xiao, A comprehensive dynamic model of double-row spherical roller bearing—model development and case studies on surface defects, preloads, and radial clearance, *Mechanical Systems and Signal Processing* 22 (2008) 467–489.

- [20] S. Sassi, B. Badri, M. Thomas, A numerical model to predict damaged bearing vibrations, *Journal of Vibration and Control* 13 (2007) 1603–1628.
- [21] M. Tadina, M. Boltežar, Improved model of a ball bearing for the simulation of vibration signals due to faults during run-up, *Journal of Sound and Vibration* 330 (2011) 4287–4301.
- [22] S.P. Harsha, Nonlinear dynamic analysis of an unbalanced rotor supported by roller bearing, *Chaos, Solutions Fractals* 26 (2005) 47–66.
- [23] S.P. Harsha, Nonlinear dynamic analysis of a high-speed rotor supported by rolling element bearings, *Journal of Sound and Vibration* 290 (2006) 65–100.
- [24] S.P. Harsha, K. Sandeep, R. Prakash, Non-linear dynamic behaviors of rolling element bearings due to surface waviness, *Journal of Sound and Vibration* 272 (2004) 557–580.
- [25] S.P. Harsha, P.K. Kankar, Stability analysis of a rotor bearing system due to surface waviness and number of balls, *International Journal of Mechanical Sciences* 46 (2004) 1057–1081.
- [26] S.P. Harsha, K. Sandeep, R. Prakash, The effect of speed of balanced rotor on nonlinear vibrations associated with ball bearings, *International Journal of Mechanical Sciences* 45 (2003) 725–740.
- [27] N. Tandon, A. Choudhury, A theoretical model to predict the vibration response of rolling bearings in a rotor bearing system to distributed defects under radial load, *Journal of Tribology* 122 (2000) 609–615.

## Chapter 5

### Stiffness Analyses in Rolling Element Bearings

This chapter has been submitted as

A. Moazen Ahmadi, C.Q. Howard, The importance of bearing stiffness and load when estimating the size of a defect in a rolling element bearing, *Journal of Sound and Vibration* (Submitted to *Journal of Sound and Vibration* on 17/03/2016).

This chapter is the third of four journal papers (submitted). In this chapter the hypothesis of using the low frequency variation in stiffness to distinguish defects that vary in size by exactly one angular ball spacing is investigated, based on analytical and experimental results. This hypothesis was initially suggested by Petersen et al. [1] based on numerical simulations, in which the author of this thesis is a co-author. However, this hypothesis was not validated with experimental test results and is the subject of the third journal paper and this chapter of the thesis. Moreover, the hypothesis suggested by Petersen et al. [1] is further improved to include the important effects of the applied load on the static stiffness in defective bearings, which were ignored previously. A time-frequency technique to detect the variation in the frequency response of the vibration signal due to stiffness variations of the bearing assembly is suggested, and the importance of including the effect of load in developing an accurate defect size estimation method is demonstrated in this chapter. Recommendations for condition monitoring are given, based on the analyses presented in this chapter. The new method that is proposed does not rely on prior historical vibration data for assessing the damage in a bearing, unlike previously suggested methods.

The methods and results presented in this chapter contribute to the wider experimental investigation of the effects of loadings on the varying static stiffnesses in defective bearings and their effects on measured vibration signatures. The force-displacement relationships for defective bearings under various static radial loadings at various cage angular positions are analytically estimated, experimentally measured and then they are compared. The study shows the importance of the effect of the applied load on the static stiffness variations in defective rolling element bearings. These findings are presented in the third of the four journal publications. The experimental measurements of the effect of the defect size and the applied load on the varying stiffnesses of bearing assemblies has not been shown previously and provides valuable knowledge for developing methods to distinguish between bearings with defects that vary in size by exactly one angular ball spacing.

- [1] D. Petersen, C.Q. Howard, N. Sawalhi, A. Moazen Ahmadi, S. Singh, Analysis of bearing stiffness variations, contact forces and vibrations in radially loaded double row rolling element bearings with raceway defects, *Mechanical Systems and Signal Processing* 50-51 (2015) 139-160. published online (DOI: 10.1016/j.ymssp.2014.04.014)

# Statement of Authorship

Title of Paper	The importance of bearing stiffness and load when estimating the size of a defect in a rolling element bearing
Publication Status	<input type="checkbox"/> Published <input type="checkbox"/> Accepted for Publication <input checked="" type="checkbox"/> Submitted for Publication <input type="checkbox"/> Unpublished and Unsubmitted work written in manuscript style
Publication Details	Journal of Sound and Vibration

## Principal Author

Name of Principal Author (Candidate)	Alireza Moazen-ahmadi		
Contribution to the Paper	Performed analytical work, interpreted data, wrote manuscript and acted as corresponding author.		
Overall percentage (%)	90%		
Certification:	This paper reports on original research I conducted during the period of my Higher Degree by Research candidature and is not subject to any obligations or contractual agreements with a third party that would constrain its inclusion in this thesis. I am the primary author of this paper.		
Signature		Date	27/9/2016

## Co-Author Contributions

By signing the Statement of Authorship, each author certifies that:

- i. the candidate's stated contribution to the publication is accurate (as detailed above);
- ii. permission is granted for the candidate to include the publication in the thesis; and
- iii. the sum of all co-author contributions is equal to 100% less the candidate's stated contribution.

Name of Co-Author	Carl Howard		
Contribution to the Paper	Supervised the research and contributed in academic discussion and manuscript review.		
Signature	10%	Date	27/9/2016

Name of Co-Author			
Contribution to the Paper			
Signature		Date	

Please cut and paste additional co-author panels here as required.





# The importance of bearing stiffness and load when estimating the size of a defect in a rolling element bearing

Alireza Moazen-ahmadi<sup>1</sup>; Carl Howard;

School of Mechanical Engineering, The University of Adelaide, Australia

---

## ABSTRACT

The change in the static stiffness of a bearing is an important discriminator when determining the size of a defect in a rolling element bearing. In this paper, the force-displacement relationships for defective bearings under various static radial loadings at various cage angular positions are analytically estimated and experimentally measured and analyzed. The study shows the importance of the effect of the applied load on the static stiffness variations in defective rolling element bearings. The experimental measurements of the effect of the defect size on the varying stiffnesses of bearing assembly, which has not been shown previously, provides valuable knowledge for developing methods to distinguish between defective bearings with defects that are smaller or larger than one angular ball spacing. The methods and results presented here contribute to the wider experimental investigation of the effects of loadings on the varying static stiffnesses in defective bearings and their effects on measured vibration signatures.

*Keywords:* rolling element bearing, varying stiffness, defective bearing, defect size estimation, bearing spall

---

<sup>1</sup> Tel.: +61 4254 9 4666  
E-mail: [alireza.moazenahmadi@adelaide.edu.au](mailto:alireza.moazenahmadi@adelaide.edu.au)

---

## 1. Introduction

Rolling element bearings are widely used in rotating machinery and bearing failure is one of the most common reasons for machinery breakdowns. Defects in bearings are commonly categorized into localized and distributed defects. Distributed defects, such as waviness, surface roughness or off-size rolling elements, are usually the result of manufacturing errors [1, 2]. Localized defects are often initiated by insufficient lubrication film between the contact surfaces. This causes metal-to-metal contact between the rolling elements and the raceways. This, in turn, generates stress waves, leading over time to the formation of sub-surface cracks. The large forces between bearing parts cause sub-surface cracks to grow into surface defects, a phenomenon called pitting or spalling [3]. This paper considers square shape defects of various dimensions on the outer-raceway that influences the static force-displacement relationships of the bearing assembly and the resulting vibration signature. In this paper, defects smaller than the angular spacing of rolling elements are referred to as line-spall and larger defects, with multiple rolling elements in the defect zone, are referred to as extended defects.

Effective bearing condition monitoring systems should be able to detect and assess the severity or estimate the size of defects in bearings at the early stages of defect development, and predict the expected remaining life of the bearing, either to enable remedial action to be taken, or to schedule the replacement of the bearing at a convenient time. The typical vibration condition monitoring process involves measuring the vibration level of a bearing housing and trending the level over time. When the level exceeds a nominated threshold, the bearing is flagged for replacement. Alternatively, the geometric arc length of a bearing defect from the vibration signal can be determined for replacement decision making, without using historical data, and this latter method is the focus of the work in this paper.

Previous studies on the vibration signatures of defective bearings with square shape defects on the raceway show that the passage of a rolling element over the defect generates

two main components [4-7]. The first component, which has low frequency content, results from the entry of a rolling element into the spall. Petersen and et al. [5, 8] have shown that the low frequency response is linked with the dynamic properties of the bearing assembly. The second component results from the impact of a rolling element into the trailing edge of the spall which excites a much broader range of frequencies, including high frequency bearing resonances [4, 6-10]. Figure 1(a) illustrates a typical defective rolling element bearing with a localized line-spall defect on the outer raceway. A typical measured vibration response generated by the defect is shown in Figure 1(b). Resonances of the bearing assembly are excited by the impact of the rolling element on the exit point of a defect and parametric excitations caused by rapid changes in the bearing stiffness when a rolling element re-stresses between the raceways [8].

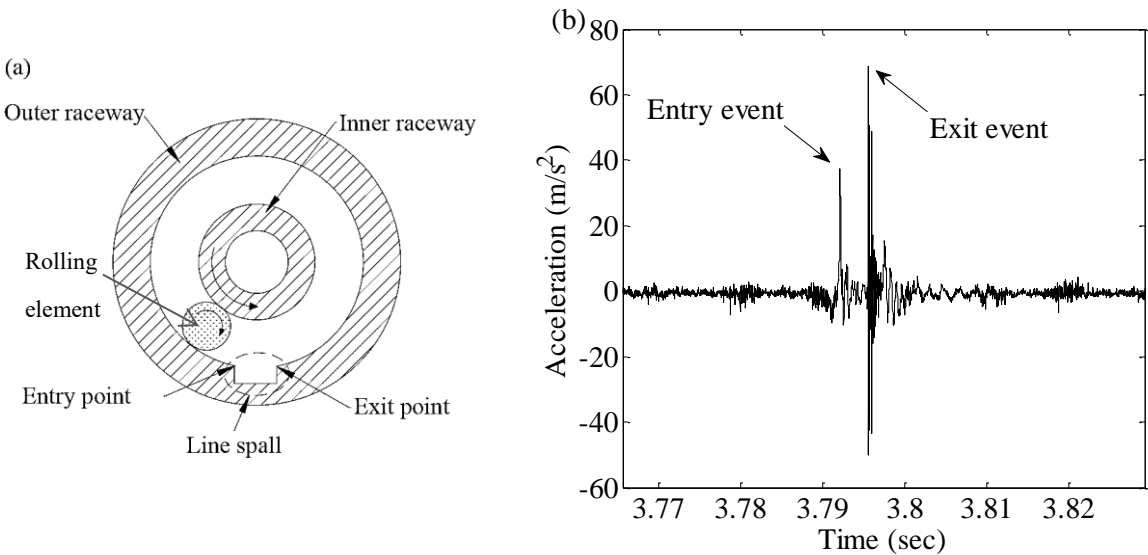


Figure 1: (a) Diagram of a rolling element travelling into a line-spall defect located on the outer raceway. (b) A typical measured vibration response of a bearing with line-spall defect located on the outer raceway.

Several defect size estimation methods have been suggested previously for bearings with line spall-defects, based on detecting the time separation between entry and exit events from the vibration signal [6, 11]. These defect size estimation methods underestimate the size of a defect that is larger than, at least, one ball angular spacing. The possibility of using stiffness variations in defective bearings as a measure to distinguish between extended defects and

line-spall defects has been suggested by Petersen et al. [5, 8]. They presented an analytical formulation of the varying static stiffness and load distribution of a ball bearing assembly as a function of cage angular position. Petersen et al. [5, 8] analyzed the static stiffness variation in defective bearings with square shaped outer raceway defects of varying circumferential extent and similar depths without experimental validation, which is shown in this paper. In the work conducted here, the effects of the applied load on the static stiffness in defective bearings, which was ignored previously, are investigated and the importance of including the effect of load in developing a reliable and accurate defect size estimation method is demonstrated.

The total deformation in rolling element bearings is composed of the deformation of the local rolling elements in the load zone between the inner and outer raceways and the global deformation of the inner and outer raceways [12]. The stiffness in rolling elements depends on the angular position of the rolling elements, which changes due to the rotation of the cage. Consequently, stiffness varies with the number of load carrying rolling elements in the load zone. The static stiffness behavior of healthy ball bearings at various cage positions has been studied analytically [8, 13, 14], numerically [15] and experimentally by measuring the force-displacement relationship [16]. However the static stiffness of defective bearings as a function of cage angular position has only been studied analytically and numerically [8] without experimental validation and analysis, and is addressed in the work presented here.

In this paper, radial bearing stiffness is analysed and examined. Therefore, the term “stiffness” is used for “radial bearing stiffness” unless otherwise stated. For the work conducted in this paper, a bearing test rig was used to measure the vibration of a “floating” bearing housing, and eddy current proximity probes were used to measure the relative displacement between the inner and outer raceways. Deep-groove ball bearings with line-spall and extended defects, machined using electro-discharged-machining (EDM) were installed on the test rig and the force-displacement curves were obtained by measuring the relative displacement signals for a range of loads. Static stiffness curves were obtained and

analyzed for two cage positions. The vibration responses of the two defective bearings are measured and a method to distinguish the two defect sizes under similar test conditions is improved. Experimental and analytical analyses in this research reveal the importance of the effect of load when using the low frequency response variation as a measure to identify extended defects.

The main contributions of this paper are (1) an experimental measurement and analysis of the varying static stiffness in defective bearings with various lengths and loads which validates previous analytical formulation of the static varying stiffness and load distribution of a ball bearing assembly as a function of cage angular position, (2) an analysis of the effects of the applied load on the static stiffness in defective bearings with extended defects , which were ignored previously, (3) an improved approach to distinguishing extended defects and line spalls using the low frequency variation in stiffness.

This paper is structured as follows: Section 2 describes the test rig and the measurement method used in the experiments; Section 3 presents the analytical and experimental outcomes, and detailed analysis of the static stiffness in defective bearings; Section 4 presents vibration measurements of the defective bearings and analysis of the characteristic frequency variation and Section 5 summarizes the findings of this research.

## **2. Test equipment and measurements**

The test rig, as shown in Figure 1, used in this study was manufactured by Spectra Quest, Inc. ([www.spectraquest.com](http://www.spectraquest.com)). The bearing housing supplied with the test-rig was replaced to enable the experiments to be conducted as proposed in this study. The test rig includes an electric motor controlled by a variable frequency drive. The motor was fitted onto a shaft via a coupling and supported by two back-to-back tapered roller bearings. Test bearings were fitted into a custom-made bearing housing at the end of the shaft with a radial loading mechanism applied by a hydraulic jack.

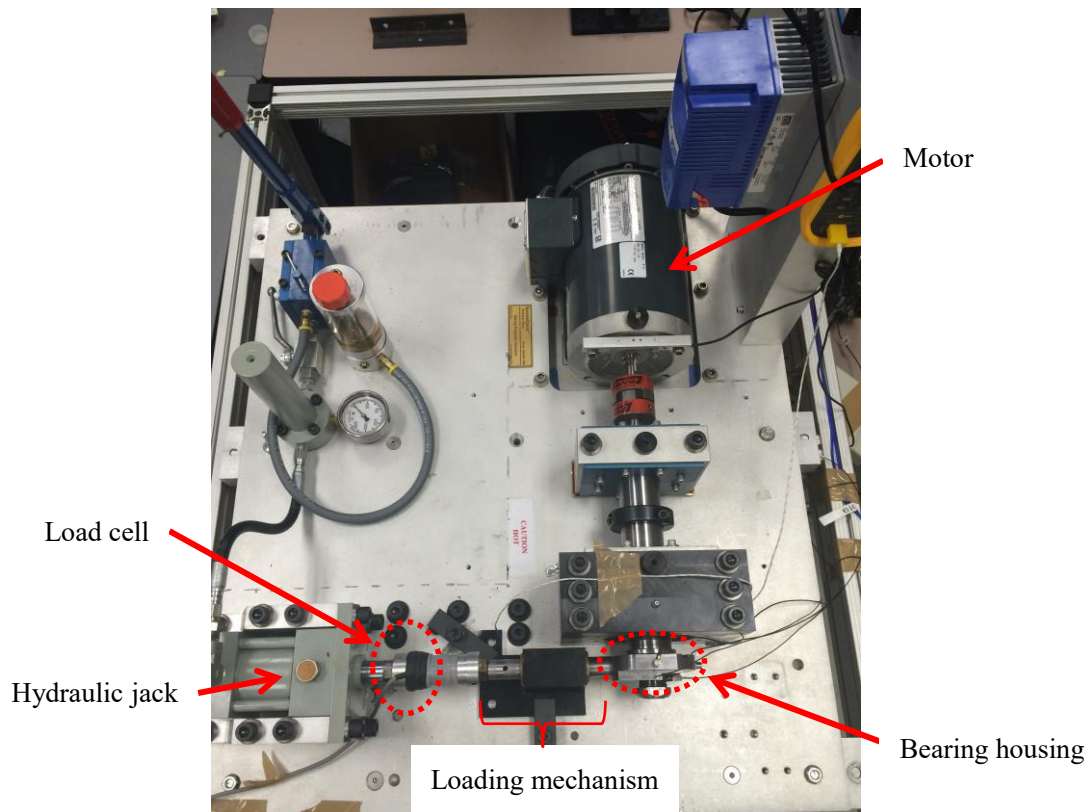


Figure 2: Top view of the test rig used in this study, shows the custom-made bearing housing that was designed to accommodate an accelerometer to measure the vibration of the housing, and eddy current proximity probes to measure the relative displacement between the inner and outer raceways of the test bearing.

Figure 3 shows the custom-made bearing housing that was designed to accommodate an accelerometer to measure the vibration of the housing, and eddy current proximity probes to measure the relative displacement between the inner and outer raceways of the test bearing.

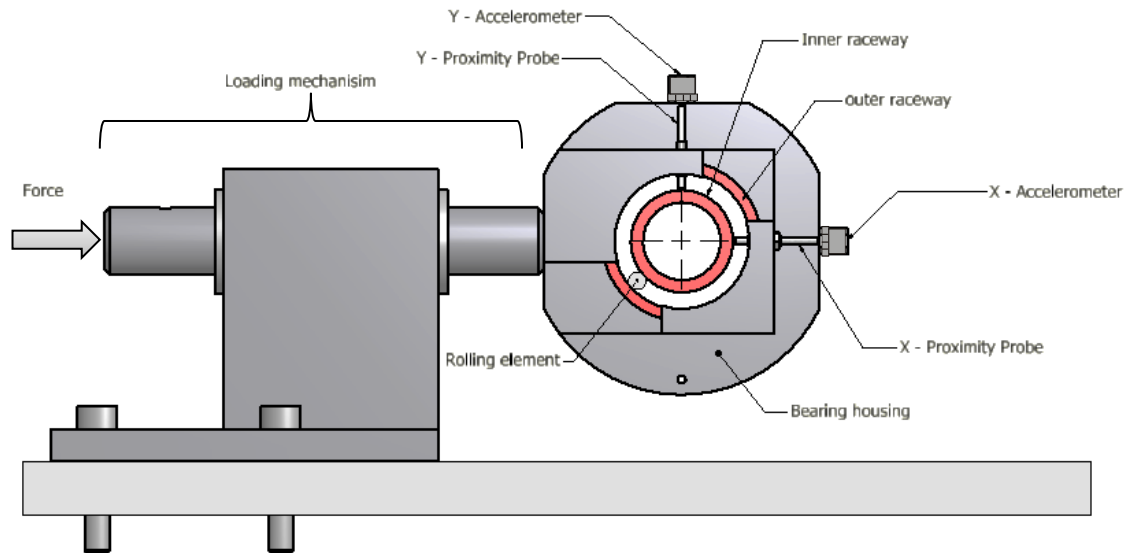


Figure 3: Schematic of the test bearing housing and the method of load application.

The stud-mounted accelerometers (Bruel & Kjaer type 4393) were attached to the bearing housing to measure vibration. The eddy current proximity probes (Micro-Epsilon type EPU05-C3) were mounted on the bearing housing to measure the relative displacement between the inner and outer raceways. A tachometer was used to measure the shaft speed and a load cell measured the force applied to the bearing housing by the hydraulic jack. The data acquisition system consisted of a National Instruments (NI) CompactDAQ system with two NI 9234 modules. Data was acquired and post-processed using MATLAB software. All signals were acquired with a sampling frequency of 25.6 kHz.

The test bearings used in this study were ball bearings manufactured by Rexnord (ER16K), incorporating 9 balls, with a ball diameter of 7.94 mm, pitch diameter of 39.32 mm, static load rating of 7830 N and a contact angle of  $0^\circ$ . Square shape defects with various circumferential lengths across the full axial extent of the outer raceway were machined using electro-discharge machining (EDM) on the outer raceway of the bearings. The size of defects in the test bearings vary in size by exactly one angular ball spacing. Table 1 lists the test bearings and the geometry of defects tested in this study.



Table 1: Test bearings and geometries of defects.

Test bearing	Defect size		
	Angular extent (degrees)	Length (mm)	Depth ( $\mu\text{m}$ )
TB1	15.8	6.52	100
TB2	55.8	23.01	100
DFB	Defect-free bearing		

Each defective bearing was installed into the bearing housing such that the center of the defect was aligned with the direction of the horizontal radial load. Two test positions were chosen such that at each position the minimum or the maximum possible number of rolling elements were located in the load zone in the case of Defect-Free Bearing (DFB). The positions of the rolling elements at each test position cases with regards to the location and the angular extents of the defects, are shown schematically in Figure 4. At Test Position 1, (TP1), the loading axis passes through one rolling element and at Test position 2, (TP2), the loading axis passes in between two rolling elements. The cage angular position for each test position differs by  $(360^\circ / 9 \text{ balls} / 2 = 20^\circ)$ .

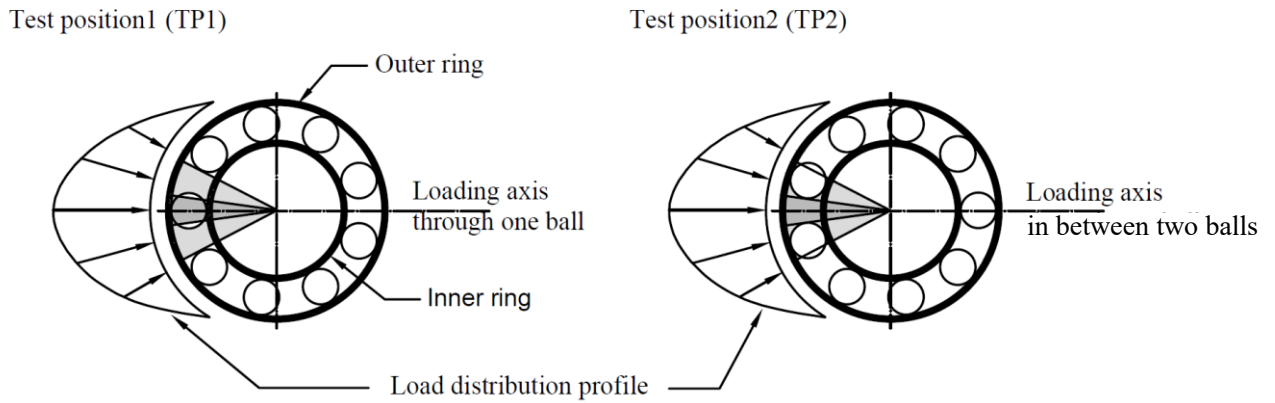


Figure 4: Schematic view of the positions of the rolling elements for the two test positions, where the cage angular position for each test position differs by  $20^\circ$ . The dark and light grey sectors show the  $15.8^\circ$  and  $55.8^\circ$  angular extents for Test Bearing 1 and 2, respectively. Test position 1 shows one rolling element inside the defect for both test bearings. Test position 2 shows zero rolling elements inside the defect for Test Bearing 1 and two rolling elements inside the defect for Test Bearing 2.

The testing procedure and the setup are designed to eliminate the potential errors in measuring the force-displacement relationship caused by the geometry imperfections of the inner raceway or the shaft. The inner raceway cylinders of all the test bearings were machined to provide a reference measurement surface for the eddy current proximity probes, as shown in Figure 5. Therefore, the relative distance measurements between the inner and the outer raceways do not contain measurement variations due to out-of-roundness faults pre-existing in inner raceways, which can occur due to heat treatment processes.

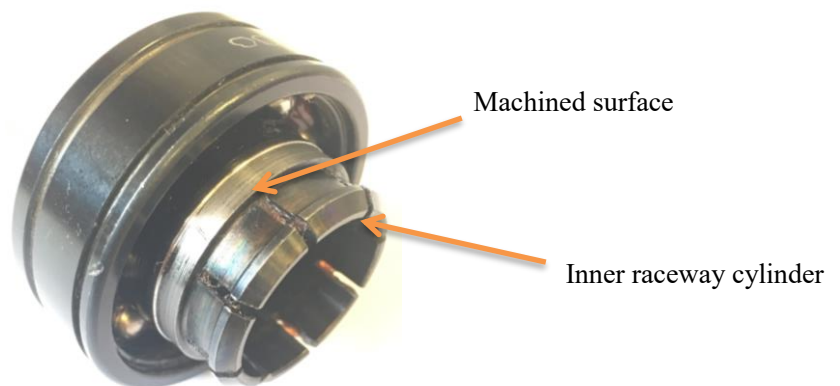


Figure 5: Picture of a Rexnord ER16K bearing assembly showing the machined surface on the inner raceway cylinder that provides a reference surface for the eddy current proximity probes.

### 3. Static stiffness analyses

#### 3.1 Analytical analysis

In this section, the analytical formulation presented by Petersen et al. [5] was implemented to study the effects of the circumferential extent and the static load on the static stiffness, and the number of the load carrying rolling elements in the defect zone for the cases of the test bearings introduced in Section 2. Note that this is different from the study presented in Petersen et al. [5] where only the effect of the circumferential extent for one static load on the static stiffness in bearing was studied, rather than including the effect of static load.

The parameter value of the load–deflection factor for the Hertzian contacts used in the model is  $7 \times 10^9 \text{ N/m}^{1.5}$ , which was chosen according to reference [3]. The bearings were subjected to static loads of 500 N and 3000 N in the horizontal direction. The analytical formulation of the load distribution and the varying stiffness of a ball bearing assembly presented by Petersen et al. [5] does not include the finite size of rolling elements. Therefore a method which effectively describes the path of the center of the ball as it traverses through the square shaped defect is suggested by Petersen et al. [5]. The profiles of the square shaped outer raceway defects considered for this study are generated according to the method described in [5]. This method does not include the finite size of a rolling element. Therefore the path of rolling element has to be modified to account for the gradual de-stressing and re-stressing of a rolling element at the entry and exit points of the defect [4, 5]. Figure 6 presents the defect depth profiles for square shaped defects of depth  $100 \mu\text{m}$  and circumferential extents  $15.8^\circ$  and  $55.8^\circ$ , with the solid and dashed lines indicating the modelled and actual defect depth profiles, respectively.

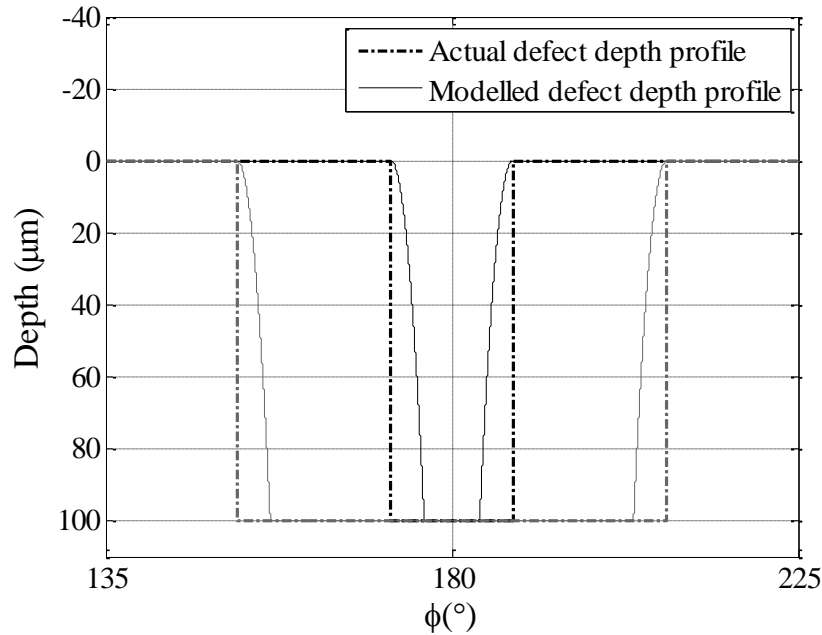


Figure 6: Defect depth profiles for square shaped defects of depth 100  $\mu\text{m}$  and circumferential extents 15.8° (black) and 55.8° (gray); (dashed line) actual defect depth profile; (solid line) modelled defect depth profile.

Figure 7 (a) and (b) show the variation of the estimated number of balls that carry the static load as a function of the applied load and cage angular position in the two cases of defects with different circumferential extents. As a result of the applied load and the number of balls supporting the load, the corresponding displacement of the outer raceway relative to the inner raceway will also vary. By knowing the force-displacement relationship, the equivalent stiffness can be determined, as shown in Figures 6 (c) and (d) for the two test bearings.

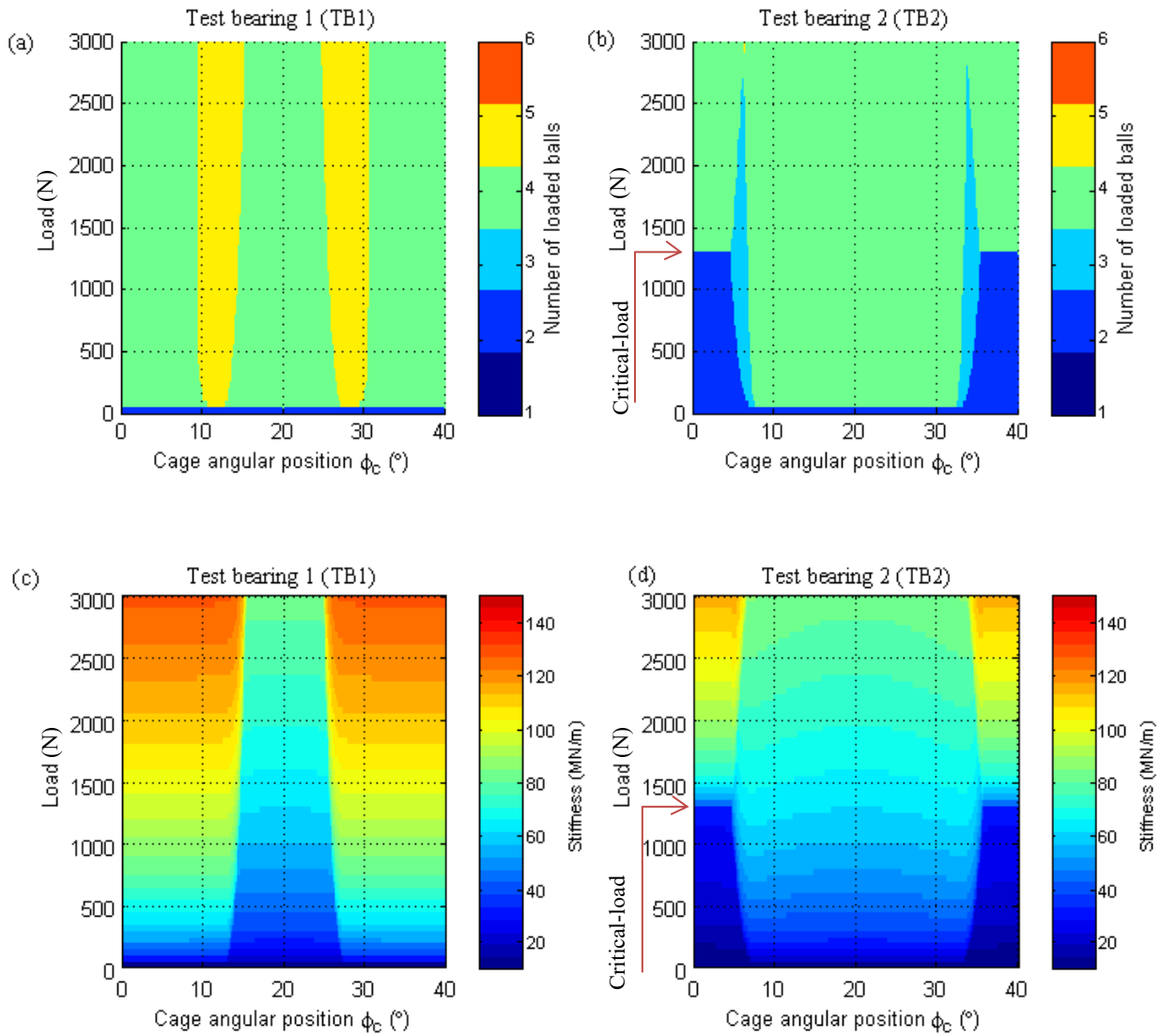


Figure 7: Contour plots showing the number of balls carrying load and radial bearing stiffness as a function of cage angular position for a square shaped outer raceway defect of depth  $100\mu\text{m}$ . Plots (a) and (b) show the number of balls carrying the static load for  $15.8^\circ$  (TB1) and  $55.8^\circ$  (TB2) defects respectively, and plots (c) and (d) show the corresponding radial bearing stiffness for  $15.8^\circ$  and  $55.8^\circ$  defects respectively.

The stiffness and the number of balls that carry the static load vary periodically for both defective bearings with the fundamental period defined by a ball angular spacing of  $40^\circ$ . Therefore Figure 7 shows only  $40^\circ$  of the cage angular position. The number of load carrying rolling elements and the varying stiffness as a function of the applied load is similar for both TB1 and TB2 at the cage angular position  $20^\circ$ . This similarity is also valid for the cage angular positions neighboring  $\varphi_c = 20$  at which only one rolling element is positioned in the defect.

Compared with the defect with the smaller circumferential extent, the stiffness and the number of load carrying rolling elements in the extended defect (TP2) suddenly increases at the cage angular position  $0^\circ$  at and above 1300 N load, see Figure 7(b) and (d). As the load applied to the bearing increases, eventually the displacement of the outer raceway causes balls within the defect zone, that were unloaded at and under 1300 N, to come into contact with the raceways again and start to become loaded. This load is called the “critical load” in this study.

At loads less than the critical-load, when the circumferential extent of the defect is greater than the ball angular spacing, as is the case of TB2, one or more balls are positioned in the defect at any one time. Therefore, the stiffness is always equal to or less than the stiffness of the bearing with a smaller circumferential defect, as is the case of TB1, depending on the cage angular position. When the rolling elements positioned in the defect start to take load at loads higher than the critical-load, varying stiffnesses of the bearing with extended circumferential defect increase dramatically and become closer to the stiffness values of the case with smaller defects.

Since the presence of the extended defect reduces the number of loaded balls compared with the bearing with smaller defects, the balls positioned outside the defect zone and inside the load zone need to carry more of the load [5]. Hence, the local relative contact deformations of the load carrying rolling elements in the larger defect are greater than the local relative contact deformations, in smaller defects. Consequently, under equal load, the relative displacement between the inner and outer is greater in the case of the extended defect, when compared with smaller defects. This force-displacement relationship can also be explained by the fact that bearings with an extended defect have lower static stiffness at loads under the critical-load, when compared with bearings with smaller defects, which can be seen in Figure 7. Therefore, the stiffness changes in a bearing assembly are not only due to the defect size but also due to the applied load. These analyses show the importance of

determining the critical load when changes in the frequency response of a bearing is being monitored.

### 3.2 Experimental analysis

This section presents an analysis of the measured signals using the test rig described in the previous section. The static measurements were conducted on the test bearings by applying various static loads at the two test positions described in the previous section. The aim was to validate the analytical analyses presented in the previous section by measuring the relative displacement between the inner and outer raceway as a function of applied static load and provide insights into the static stiffness behavior of the tested bearings. Figure 8 shows the obtained force-displacement relationships for the three bearings TB1, TB2, and defect free bearing.

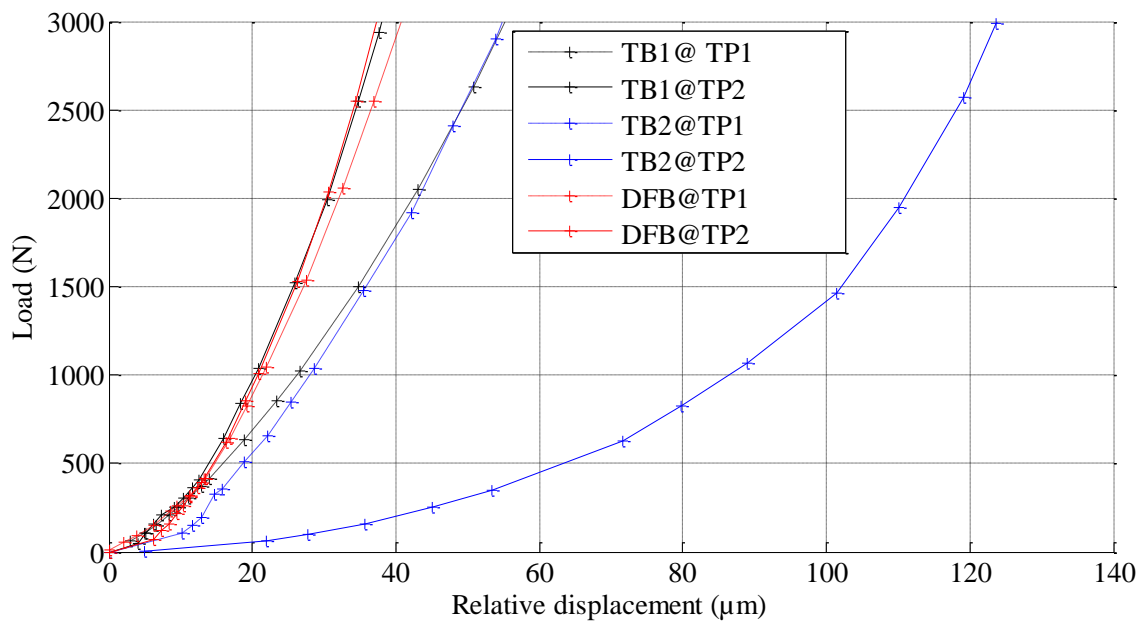


Figure 8: Force-displacement relationships for Test bearings 1 (TB1) and 2 (TB2), at the two Test positions 1 (TP1) and 2 (TP2), and the Defect Free Bearing (DFB), as described in Section 2.

The slope of each force-displacement curve in Figure 8 represents the static stiffnesses of the bearing assembly at a particular test position. The slopes for TB2 are lower at both test positions when compared with similar results for the DFB case. Studying the force-

displacement relationship of the TB2 at the TP2 is particularly important as the relative displacement value reaches the value of the depth of the defect, 100  $\mu\text{m}$ , at about 1400 N load, see Figure 8. At this value, the slope of the force-displacement curve dramatically increases. The static load of 1400 N, by definition, is called the critical-load which agrees with the critical-load estimated in Section 3.1 and shown in Figure 7.

The obtained force-displacement relationships are further analyzed by investigating the slope of the measured force-displacement curves. Firstly, polynomial curves of the order of four were fitted to the measured force-displacement data and then the derivatives at each displacement point were calculated. Figure 9 shows the slopes of measured force-displacement curves as a function of the applied load.

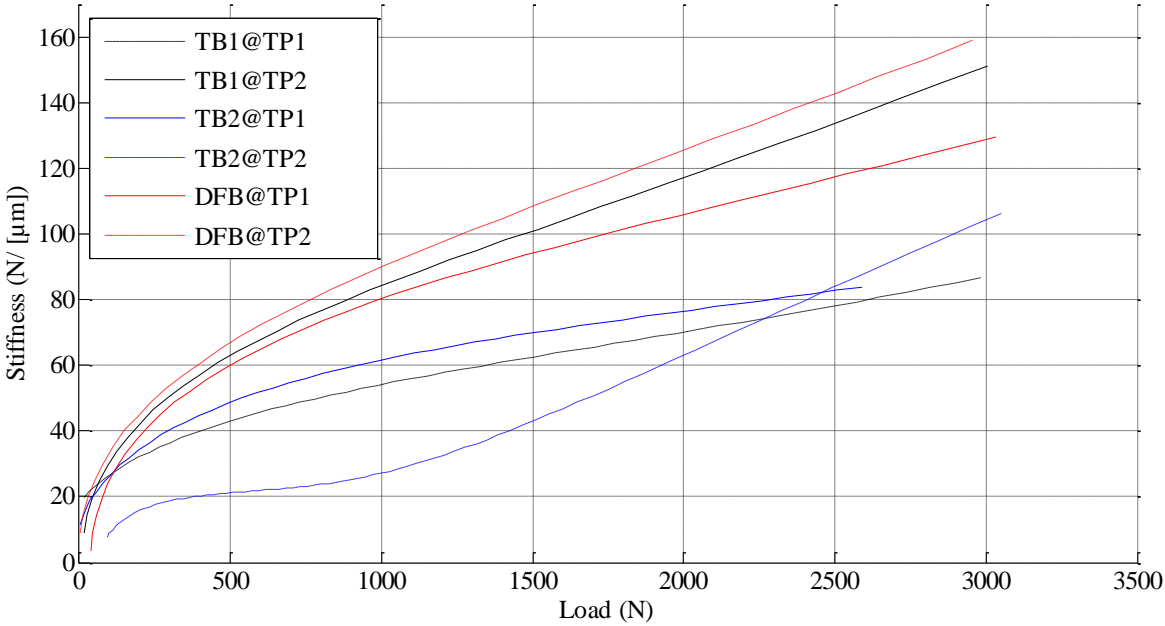


Figure 9: Stiffness curves for test bearings at the two test positions, TP1 (solid line) and TP2 (dashed line).

The stiffness-load curves reveal that the static stiffness varies linearly with applied load above 1000 N with similar slopes, except for the static stiffness curve obtained for the TB2 at the TP2. The slope of the static stiffness curve for TB2 at TP2 varies linearly with applied load above 1300 N with a slope which is much greater than the slopes of the rest of the curves.



At this critical-load the relative displacement between the inner raceway and the outer raceway, in the direction of the load, approaches the depth of the defect, 100  $\mu\text{m}$ , in TB2 at TP2. Therefore, the number of load carrying rolling elements increases and equals the number of load carrying rolling elements in the case of DFB. Although at higher static loads the number of load carrying rolling elements in TB2 and DFB are equal, the load distributions in the two bearings will be different. Consequently, at loads above the critical-load, the rate of changes of the static stiffness curves become similar in all the test bearings (TB1, TB2 and DFB) at TP2, due to equal numbers of rolling elements in the load zone. The measured experimental static stiffnesses match the estimated stiffnesses, shown in Figure 7 (c) and (d), for the TB1 and TB2 at 20° and 0° (TP1 and TP2 respectively).

Analyses of the experimental force-displacement results, shown in Figure 8 and Figure 9 are listed below.

- The force-displacement relationships for each tested bearing vary for the two test positions, TP1 and TP2. The variation is due to the angular position of the cage in each test bearing, and is the smallest for the defect free case, DFB, and the largest for the bearing with the extended defect, TB2. These variations are due to the difference in the number of the rolling elements carrying the static load and the magnitude of the applied static load.
- The resemblance between the force-displacement relationships for TB1 at TP1 and the DFB at TP1, suggests similar non-linear static stiffness at TP1 for both defective test bearings. Therefore, at this angular position, TP1, the applied load and the defect size has no effect on the static stiffness.
- The force-displacement relationships for TB1 only deviate from the static stiffness of the DFB at TP1 when a rolling element is positioned inside the defect.
- Force-displacement relationships for TB2 at TP1 and TP2 deviate entirely from the force-displacements for the DFB as at least one rolling element is positioned inside

the defect at any given angular position of the cage. Therefore, lower static stiffness for the extended defect, TB2, is expected at any cage angular position when compared with a healthy bearing.

- Force-displacement relationship curves for TB1 and TB2 are similar at TP1, whereas the force-displacement relationship curves vary for TP2. This suggests that the dynamic stiffnesses of the two defective bearings are not expected to be similar.

## **4. Dynamic analyses**

### **4.1 Vibration measurement**

The bearing test rig in Figure 2 was used to measure the vibration response of two bearings with manufactured square defects TB1 and TB2, which vary in size by exactly one angular ball spacing. Each bearing was tested with 500N and 3000 N radial loads and the shaft supporting the bearing was rotated at 600 rpm. The vibration response in the horizontal direction (the direction of the loading axis) is measured using the accelerometer mounted on the bearing housing. Figure 10 shows the experimental vibration results in the horizontal direction as a function of the cage angular position for the two defective bearings. In this figure the cage position is calculated with the assumption of no cage slippage in the bearing. The figure shows the sizes (in degrees) of the defects on each test bearing. It can be seen that the angular extents between any two successive entry and exit events appear nearly identical for both TB1 and TB2 despite TB1 having a defect size of  $15.8^\circ$  and TB2 having a defect size that is  $40^\circ$  larger at  $55.8^\circ$ . This is because the balls will enter and exit the defects in TB1 and TB2 with the same period as defects vary in size by exactly one angular ball spacing.

Hence, current defect size estimation methods are unable to correctly estimate the size of the larger defect in bearing TB2.

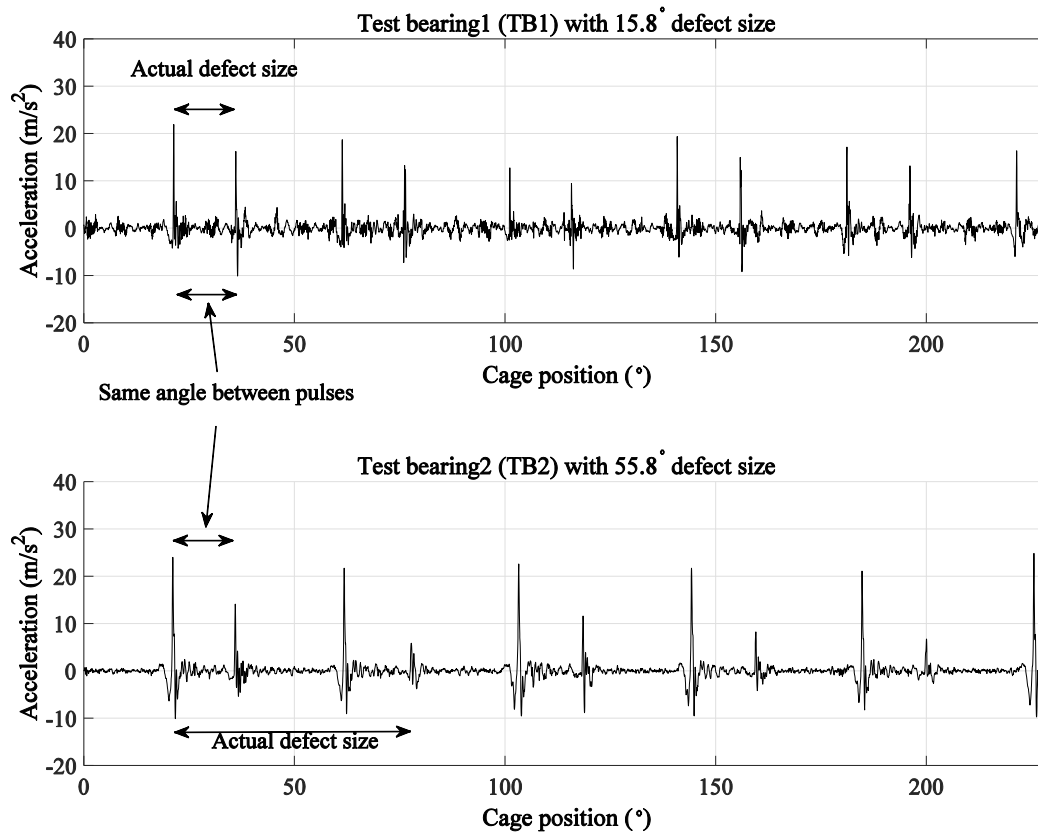


Figure 10: Experimentally measured acceleration in the horizontal direction of bearings TB1 (15.8° defect size) and TB2 (55.8° defect size) as a function of angular cage position at 500N of load and a shaft speed of 600 rpm. The corresponding sizes of the defects are indicated on the figures.

To resolve this inability to differentiate the size of the defects, the following section shows how knowledge of dynamic stiffness and measurement of the resonance frequency of the bearing assembly can be used to differentiate the size of the defects.

#### 4.2 Detection of dynamic stiffness variations

In this section, the effects of the dynamic stiffness variation on the measured vibration responses are investigated. In this paper, the dynamic stiffness is the frequency dependent ratio between a dynamic force, due to defect size variation, and the resulting dynamic displacement. The purpose of these experimental analyses is to justify the hypothesis that the low frequency variations of the entry and exit vibration events can be used as a feature to distinguish defects that vary in size by exactly one angular ball spacing. Test bearings are loaded with 500N and 3000N to investigate the effect of load. These loads are selected to be

smaller and greater than the critical load estimated in section 3.1 and experimentally shown in section 3.2.

The low frequency vibration events that occur when a rolling element enters and exits a defect, as discussed in Section 1, are due to the stiffness changes of the bearing assembly [8]. It has been shown in this paper, both analytically and experimentally, that the stiffness of the bearing assembly is noticeably different when comparing line spall and extended defects. The change in the bearing assembly stiffness can be detected by inspecting the characteristic frequency of the low-frequency events. This can be achieved by using time-frequency signal-processing techniques, as shown below.

Firstly, peaks of the entry and exit transient events are detected on the measured vibration data. Then, the entry and exit events are separated and individually captured using a square window with the length of 1155 samples that starts 155 samples before a detected event's peak. Square window is selected for these analyses due to the fact that the measured vibration signal at the start and end of each block is near zero and amplitude accuracy of the captured events is important. Next the captured events are ensemble averaged and the spectrograms of the resultant ensemble averaged signals are created using the Discrete Gabor Transform (DGT) to perform time-frequency analyses [17, 18]. Figure 11 (a) to (d) and (m) to (p) show the 20ms of the 30 events captured from the measured vibration signals of the test bearings, TB1 and TB2, under 500N and 3000N static loads. Figures 12(e) to (h) and (q) to (t) show the ensemble averages of the related captured signals and their standard deviation (SD). Figures 12 (i) to (l) and (u) to (x) show the spectrograms of the resultant ensemble averaged signals. The vibration energy densities on the DGT spectrograms for each event are normalized

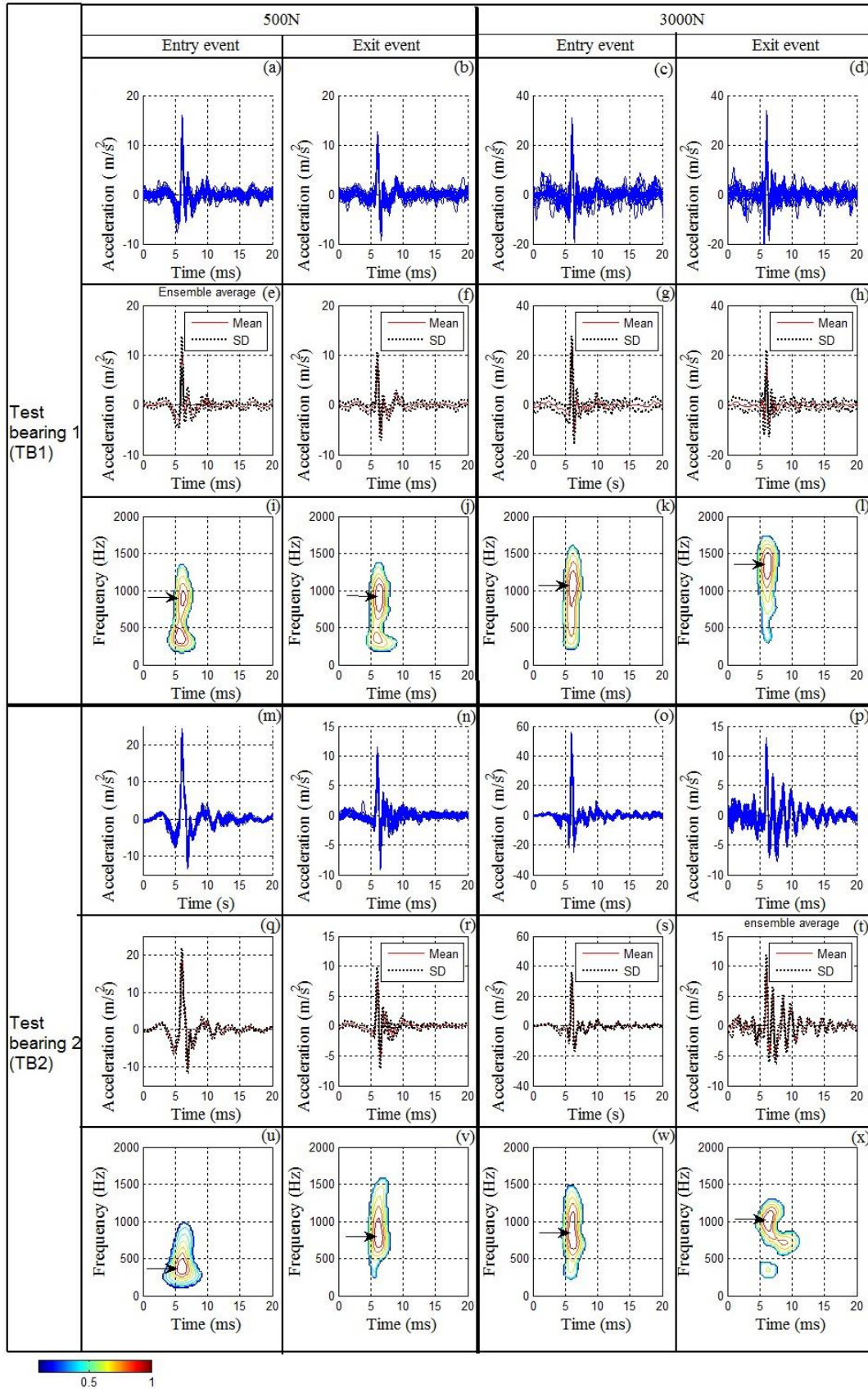


Figure 11: Comparing acceleration results and their spectrogram using the Discrete Gabor Transform (DGT) for the test bearings, TB1 and TB2, under 500N and 3000N loads. (a) to (d) and (m) to (p) show 20ms the captured 30 entry and exit events, (e) to (h) and (q) to (t) show the

ensemble average and its standard deviation for the captured events, (i) to (l) and (u) to (x) show the spectrograms for the calculated entry and exit mean signals.

The observed low frequency entry and exit events shown in Figure 11, for both the acceleration results and the spectrograms, are caused by varying stiffness excitations of the rigid body modes that occur when a ball enters or exits the defect (also called parametric excitation) [22]. Some comments about the spectrograms in Figure 11 are as follows:

Dominant characteristic frequencies of entry events appearing on the spectrograms are generally lower than the dominant characteristic frequency of the exit events for every individual test bearing. These results are consistent with the theoretical analysis and experimental measurements of static stiffness of the test bearings presented in Section 3.1 and Section 3.2.

The difference between the dominant characteristic frequencies of the entry events in a particular test bearing and under different loads is larger in the case of TB2 when compared with the similar events in the case of TB1, compare Figure 11 (i) and (k) to (u) and (w). This phenomenon can be explained by the fact that when bearing TB2 is loaded with 500N, as the rolling elements enter the defect they don't carry load. Whereas, if the bearing TB2 was loaded with 3000N, the rolling elements would carry some load when they enter the defect zone. Hence, unlike the TB1, the TB2 will be stiffer at higher loads. Under similar loading conditions, the dominant characteristic frequencies of entry and exit events are higher in the case of TB1 than TB2, compare Figure 11 (i) with (u), (j) with (v), (k) with (w) and (l) with (x). However, the entry events of TB1 and TB2 under 500N have the largest difference between the dominant characteristic frequencies among the rest, as shown Figure 11 (i) and (u).

It has been shown in Section 3.1 and Section 3.2 that the static stiffness of the bearing assembly with the larger defect TB2, when the balls were in position TP2, is lower for applied loads less than the critical-load when compared with the static stiffness of the rigid body

modes of TP1. As a result, the rigid body modes of the test bearing have lower dominant characteristic frequencies.

This experimental analysis shows that it is practically possible to use the shifting of the characteristic frequencies of the low frequency events to distinguish between two defects that vary in size by exactly one angular ball spacing when estimating the size of the defect. Further, it has been demonstrated that the applied load must be considered for such analyses. Under relatively high loads (above critical-loads), shifting of the characteristic frequencies of the low frequency events due to the presence of the extended defect may not be significant enough to be detected clearly. Successful implementation of low frequency variation detection to distinguish two different defect sizes requires an analysis to determine the critical-load.

#### **4.3 Recommendations for condition monitoring**

In this section, recommendations are provided to implement a defect size estimation method utilizing the low frequency entry event as a roller enters a defect. According to the discussion presented in this study, the applied load has a significant effect on the bearing assembly stiffness and consequently the low frequency characteristics of the bearing, and hence determining the critical load is helpful. The critical load can be estimated using the method discussed in Section 3.1. The minimum acceptable depth of a defect should be defined to determine the critical-load of the bearing under condition monitoring. If the minimum acceptable depth of a defect is not known, defective bearings should be tested under loads close to their minimum recommended load carrying capacity. Spectrograms should be constructed for entry and exit events separately in accordance with the method described earlier in section 4.2. Presence of the following characteristics in the spectrograms is an indication of existing extended defects.

1. Lower dominant characteristic frequencies of entry and exit events on the spectrograms of the vibration data under similar loads as the defect grows. This

analysis requires historical trend data of the bearing being monitored and the bearing should be tested under similar loads.

2. Significant increase in the dominant characteristic frequencies of the entry events by increasing the applied load when compared with the increase of the dominant characteristic frequency of the exit events. It should be possible to test a bearing at two different loads. This analysis does not require historical data of the bearing being monitored.

Note that while the first characteristic might be detectable in power spectra density results, as showed previously by simulations [5], detection of the second characteristic is only possible by performing time-frequency analysis, similar to the one presented in this study. This proposed method, which is an original contribution of this paper, does not require historical data for comparison, unlike the method suggested in [5].

## **5. Conclusions**

This paper investigates the relationship between the applied load and the relative displacement between the raceways of defective rolling element bearings with outer raceway defects. Analytical estimations and experimental measurements of the static stiffness show that stiffness variation is a function of load, defect size and cage angular positions. Experimental analysis of the bearing stiffness variations in this paper confirms that the static stiffness decreases in the loaded direction at cage angular positions where rolling elements are positioned in the defect. It is shown that the static stiffness variation in defective bearings with extended defects is more sensitive to applied loads than it is to the cage angular position, when compared with smaller defects. It was shown in this study that the stiffness of the bearing assembly in defective bearings changes dramatically when test bearings are applied with loads above the critical-load. The critical-load depends on the depth and size of the defect. In a defective bearing, once the applied load reaches the critical-load, the number of load carrying rolling elements will increase as there is sufficient deflection of the assembly



to cause the unloaded rolling elements in the defect zone to regain contact with the inner and outer raceways and support the applied load.

The feasibility of using the variation of the low frequency entry event to distinguish defects that vary in size by exactly one angular ball spacing is investigated by measuring the vibration response of two defective bearings. Time-frequency analyses are used to detect the changes in the characteristic frequencies of the low frequency vibration events. Careful time-frequency analyses of different defective bearings under different applied loads showed the feasibility of this method in distinguishing the two defect sizes. It is shown that a successful implementation of this method to distinguish the two different defect sizes requires analysis to determine the critical-load introduced in this research. Recommendations for condition monitoring methods are given based on the analyses presented in this study. The new method proposed in this paper does not require historical data, whereas previously suggested methods require historical data.

## References

1. Y.T. Su, M.H. Lin, and M.S. Lee, *The effects of surface irregularities on roller bearing vibrations*. Journal of Sound and Vibration, 1993. **165**(3): p. 455-466.
2. C. Sunnersjö, *Rolling bearing vibrations-the effects of geometrical imperfections and wear*. Journal of Sound and Vibration, 1985. **98**(4): p. 455- 474.
3. T.A. Harris, *Rolling Bearing Analysis*. 2001, USA: Wiley.
4. A. Moazen Ahmadi, D. Petersen, and C.Q. Howard, *A nonlinear dynamic vibration model of defective bearings – the importance of modelling the finite size of rolling elements*. Mechanical Systems and Signal Processing, 2015. **52–53**: p. 309-326.
5. D. Petersen, C. Howard, and Z. Prime, *Varying stiffness and load distributions in defective ball bearings: analytical formulation and application to defect size estimation*. Journal of Sound and Vibration, 2015. **337**(0): p. 284-300.
6. N. Sawalhi and R.B. Randall, *Vibration response of spalled rolling element bearings: observations, simulations and signal processing techniques to track the spall size*. Mechanical Systems and Signal Processing, 2011. **25**(3): p. 846-870.
7. S. Singh, U.G. Köpke, C.Q. Howard, and D. Petersen, *Analyses of contact forces and vibration response for a defective rolling element bearing using an explicit dynamics finite element model*. Journal of Sound and Vibration, 2014. **333**(21): p. 5356–5377.
8. D. Petersen, C.Q. Howard, N. Sawalhi, A. Moazen Ahmadi, and S. Singh, *Analysis of bearing stiffness variations, contact forces and vibrations in radially loaded double row rolling element bearings with raceway defects*. Mechanical Systems and Signal Processing, 2015. **50-51**: p. 139-160.
9. I. Epps and H. McCallion. *An investigation into the characteristics of vibration excited by discrete faults in rolling element bearings*. in *Annual Conference of the Vibration Association of New Zealand*. 1994. Christchurch.
10. A. Moazen Ahmadi, D. Petersen, and C.Q. Howard. *A nonlinear dynamic model of the*

- vibration response of defective rolling element bearings*. in *Proc of Australian Acoustical Society*. 2013. Victor Harbor.
11. S. Zhao, L. Liang, G. Xu, J. Wang, and W. Zhang, *Quantitative diagnosis of a spall-like fault of a rolling element bearing by empirical mode decomposition and the approximate entropy method*. *Mechanical Systems and Signal Processing*, 2013. **40**(1): p. 154-177.
  12. J.E. Shigley, *Mechanical engineering design*. 1972.
  13. N. Aktürk, M. Uneeb, and R. Gohar, *The effects of number of balls and preload on vibrations associated with ball bearings*. *Journal of Tribology*, 1997. **119**(4): p. 747-753.
  14. H.-V. Liew and T.C. Lim, *Analysis of time-varying rolling element bearing characteristics*. *Journal of Sound and Vibration*, 2005. **283**(3-5): p. 1163-1179.
  15. Y. Guo and R.G. Parker, *Stiffness matrix calculation of rolling element bearings using a finite element/contact mechanics model*. *Mechanism and Machine Theory*, 2012. **51**: p. 32-45.
  16. M. Dougdag, N.E. Titouche, M. Djaoui, and M. Ouali, *The calculation of ball bearing nonlinear stiffness theoretical and experimental study with comparisons* *Journal of Engineering and applied sciences*, 2008. **3**(11): p. 872-883.
  17. K. Gröchenig, *Foundations of time-frequency analysis*. 2013: Springer Science & Business Media.
  18. H.G. Feichtinger and T. Strohmer, *Gabor analysis and algorithms: Theory and applications*. 2012: Springer Science & Business Media.

## Chapter 6

### Defect Size Estimation in Rolling Element Bearings

This chapter has been submitted as

A. Moazen-ahmadi, C.Q. Howard, A defect size estimation method based on operational speed and path of rolling elements in defective bearings, *Journal of Sound and Vibration* (Submitted to *Journal of Sound and Vibration* on 17/03/2016).

This chapter is the fourth of four journal papers (submitted) and presents investigations into the effect of the centrifugal and inertia forces acting on the rolling elements on the measured vibration signature in defective bearings. The sources of inaccuracy and the speed-dependency in the existing defect size estimation algorithms are identified and explained. The speed dependency of the angular extents between the low frequency entry events and the high frequency exit events on the vibration signal have been shown by experimental measurements and simulation. The simulation in this chapter is carried out using the model developed in Chapter 3. The analyses presented in this study are essential to develop accurate and reliable defect size estimation algorithms, which are also suitable for bearings under various operational speeds. The simulations and experimental measurements in this study have led to the derivation of a hybrid method to more accurately estimate the size of a defect in a bearing, which is shown not to be biased for operational speed, unlike previous methods. The hybrid method, presented in Chapter 6, uses the analyses presented in this chapter; the model presented in Chapter 3 and the defect size estimation algorithm proposed in Chapter 4.



# Statement of Authorship

Title of Paper	A defect size estimation method based on operational speed and path of rolling elements in defective bearings		
Publication Status	<input type="checkbox"/> Published	<input type="checkbox"/> Accepted for Publication	<input type="checkbox"/> Unpublished and Unsubmitted work written in manuscript style
	<input checked="" type="checkbox"/> Submitted for Publication		
Publication Details	Journal of Sound and Vibration		

## Principal Author

Name of Principal Author (Candidate)	Alireza Moazen-ahmadi		
Contribution to the Paper	Performed analytical work, interpreted data, wrote manuscript and acted as corresponding author.		
Overall percentage (%)	90%		
Certification:	This paper reports on original research I conducted during the period of my Higher Degree by Research candidature and is not subject to any obligations or contractual agreements with a third party that would constrain its inclusion in this thesis. I am the primary author of this paper.		
Signature		Date	27/9/2016

## Co-Author Contributions

By signing the Statement of Authorship, each author certifies that:

- i. the candidate's stated contribution to the publication is accurate (as detailed above);
- ii. permission is granted for the candidate to include the publication in the thesis; and
- iii. the sum of all co-author contributions is equal to 100% less the candidate's stated contribution.

Name of Co-Author	Carl Howard		
Contribution to the Paper	Supervised the research and contributed in academic discussion and manuscript review.		
Signature	10%	Date	27/9/2016

Name of Co-Author			
Contribution to the Paper	Supervised the research and contributed in academic discussion and manuscript review.		
Signature		Date	

Please cut and paste additional co-author panels here as required.



## **A defect size estimation method based on operational speed and path of rolling elements in defective bearings**

Alireza Moazen-ahmadi and Carl Q. Howard

<sup>1</sup>The University of Adelaide, Australia

### **1. Abstract**

This paper investigates the effect of inertia and centrifugal force, which act on a rotating rolling element, on the measured vibration signature in defective bearings. These effects are more important in bearings as speed increases. The sources of inaccuracy and the speed-dependency in the existing defect size estimation algorithms are identified and explained. Significant speed dependency of the characteristic events that are generated at the angular extents of the defect are shown by simulation and experimental measurements as speed increases. The analyses presented in this study are essential to develop accurate defect size estimation algorithms, which are also suitable for bearings under various operational speeds. A complete defect size estimation algorithm is proposed that is more accurate and less biased by shaft speed when compared with existing methods.

Keywords: Rolling element bearing, spall, defect size estimation, speed dependency

---

### **2. Introduction**

Rolling element bearings are widely used in rotary machinery and the failure of bearings is the most common reason for machine breakdowns. Effective bearing condition monitoring systems should be able to detect and estimate the size of defects in bearings correctly at early stages of the defect development in order to enable



remedial action to be taken. Therefore, appropriate models and signal processing algorithms to track the growth of defects are beneficial.

Defects in bearings are commonly categorized into localized and distributed defects. Distributed defects, such as waviness, surface roughness, or off-size rolling elements are usually the result of manufacturing errors [1, 2]. Localized defects are often initiated by insufficient lubrication film between the contact surfaces. This causes metal-to-metal contact between the rolling elements and the raceways, which in turn generates stress waves, leading to the formation of sub-surface cracks over time. The large forces in bearings cause the sub-surface cracks to grow into surface defects. This phenomenon is called pitting or spalling [3]. This paper considers the vibrations and contact forces generated in bearings with raceway spalls, also known as line spalls.

Effective bearing condition monitoring systems should be able to detect and assess the severity of defects in bearings at the early stages of defect development, either to enable remedial action to be taken, or to schedule the replacement of the bearing at a convenient time. The typical vibration condition monitoring process involves measuring the vibration level of a bearing housing and trending the level over time. When the level exceeds a nominated threshold, the bearing is flagged for replacement. Alternatively, the geometric arc length of a bearing defect from the vibration signal can be determined to assist replacement decision making.

Previous studies on the vibration signature of defective bearings with raceway spalls show that the passage of a rolling element over the spall generates two main components, namely entry and exit events [4-8]. These events and their characteristics are reviewed in section 2.1. Several defect size estimation methods were previously suggested, based on the extraction of the time separation between these two components from the vibration signal. These methods are reviewed in section 2.1.

Current models developed for defective bearings are reviewed in section 2.2 and a model suitable for this study is selected from these reviews. Section 3 describes the test rig, the model used in this study, and the detailed analysis of the simulation outcomes. Section 4 describes a proposed method designed to estimate the defect size, which is more accurate and less biased by shaft speed when compared with existing methods. Section 5 summarizes the findings of this research.

This paper contributes to current knowledge by providing greater understandings of the vibration signature originating from the entry and exit events. The focus of this research is to demonstrate the speed dependency of the angular extents between the low frequency entry events and the high frequency exit events on the vibration signal. The secondary purpose of these investigations is to eliminate the speed dependency of the current defect size estimation algorithms, and propose a new algorithm based on the analyses presented in this study. In this paper the acceleration time signal responses resulting from a rolling element entry into, and exit from, a typical spall is investigated. The experimental data was provided by the University of New South Wales (UNSW), which has carried out tests on bearings with an outer raceway defect.

## **2.1 Vibration signature and defect size estimation methods**

Figure 1(a) illustrates a defective rolling element bearing with a line spall defect on the outer raceway. A typical measured vibration signal due to such a defect is shown in Figure 1(b). It has been shown by previous studies that the passage of a rolling element over the defect generates two main components: numerically [9], analytically [4, 10] and experimentally [5].

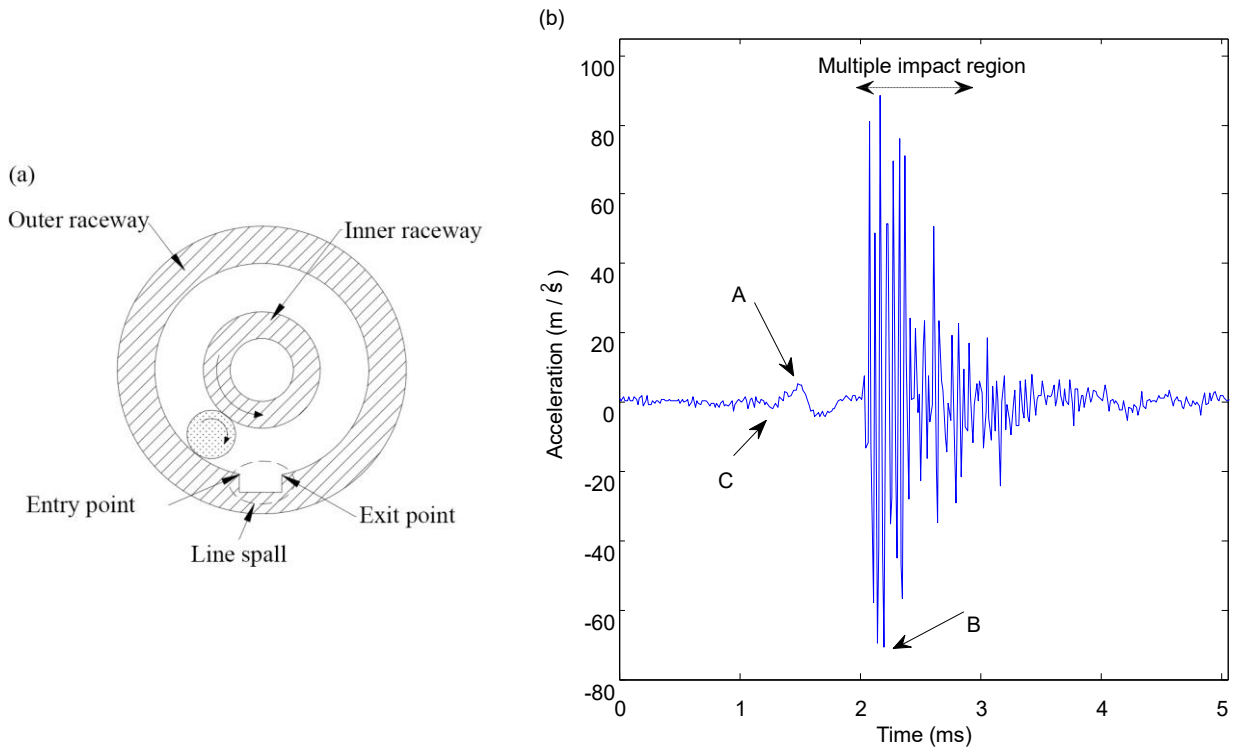


Figure 1: (a) Diagram of a rolling element travelling into a line spall defect located on the outer raceway. (b) A typical measured vibration response. Points A and B are typically identified as entry and exit points, as suggested by previous studies [8, 11], whereas the analysis in this paper shows that point C is the entry point and the exit point happens in the multiple impact region.

Sawalhi and Randall [8] measured the vibration of several defective ball bearings with a line spall defect and suggested that the high frequency impulsive event in the measured vibration response corresponds to the excitation of high-frequency bearing resonant modes, which occur when the center of a rolling element is halfway through the defect. These researchers assumed that point A, shown in Figure 1 (b), corresponds to the entry point, while the largest high frequency responses in magnitude, shown as point B in Figure 1, in the multiple impact region, correspond to the exit point of a defect. Moazen Ahmadi et al. [5] showed that the defect size estimation based on finding point A (the low frequency local maxima) and point B (the high frequency

event) and by doubling the distance between these two points, is inaccurate and unreliable. Previous defect size estimation methods that are based on these hypotheses are shown to be inaccurate and biased by shaft speed [5, 8].

Petersen et al. [10, 12] and Moazen Ahmadi et al. [4, 5] studied the entry and exit events and have shown that the low frequency response is linked with the dynamic properties of the bearing assembly. The entry of a rolling element into a line spall defect produces a vibration signal with low frequency content [6, 8]. The exit of the rolling element excites a much broader range of frequencies, including the high frequency bearing resonances. These resonances are excited by the impact of the rolling element mass on the exit point of a defect, as well as the parametric excitations caused by rapid changes in the bearing stiffness, which occur when the rolling element re-stresses between the raceways [10]. The high frequency event observed in experimental results [6, 13] often appears to have been caused by multiple impacts rather than a single impact. Simulation results of defective bearings presented by Singh et al. [14] indicate that the multiple impacts occur when the rolling element successively impacts on the inner and outer raceways as it re-stresses at the exit point.

Moazen-ahmadi et al. [5] indirectly investigated the path of rolling elements in the defect zone by measuring the displacements between raceways generated in bearings with an outer raceway line spall of various dimensions, speeds and loads. They have related the relative displacement signal between the inner and outer raceways as a rolling element passes through a line spall defect. By synchronizing the vibration and displacement signals, they were able to propose a hypothesis to explain the path of rolling elements in the defect zone, which explains the discrepancies in the previous assumptions of the path of rolling elements in the defect zone and the corresponding features on the vibration response to the entry and exit events. The key findings in their

study, which are essential for the analyses presented in this study, are listed below:

- The entry transient event to the defect starts before the local maxima of the low frequency response: point C as opposed to point A, shown in Figure 1.
- The exit impact events shown by acceleration impulses can occur before the center of a rolling element reaches the center of a defect. Therefore, the exit impacts do not necessarily happen midway through a defect.
- The exit transient event (the moment that a rolling element comes into contact with both raceways at the exit) causes a low frequency event on the vibration result. This event, however, can be superpositioned by the excited high frequency modes. Depending on the dynamics of a bearing assembly and its pedestal, the two events, namely the high-frequency impact response and the low-frequency response, could be separated or superpositioned. Because of the location randomness of the high frequency event, detection of the maximum local amplitude of the high frequency response cannot be used as an accurate marker to indicate the exit point of the defect.
- The distance between the entry and exit low frequency transient events on the vibration response is independent of the speed.
- The distance between points C and A is independent of the speed but dependent on the load.

These key findings are essential in developing methods to estimate defect sizes in bearings and also to explain the deficiencies in current defect size estimation methods. Moazen-ahmadi et al. [5] have suggested a more accurate estimation method by identifying sources of error in previous defect size estimation methods. Their new method was based on the detection of low frequency entry and exit events, instead of

the detection of the low frequency entry events and high frequency exit events. This method effectively uses the time measured between the entry point, shown as point C in Figure 1 (b), to the exit point, a low frequency event obscured by the multi-impact region in the vibration signal, shown in Figure 1 (b). Since detection of the entry transient event, point C shown in Figure 1(b), is not always an easy task, mainly due to possible background noise, Moazen-ahmadi et al. [5] proposed a formula to estimate the location of point C based on detection of point A. They showed that the distance between C and A is associated with the de-stressing phase of the rolling element, as the center of a rolling element traverses from a loaded to an unloaded state. This distance depends on the maximum total elastic contact deformation of the bearing components in the transient phase at the entry and exit, and is independent of speed. They have also suggested a signal processing method to find the low frequency exit transient event in the multi impact region. Since the high frequency exit events are often superpositioned on the low frequency exit events, detection of the low frequency exit event may not always be possible [5], whereas detection of the high frequency exit events is a relatively easy task and many signal processing methods have been developed to detect them [5]. Very limited previous detailed studies have been found to investigate the speed dependence of the travel path of a rolling element from point A, the end of the entry transient event, to the first impact point of a rolling element at the exit. Smith et al. [15] tried to identify systematic errors in conventional spall size estimation methods being speed dependent. However, detailed simulations have not been done to explain and investigate the physics of the interaction between rolling elements and defects. In order to develop an accurate defect size estimation method based on the detection of the high frequency event, detailed analyses of the effect of speed on the angular extent between entry and first exit impact events are essential; and these analyses are

addressed in this study. The analyses have been undertaken experimentally and analytically by modeling the path of rolling elements in defective bearings.

This paper aims to provide a detailed understanding of the effect of speed on the position of the high frequency events on the vibration response. These studies are then used to provide an effective defect size estimation algorithm, based on the detection of the high frequency exit event (see point B in Figure 1), and low frequency entry event at point A, without being biased by the operational speed.

## **2.2 Vibration models for line spall defects**

Studies of the effect of the speed on the path of rolling elements when unloaded in the defect zone should include investigations of the centrifugal forces acting on a rolling element and the finite size of that rolling element. Numerous multi-body dynamic models have been developed for modelling line spall defects [16-22], some of which do not consider the mass and none of which consider the finite size of the rolling element. The authors were unable to find numerical models that included the finite size of the rolling element. In these models, rolling elements are modelled as a point at its centroid that follows the geometry of the modelled defect. Harsha [23-26] has considered the mass and centrifugal forces acting on a rolling element, but not the finite size of the rolling element in his multi-body dynamic model. This model was initially developed to predict the vibration response of defective bearings with distributed defects [27]. Later, the model was improved to include the mass of the rolling elements to predict the nonlinear dynamic behavior of a rolling element bearing due to waviness and unbalanced rotor support [23-26]. The improved version of the model was further modified by Tadina [22] to predict the vibration response of bearings with localized spall defects on raceways. All of the aforementioned models are designed for defects with curvatures larger than the curvature of the rolling element, which maintains

contact between the raceways in the load zone. Therefore, none of the above multi-body dynamic models are suitable for modelling the path of a rolling element in the defect zone of a defective bearing with a line spall defect.

Recently, a more comprehensive multi-body dynamic model was developed by Moazen-ahmadi et al. [4, 13] which considers the inertia and centrifugal forces acting on rolling elements and, more importantly, the finite size of the rolling element. They showed that in order to predict the path of a rolling element and the corresponding features in the vibration response correctly, it is important to include the finite size of rolling elements when modelling localized defects. The key findings of this model are further validated and studied experimentally by Moazen-ahmadi et al. [5]. This model is chosen to simulate the vibration response and the path of rolling elements in this study.

### **3. Measurements and simulations**

#### **3.1 Test equipment**

The experimental data used here for the validation of the proposed algorithm, is from a previous study discussing the development of spall size estimation techniques for defective bearings [8]. The test rig includes a fan disk with 19 blades fitted on a shaft, which is supported by two Nachi 2206GK double row self-aligning ball bearings. These bearings have 14 balls on each row, a pitch diameter of 45mm, a ball diameter of 8mm, and a contact angle of  $0^\circ$ . The balls are retained in a staggered arrangement by a single cage, with the angular offset between the two rows being equal to half the angular ball spacing on the individual rows. The shaft is driven by a motor via a V-belt and the rotational speed is controlled using a variable voltage and frequency drive. Line spalls of varying sizes were machined on the outer raceway, and the vibration response was



measured at various speeds using an accelerometer. A detailed description of the test rig and the defects that were inserted can be found in reference [8].

### 3.2 Model description and analysis

This section presents a comparison between the simulated and experimental vibration results. The aim of the simulations is to show that the model can predict characteristics observed in the measured vibration response and to investigate the path of a rolling element in the defect zone. The nonlinear multi-body dynamic model introduced in Section 2.2 was implemented to simulate the path of rolling elements and the measured vibration responses of the test bearings. The numerical model is calculated in the continuous time-domain, and the results were discretised at time steps equivalent to  $1/65,536$  sec. The natural frequency and damping ratio of the high-frequency resonant mode included in the model were set to 20 kHz and 3%, respectively. This corresponds to the high-frequency bearing resonant mode observed in the measured vibration response. A static load of 100 N and a clearance of  $3\mu\text{m}$  were used in the model. The parameter values used in the model were chosen according to references [10, 13, 16, 17] and are listed in Table 1.

Table 1: Model parameter values used for simulation

Load-deflection factor between a ball bearing and the outer raceway	10.3 GN/m <sup>1.5</sup>
Load-deflection factor between a ball bearing and the inner raceway	18.9 GN/m <sup>1.5</sup>
Support stiffness	8 MN/m
Support damping	10%
Mass of the inner raceway and shaft	2 kg
Mass of the outer raceway	3 kg
Viscous damping constant	75 N s/m

### 3.3 Results comparison and analysis

Figure 2(a) shows 0.025 seconds of the acceleration data that was experimentally measured on the test bearing at a speed of 800 rpm and 100 N static radial load. The simulated acceleration response is included in Figure 2(b). The experimental data was low-pass filtered at 22 kHz as the bearing resonances at higher frequencies are not considered in the model.

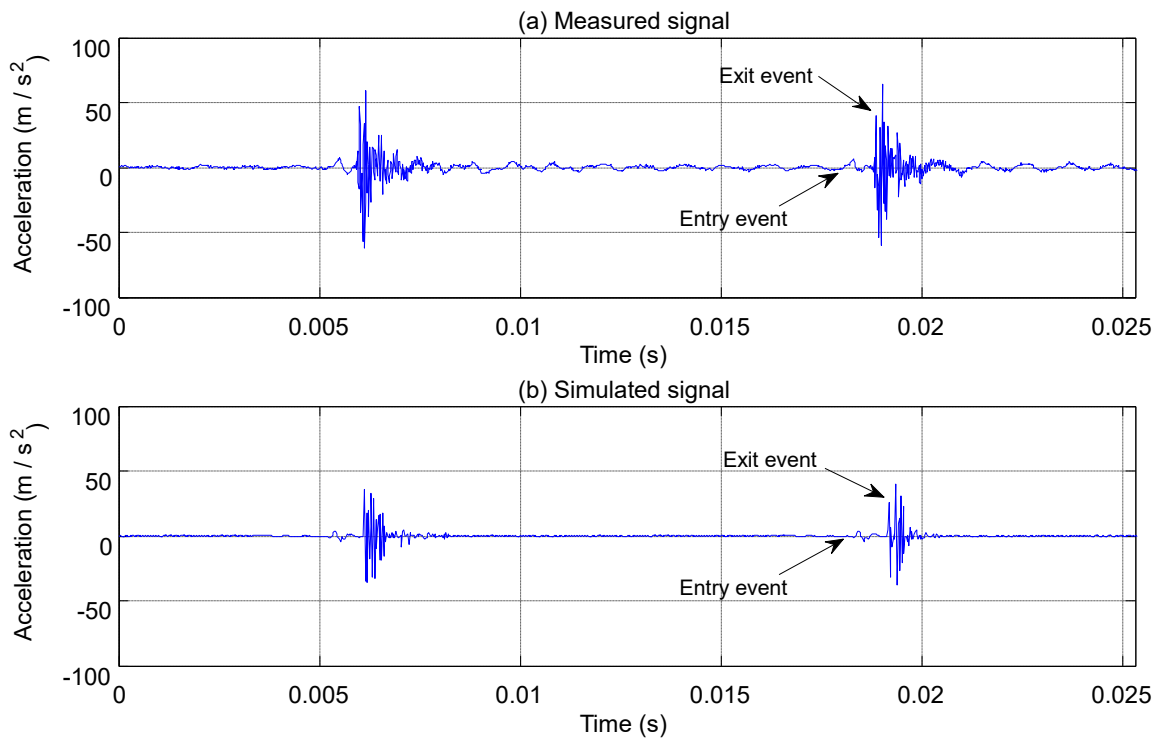


Figure 2: (a) Measured bearing vibration response, (b) Simulated bearing vibration response, over 0.025 seconds, at 800 rpm with a defect 1.2mm long.

Figure 3(a) shows a zoomed-in section of the signals presented in Figure 2, where the zoomed-in section corresponds to the period of time in which a roller approaches and leaves the defect on the defective raceway. Figure 3(b) shows the predicted path of the radial position of the rolling element. In Figure 3(b), the small difference between

the roller path and the defect geometry, outside the defect zone, is the roller contact deformation and is shown by  $\delta$ .

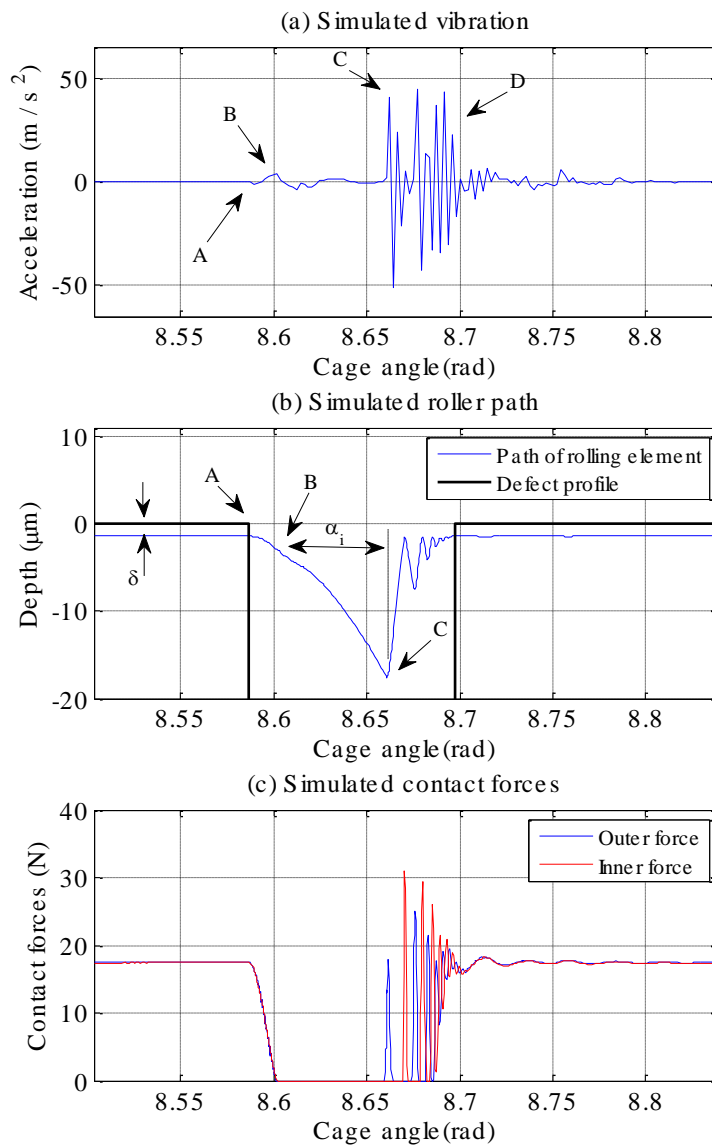


Figure 3: (a) Simulated vibration response of the test bearing at 800 rpm with 1.2mm defect size (b) Simulated path of the centroid of the rolling element plus the radius of the rolling element as it travels through the defect zone.  $\alpha_i$  is the cage angle to impact. (c) Simulated inner and outer contact forces acting on the same rolling element.

The key vibration characteristics of the simulation result are listed below.

**Rolling element entry:** The entry of the rolling element into the defect generates low frequency content in the vibration response, predominantly. This low frequency

vibration is due to the gradual de-stressing of the rolling element, which starts at entry point A, and ends when contact forces drop to zero at C, as shown in Figure 3. The entry of the rolling element into the defect from A to C can be considered as two events. The first is the entry transient (A-B) that is the gradual de-stressing of the rolling element as it enters the defect and lasts until the contact forces acting on the rolling element become zero as it loses contact with both raceways. The gradual decay of the contact forces can be seen in Figure 3(c). Moazen-ahmadi et al. [5] showed that the de-stressing angular travel of the center of a rolling element at this stage only depends on the maximum total elastic contact deformation that a rolling element needs to lose in the transient phase at the entry and exit [5]. The second event is the “drop”, (B-C), which is caused by the centrifugal force due to rotation, shown in Figure 3(b). The angular distance that the center of the roller travels from point B to C is shown as  $\alpha_i$  in Figure 3(b). During this process, the rolling element has no contact with the raceways and it carries no load. Therefore, the only forces acting on the rolling element at this stage are the inertia and the centrifugal forces.

**Rolling element exit:** This event is mostly associated with the excitation of high frequency modes of the bearing assembly. The exit of the rolling element from the bearing defect can be considered as two events. The first event is when the rolling element strikes the exit point of the defect for the first time at point C, just under 8.7 radians in Figure 3(b). Note that the results shown in Figure 3 are the trajectory of the centre of a rolling element in the defect zone. The direction change of the trajectory at point C, is due to the impact of the circumference of a ball hitting the exit point of the defect (just under 8.7 radians in Figure 3(b)). The high-frequency event in the vibration response observed at point C, as shown in Figure 3, is associated with this event, where the rolling element has to change direction suddenly. This abrupt change

in the direction of movement causes a step change in velocity and generates an impulse in the acceleration signal, which excites the high frequency resonance mode of the bearing assembly that is included in the model. Secondly, when the rolling element re-stresses between the raceways at the defect exit, multiple impacts occur as it alternately strikes the outer and inner raceway and re-stresses back to its normal load carrying capacity [28]. The multiple impacts at the exit of the defect can be seen in the experimental results in Figure 1(b), and have also been observed in experiments presented in previous studies [13, 14]. Moazen-ahmadi et al. [4, 5] showed that the re-stressing of the rolling element at point D is associated with low frequency events at the exit and the exit event is a superposition of a low frequency event potentially coupled with multiple high frequency events.

The 'drop' event, that is point B to C, as shown in Figure 3, is simulated and analyzed for different speeds in the following section. This section of the travel path is the only section where the contact forces are zero. Consequently, the boundaries of the rolling element and both raceways do not dictate the profile of the path of the rolling element.

### **3.4 Rolling element path simulation**

The model introduced earlier, is used to simulate the radial movement of a rolling element as a function of its cage angular position,  $H(\alpha)$ , for two different operational speeds. Since the aim of this section is to study the unloaded section of the path (the 'drop' event) of a rolling element in the defect zone, simulations are done for a sufficiently large defect (2.4 mm) to avoid the effect of the defect's exit point on the path of the unloaded rolling element. Simulation results of the paths of a rolling element in the defect zone for different speeds are obtained and polynomial curves are fitted to the results. Figure 4 illustrates the polynomial curve fitting results of order 4 for 0.05 rad of the simulated radial movement of a rolling element, as a function of its cage

angular position. These curves represent a section of the path of a rolling element where the rolling element is in the 'drop' section of the entry event: see the 'rolling element entry' section, described in section 3.2.

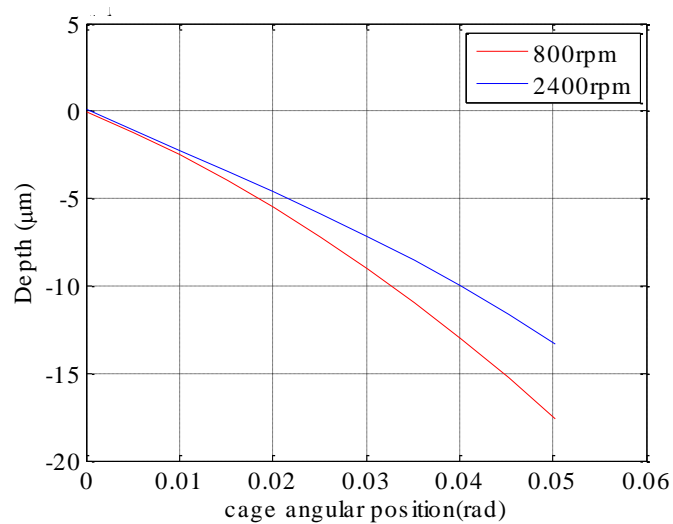


Figure 4: Polynomial curve fit results of order 4 for 0.05(rad) of the traveling path of the center of a rolling element in the defect zone for two shaft speeds.

Simulation of the path of rolling elements presented in Figure 4 shows the dependency of the radial movement of a rolling element as a function of its cage angular position in relation to the speed, when the rolling elements are unloaded in the defect zone. This dependency is particularly important as the angular distance that a rolling element travels in a defect zone to hit the exit point,  $\alpha_i$  shown in Figure 3, depends on the radial displacement traveled by a rolling element and the geometry of the bearing assembly and the defect. Therefore, the angle to impact,  $\alpha_i$ , depends on the rotational speed.

Comparing the simulation results, for any angular extent that a roller travels, it moves further in the radial direction at lower speeds when compared to higher speeds. As a result, the rolling element hits the exit ending the 'drop' event earlier (in terms of

angle) at lower operational speeds than at higher operational speeds. Note that the results shown in Figure 4 are the trajectory of the centre of a rolling element in the defect zone which is only for the ‘drop’ stage of the travel. Since the centre of the rolling element with lower operational speed travels more in vertical direction, a point on the circumference of the rolling element, hits the exit point of a defect earlier (in terms of angle) when compared with a rolling element with higher operational speed. Consequently, the radial distance traveled by the rolling element before it hits the exit increases by increasing the operational speeds for a certain time. If these analyses are ignored, estimating the defect size by measuring the distance between the entry and impact events results in either underestimation or overestimation, depending on the radial speed.

#### **4. Proposed hybrid method to estimate the defect size**

##### **4.1 Formulation**

In this section, the analysis presented in the previous section is used to improve current methods to estimate the bearing’s defect size, to enable greater accuracy and less bias for operational speed. Bearings with 0.6 mm and 1.2 mm defects, described in section 3.1, are used for validation of the proposed method. The aim is to use distinct features of the vibration signal that can be detected relatively easily. The method is based on the detection of the local maxima of the low frequency event (point B in Figure 3) and the first high frequency event, which corresponds to the first impact of a roller to the defect’s exit point, after the entry event (point C in Figure 3). The overall estimation of the length of the defect is broken down into estimations of three distances; namely  $L_1$ ,  $L_2$  and  $L_3$ . Figure 5 shows the zoomed section of the travel path of a rolling element in the defect zone and the three distances to be estimated.

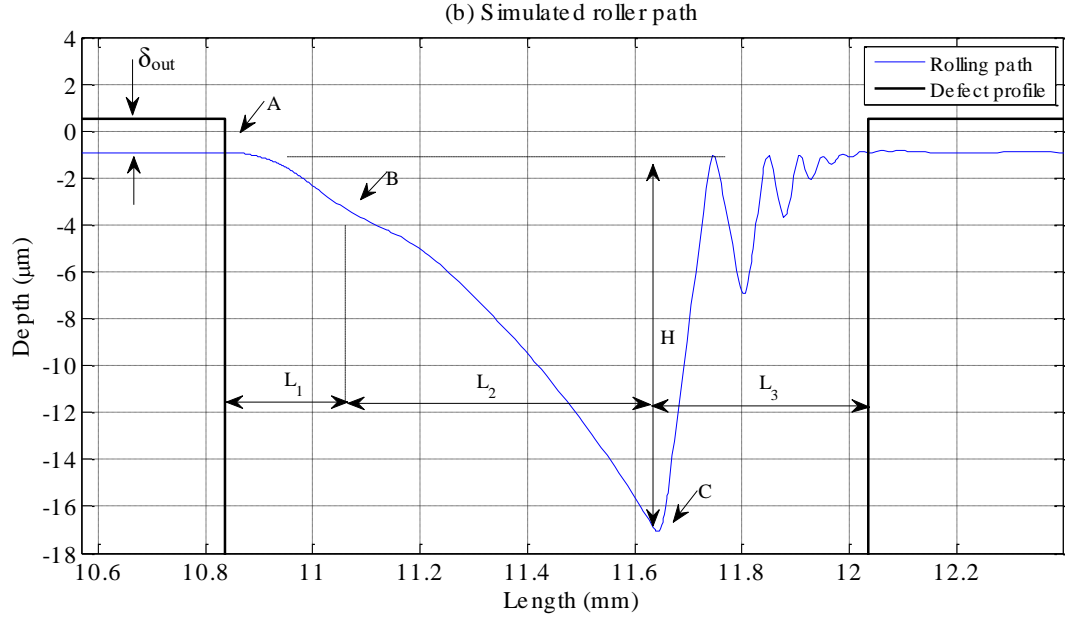


Figure 5: Schematic of the travel path of a rolling element in the defect zone.  $L_1$  is the distance from the point of entry to the point that rolling elements lose contact with both race ways,  $L_2$  is the distance to be measured from the vibration result and  $L_3$  is the distance to be estimated,  $H_i$  is the vertical relative movement of a rolling element at the time of first impact and  $\delta_{out}$  is the maximum relative deformation between a rolling element and the outer raceway in the load zone

**Estimation of  $L_1$ :** Moazen-ahmadi et al. [5] showed that angular travel of the center of a rolling element  $L_1$ , depends on the maximum total elastic contact deformation that a rolling element needs to lose in the transient de-stressing phase at the entry and exit. The angular travel  $L_1$ , can either be simulated using the mathematical model presented in Moazen-ahmadi et al. [4, 13], or estimated by geometrically relating the relative elastic contact deformation to the geometry of the bearing, using the following equation:

$$L_1 = \sin\left(\frac{(2r_b\delta_{max} - \delta_{max}^2)^{1/2}}{r_b + R}\right) \times R \quad (1)$$



where  $R$  is the radius of the outer raceway,  $r_b$  is the radius of the rolling element and  $\delta_{\max}$  is the maximum total elastic contact deformation between a rolling element and the raceways. It can be calculated using the following equation:

$$\delta_{\max} = \left( \frac{Q_{\max}}{k_n} \right)^{1/n} \quad (2)$$

where  $n$  is the load-deflection exponent ( $n = 1.5$  for point contact),  $Q_{\max}$  is the maximum radial distributed load in the direction of the applied load and  $k_n$  is the total load-deflection factor of a bearing which depends on the curvature of the rolling elements and raceways. Detailed descriptions and formulae for  $Q_{\max}$  and  $k_n$  for ball bearings can be found in Harris [3].

**Estimation of L2:** Is the estimation of the length to which the center of a rolling element travels from the point of entry (point B in Figure 5) and the first impact to the exit point (point C in Figure 5). This distance can be calculated by measuring the time to impact, ( $t_i$ ), which will be measured directly from the vibration signal.

$$L_2 = \sin(t_i \times \omega_c) \times d, \quad (3)$$

where  $\omega_c$  (Hz) is the rotational speed of the cage,  $d$  is the radius of the outer raceway and  $t_i$  is the measured time between the local maxima of the rising point of the first low frequency oscillation and the first high frequency oscillation on the vibration response.

**Estimation of L3:** The length between the impact point on the circumference of the rolling element to the center of the rolling element,  $L_3$ , depends on the radial distance travelled by a rolling element,  $H_i(t_i)$ , before the first impact, shown as point C in Figure 5. This distance,  $L_3$  can be determined geometrically by relating  $H_i(t_i)$  to the dimensions of the rolling elements as

$$L_3 = r_b \times \cos(\text{asin}(r_b - (H_i + \delta_{\text{out}})/r_b)), \quad (4)$$

where  $r_b$  is the radius of a rolling element and  $\delta_{\text{out}}$  is the maximum relative deflation between a rolling element and the outer raceway in the load zone.  $\delta_{\text{out}}$  depends on the curvature of the rolling elements and raceways, and the applied load [3]. The path of the center of a rolling element after losing contact with both raceways depends on the mass of a rolling element and the rotational speed of the shaft [4, 13]. Function  $H_i(t_i)$  which provides the radial displacement of a rolling element at the time to impact,  $t_i$ , can be obtained by the simulation explained in section 3.2. The time to impact,  $t_i$ , is measured directly from the experimental vibration signal.

The described method in this section is shown in a flowchart presented in Appendix A.

## 4.2 Validation and comparison

The hybrid method described in section 4.1 was used for 100 measured impacts and the mean and the standard deviation of estimation results for two test bearings (with 0.6mm and 1.2mm defect sizes) and under different operational speeds are presented in Figure 6. The hybrid method uses the polynomial curve fit functions obtained from the simulations in conjunction with the measured vibration signal of the test bearings. The curve fit functions of a defective bearing with a 2.4mm defect size for different speeds presented in section 3.4 are used for the hybrid method. The estimation results are compared against the defect size estimation results, using the method suggested by Sawalhi and Randall on the same bearings [8].

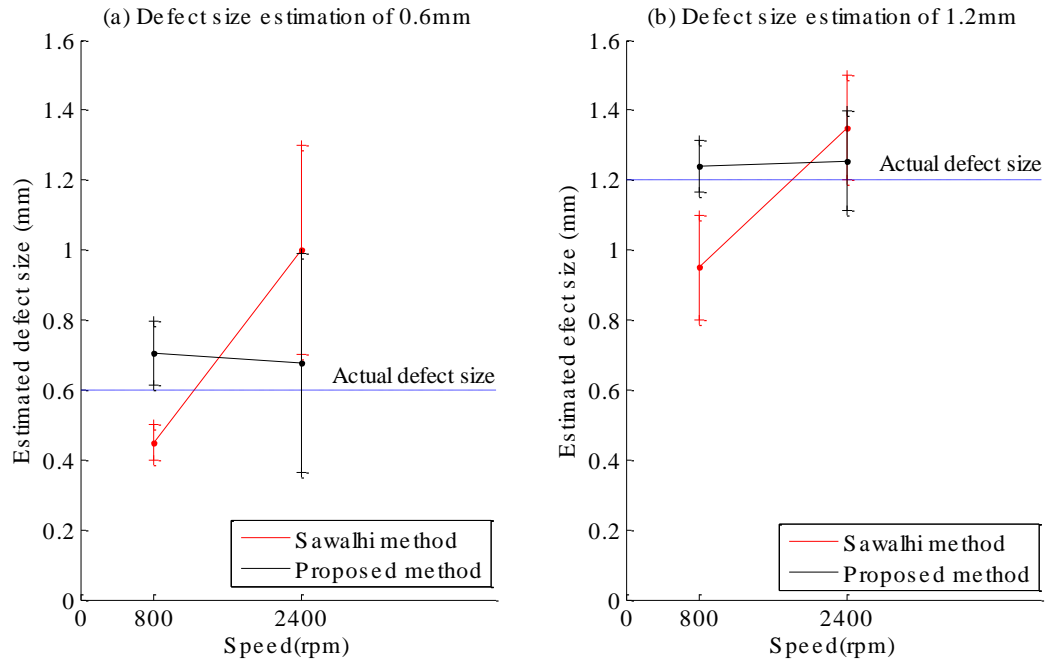


Figure 6: Comparison between the estimated mean and standard deviation of outer raceway defects using the method suggested by Sawalhi and Randall [8] and the proposed method in this paper for: a) 0.6mm and b) 1.2mm outer raceway defects

Figure 6 shows that the estimation method presented in this study is generally more accurate and less biased by operational speed. The hypothesis that the path of the unloaded rolling elements in the defect zone depends on the speed is indirectly validated by the fact that the method based on this hypothesis was able to remove the speed dependency in estimating defect sizes successfully.

Two sources of errors are identified in previous estimation methods. The first is the inaccurate assumption of the location of the entry event on the vibration signal, where the entry transient phase starts. This oversight creates an error with the opposite speed-related effect to that observed in Sawalhi and Randall's results [8, 15]. The second is due to ignoring the dependency of the unloaded rolling elements in the defect zone on the operational speed. The authors of this research believe that the high standard

deviation around the mean of the estimated defect size is due to the randomness inherent in the vibration result which causes some variation in the time to impact (time from the entry to the exit point). This randomness is partially due to the cage slippage [18]. Although the cage slippage is included in the model introduced by Moazenahmadi et al. [4], this feature was turned off in the simulation of the path of rolling elements. The reason for this is that the algorithm presented in this study requires only one path of a rolling element, whereas several different paths would be obtained by turning on the slippage in the model. By turning off the slippage (randomness) in the model, the resultant simulation of the path of a rolling element, used in the estimation algorithm, is essentially close to the mean path of rolling elements in the defect zone.

## **5. Conclusions**

This paper has demonstrated the importance of understanding the effect of inertia and centrifugal force, which acts on a rolling element, on the measured vibration signature in defective bearings. Significant speed dependency of angular extents between the low frequency entry events and the high frequency exit events on the vibration signal is shown by simulation and experimental measurements for high-speed operation. The sources of inaccuracy and the speed-dependency in the existing defect size estimation algorithms are identified and explained.

It is shown that for any angular extent that a roller travels, it moves further in the radial direction at lower operational speeds. Consequently, in defective bearings, the angular distance travelled by the rolling element in the defect zone before it hits the exit, increases by increasing the operational speed. If these important trends are ignored, then estimates of the defect size by measuring the distance between the entry and impact events, results in either underestimation or overestimation of the defect size, depending on the radial speed.

The analyses presented in this study are essential for developing algorithms to estimate the size of a bearing defect which is not biased for speed. A complete defect size estimation algorithm is proposed that is more accurate and less biased by shaft speed when compared with existing methods. The method presented here uses the model developed by Moazen Ahmadi et al. [4] and the measured vibration signal to predict the radial displacement traveled by a rolling element to estimate the defect size. Experimental estimation of different defect sizes, using the vibration signal, validates the analyses and the defect size estimation method presented in this paper.

### **Acknowledgments**

Thanks are due to Dr Nader Sawalhi for kindly providing the experimental data used in this study.

Appendix A

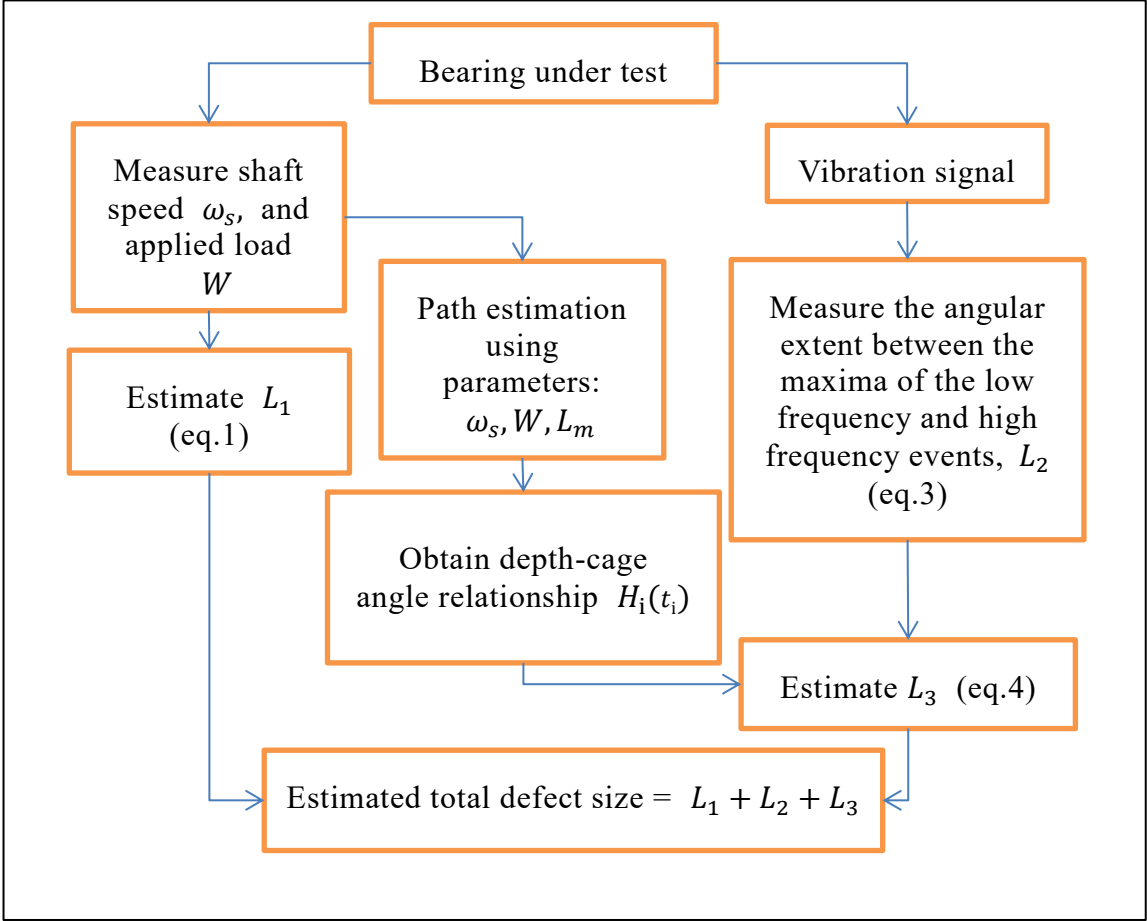


Figure 7: The flowchart for the proposed hybrid defect size estimation method, presented in section 4.1

## References

1. Y.T. Su, M.H. Lin, and M.S. Lee, *The effects of surface irregularities on roller bearing vibrations*. Journal of Sound and Vibration, 1993. **165**(3): p. 455-466.
2. C. Sunnersjö, *Rolling bearing vibrations-the effects of geometrical imperfections and wear*. Journal of Sound and Vibration, 1985. **98**(4): p. 455- 474.
3. T.A. Harris, *Rolling Bearing Analysis*. 2001, USA: Wiley.
4. A. Moazen Ahmadi, D. Petersen, and C.Q. Howard, *A nonlinear dynamic vibration model of defective bearings – the importance of modelling the finite size of rolling elements*. Mechanical Systems and Signal Processing, 2015. **52–53**: p. 309-326.
5. A. Moazen Ahmadi, C.Q. Howard, and D. Petersen, *The path of rolling elements in defective bearings: observations, analysis and methods to estimate spall size*. Journal of Sound and Vibration, 2016. **336**: p. 277-292.
6. I. Epps and H. McCallion. *An investigation into the characteristics of vibration excited by discrete faults in rolling element bearings*. in *Annual Conference of the Vibration Association of New Zealand*. 1994. Christchurch.
7. N. Sawalhi, R. Randall, and H. Endo, *The enhancement of fault detection and diagnosis in rolling element bearings using minimum entropy deconvolution combined with spectral kurtosis*. Mechanical Systems and Signal Processing, 2007. **21**(6): p. 2616-2633.
8. N. Sawalhi and R.B. Randall, *Vibration response of spalled rolling element bearings: observations, simulations and signal processing techniques to track the spall size*. Mechanical Systems and Signal Processing, 2011. **25**(3): p. 846-870.
9. S. Singh, U.G. Köpke, C.Q. Howard, and D. Petersen, *Analyses of contact forces and vibration response for a defective rolling element bearing using an explicit dynamics finite element model*. Journal of Sound and Vibration, 2014. **333**(21): p. 5356–5377.
10. D. Petersen, C.Q. Howard, N. Sawalhi, A. Moazen Ahmadi, and S. Singh, *Analysis of bearing stiffness variations, contact forces and vibrations in radially loaded double row rolling*

*element bearings with raceway defects*. Mechanical Systems and Signal Processing, 2015. **50-51**: p. 139-160.

11.S. Zhao, L. Liang, G. Xu, J. Wang, and W. Zhang, *Quantitative diagnosis of a spall-like fault of a rolling element bearing by empirical mode decomposition and the approximate entropy method*. Mechanical Systems and Signal Processing, 2013. **40**(1): p. 154-177.

12.D. Petersen, C. Howard, and Z. Prime, *Varying stiffness and load distributions in defective ball bearings: analytical formulation and application to defect size estimation*. Journal of Sound and Vibration, 2015. **337**(0): p. 284-300.

13.A. Moazen Ahmadi, D. Petersen, and C.Q. Howard. *A nonlinear dynamic model of the vibration response of defective rolling element bearings*. in *Proc of Australian Acoustical Society*. 2013. Victor Harbor.

14.S. Singh, U. Köpke, C.Q. Howard, and D. Petersen, *Analyses of contact forces and vibration response for a defective rolling element bearing using an explicit dynamics finite element model*. Journal of Vibration and Control, 2014. **333**(21): p. 5356–5377.

15.W.A. Smith, C. Hu, R.B. Randall, and Z. Peng. *Vibration-Based Spall Size Tracking in Rolling Element Bearings*. in *Proceedings of the 9th IFToMM International Conference on Rotor Dynamics*. 2015. Springer.

16.J. Sapanen and A. Mikkola, *Dynamic model of a deep-groove ball bearing including localized and distributed defects. Part 1: theory*. Proceedings of the Institution of Mechanical Engineers, Part K: Journal of Multi-body Dynamics, 2003. **217**(3): p. 201-211.

17.J. Sapanen and A. Mikkola, *Dynamic model of a deep-groove ball bearing including localized and distributed defects. Part 2: implementation and results*. Proceedings of the Institution of Mechanical Engineers, Part K: Journal of Multi-body Dynamics, 2003. **217**(3): p. 213-223.

18.N. Sawalhi and R. Randall, *Simulating gear and bearing interactions in the presence of faults: Part I. the combined gear bearing dynamic model and the simulation of localised bearing faults*. Mechanical Systems and Signal Processing, 2008. **22**(8): p. 1924-1951.



- 19.N. Sawalhi and R. Randall, *Simulating gear and bearing interactions in the presence of faults: Part II: Simulation of the vibrations produced by extended bearing faults*. Mechanical Systems and Signal Processing, 2008. **22**(8): p. 1952-1966.
- 20.M. Cao and J. Xiao, *A comprehensive dynamic model of double-row spherical roller bearing—model development and case studies on surface defects, preloads, and radial clearance*. Mechanical Systems and Signal Processing, 2008. **22**(2): p. 467-489.
- 21.S. Sassi, B. Badri, and M. Thomas, *A numerical model to predict damaged bearing vibrations*. Journal of Vibration and Control, 2007. **13**(11): p. 1603-1628.
- 22.M. Tadina and M. Boltežar, *Improved model of a ball bearing for the simulation of vibration signals due to faults during run-up*. Journal of Sound and Vibration, 2011. **330**(17): p. 4287-4301.
- 23.S.P. Harsha, *Nonlinear dynamic analysis of an unbalanced rotor supported by roller bearing*. Chaos, Solutions & Fractals, 2005. **26**(1): p. 47-66.
- 24.S.P. Harsha, *Nonlinear dynamic analysis of a high-speed rotor supported by rolling element bearings*. Journal of Sound and Vibration, 2006. **290**(1–2): p. 65-100.
- 25.S.P. Harsha, K. Sandeep, and R. Prakash, *Non-linear dynamic behaviors of rolling element bearings due to surface waviness*. Journal of Sound and Vibration, 2004. **272**(3–5): p. 557-580.
- 26.S.P. Harsha and P.K. Kankar, *Stability analysis of a rotor bearing system due to surface waviness and number of balls*. International Journal of Mechanical Sciences, 2004. **46**(7): p. 1057-1081.
- 27.S.P. Harsha, K. Sandeep, and R. Prakash, *The effect of speed of balanced rotor on nonlinear vibrations associated with ball bearings*. International Journal of Mechanical Sciences, 2003. **45**(4): p. 725-740.
- 28.N. Tandon and A. Choudhury, *A theoretical model to predict the vibration response of rolling bearings in a rotor bearing system to distributed defects under radial load*. Journal of Tribology, 2000. **122**(3): p. 609-615.

# Chapter 7

## Conclusion and Future Work

### 7.1 Conclusion

In this project, the vibration signature of bearings with an outer raceway defect has been investigated by using simulations and validated with experimental testing. The work has revealed the path of rolling elements in the defect zone and the associated features of the vibration signature. This led to the improvement of methods to estimate the size of a defect using measured vibration signals, and without historical trend data. The primary contributions of this thesis are the creation of a comprehensive multi-body nonlinear dynamic model of a bearing, which was used to create a new method for determining the size of a defect in a bearing, and in doing so identified the short-comings of previous methods. Further, modelling and experimental testing were used to show that the stiffness of the bearing assembly can be used to discriminate between a small defect and a large defect, even though the vibration signatures from both fault sizes appear similar. An outcome of these studies was a defect size estimation method that was shown to be accurate for two sizes of defects and, unlike previous methods, was not biased by shaft speed or applied load. The following sections outline the specific conclusions, outcomes and contributions of this research.

#### 7.1.1 Multi-body nonlinear dynamic model of a defective bearing

To address the lack of knowledge of the relationship between the path of a rolling element in the defect zone and the corresponding features of the vibration response, an improved

nonlinear dynamic model was proposed that included the contact forces of the bearing components and the associated vibration response. A method for accounting for the finite size of a rolling element was presented and included in the model. Unlike previous analytical models, the proposed model did not include a pre-defined path for the motion of the rolling elements, and can be used to simulate the vibration response caused by a variety of defect geometries. Comparisons with experimental results showed that the time–frequency characteristics of the significant events observed in the experimentally measured vibration response were more accurately predicted using this new model, compared with previous models that do not account for the finite size of the rolling elements. The significant events include the low-frequency pulse that occurs when a rolling element enters the defect, multiple high-frequency pulses that occur when a roller exits the defect, and impulses that occur when the rolling element strikes the raceway mid-way through the defect. Unlike previous models, the proposed model does not need to artificially modify the profile of the defect geometry to obtain a reasonable agreement with the experimental results, and no assumptions of the path of the rolling element at the entry and exit of the defect are needed. This proposed model enabled the development of a new method to determine the size of a bearing defect.

The outcome of the simulations presented is a hypothesis to explain the path of rolling elements in the defect zone, which explains both the discrepancies in the previous assumptions of the path of rolling elements in the defect zone and the corresponding features of the vibration response to the entry and exit events.

### **7.1.2 Experimental testing**

Experiments were conducted to validate the proposed numerical bearing model by comparing the predicted and measured vibration responses and shaft displacements when a

rolling element passes through a defect on the outer raceway. Experiments were conducted with machined defects of various sizes, and were conducted at various speeds and loads. The accurately measured displacement results were analysed to explain the relationship between the entry and exit events and the corresponding vibration response. The experimental results showed that:

- Exit impacts do not necessarily occur at the moment that the rolling element is midway through a defect. The exit impact events shown by acceleration impulse responses can occur before the centre of a rolling element reaches the end of a defect and are not apparent in the relative displacement measurements.
- The relative displacement measurements indicate that the transient event at the entry to the defect starts before the local maxima of the low frequency response.
- The angular extent for a rolling element to de-stress or re-stress between the raceways (low-frequency pulse on the vibration signal) increases with increasing applied load. These angular extents are not speed dependent. Therefore the relative angular extents between the low frequency entry and exit transient pulses decrease with increasing load.
- The assumption of the path of rolling elements in the defect zone, used in previous defect size estimation methods, is only valid for very small defects, of an order smaller than the patch of the relative deformation between a rolling element and the raceways. Ignoring the effect of the applied load, which is done in other defect size estimation methods, results in errors in the estimate of larger defect sizes.
- The angular extents between the low frequency entry pulse and the high frequency exit pulses on the vibration signal is speed dependent.

The analyses of these results improves the understanding of the characteristics of vibration signatures in defective bearings. The characteristics of the vibration response in defective bearings are categorized into several events, which are related to the different stages of the probable path of a rolling element in the defect zone. A method for estimating the size of a defect based on an explanation of the path of a rolling element was presented. It was shown that the proposed method is more accurate in estimating the size of a bearing defect compared with previous methods.

### **7.1.3 Stiffness analyses in defective bearings**

A method was presented in this study for calculating the quasi-static load distribution and stiffness variations of a radially loaded rolling element bearing with a raceway defect. Analysis of the load distributions showed that when rollers pass through the defect and lose all or part of their load carrying capacity, the load is redistributed to the other loaded balls. This includes the balls that are positioned outside the defect, such that good raceway sections are subjected to increased static loading when a raceway defect is present. Analysis of the bearing stiffness variations showed that when balls are positioned in the defect, the stiffness decreases in the loaded direction and increases in the unloaded direction. For an extended spall, which always has one or more balls positioned in the defect, the average stiffness in the loaded direction is reduced, compared with both the line spall and the undamaged bearing cases. The bearing stiffness variations due to the defect result in parametric excitations of the bearing assembly and play an important role in the resulting vibration response. The qualitative character of the resulting vibration response correlates strongly to the character of the stiffness variations. Rapid stiffness changes, which typically occur in a defect that has a sharp exit profile, produce high frequency impulses in the vibration response. Slower stiffness variations due to an extended spall produce low frequency parametric excitations. This was demonstrated by simulation based on the developed multi-body nonlinear dynamic

model developed in this study and measuring the vibration responses of defective bearings. The predicted contact forces were shown to fluctuate around the quasi-static loads on the balls, with rapid stiffness changes producing high magnitude impulsive force fluctuations. Furthermore, the low frequency pulse that occurs when a ball enters a line spall was linked to the dynamic properties of the bearing assembly. These findings were validated experimentally and confirm that the static stiffness decreases in the loaded direction at cage angular positions where rolling elements are positioned in the defect.

The analyses of varying stiffnesses in defective bearings were further investigated with the focus on the time-frequency characteristics of the vibration response. Analytical estimates and experimental measurements showed that the variation of bearing stiffness is a function of load, defect size and cage angular positions. Moreover it was shown that in defective bearings with extended defects, the static stiffness variation is greater due to the applied loads than cage angular position, when compared with smaller defects. It was found that when the applied load on the bearing is above the “critical load”, as defined in this study, the stiffness of the bearing assembly changes dramatically. This load depends on the depth and size of the defect. Above the critical-load, the deflection of the bearing causes more rolling elements to come into contact with the raceways and to support the applied load, which causes a change in the stiffness of the bearing assembly.

#### **7.1.4 Comprehensive defect size estimation algorithm**

One of the major objectives of this research project was to devise a reliable algorithm for estimating the size of a defect in a rolling element bearing based on measured vibration from a bearing. Simulations, which were validated by experimental testing, improved the understanding of the motion of rolling elements and the associated vibration response and

made it possible to propose an improved signal processing algorithm to estimate the size of a line spall defect, and was presented in Chapter 4.

In this research project, a study was conducted to investigate the change in the vibration response of a defective bearing as the shaft speed is increased. The speed dependency of the angular extents between the low frequency entry pulse and the high frequency exit pulse on the vibration signal have been shown by experimental measurements and simulations. It was found that the angular distance travelled by a rolling element in the defect zone before it hits the exit increases with shaft speed. If these important trends are ignored, then estimates of the defect size by measuring the distance between the entry and impact pulses, results in either underestimation or overestimation of the defect size, depending on the shaft speed. The simulations and experimental measurements in this study have led to the derivation of a reliable method to estimate the size of a line spall in defective bearings, which was shown to be unaffected by shaft speed, whereas previous methods estimated varying sizes depending on the shaft speed. The method is presented in Chapter 6 and uses the model presented in Chapter 3, and the defect size estimation algorithm proposed in Chapter 4.

It was shown that a bearing with a large line spall defect has a vibration signature that is similar to a bearing with a small line spall defect. A method to differentiate the size of the defect based on the vibration signature was devised. The method involves identifying the low frequency variation of the stiffness of the bearing assembly to distinguish defects that differ in size by exactly one angular ball spacing using a time-frequency signal processing method. It was shown that there is a critical-load such that the inner and outer rings displace sufficiently to cause more rolling elements to participate in supporting the applied load, with a consequential change in the stiffness of the bearing assembly. Hence, it is important to include the effect of load to obtain accurate estimates of the size of a defect. Recommendations for condition monitoring are given based on the analyses presented in

this study. The new method does not rely on historical data, unlike the previously suggested methods.

## **7.2 Recommendations for future work**

The comprehensive model created in this project enables the simulation of bearings with an arbitrary profile of the outer raceway. The model includes predictions of the contact forces between components, motion of the rolling elements and inner and outer rings, and the vibration of the bearing housing. This model can be used for future work to study defective bearings with different operating conditions, defect profiles and defect locations.

### **7.2.1 Effect of defect entry and exit geometry on the vibration signature**

Throughout this research, all investigations were conducted for rectangular shape line-spall defects, which are used in a large number of studies presented in the research literature. This geometry has 90 degree entry and exit angles and no rough surfaces. Further investigations are warranted to study how the entry and exit shapes of a defect affect the vibration signature. These further studies could also include rough surfaces.

Future studies could also examine different types of defects in bearings. All investigations in this project have been conducted for localized defects on the outer raceway. Therefore, possibilities for future work exist to analyse the effect of distributed defects, which occur around the circumference of a bearing component, such as generalised roughness, on the vibration signature. Since generalised roughness defects have scattered small pits and spalls with varying depths and sizes, there is a need for further research to develop a comprehensive model that can predict the vibration signal due to both small distributed defects and large line spall defects.



### **7.2.2 Deformable components**

The analytical model presented in this study assumes that the inner and outer rings are non-flexible but can translate in two degrees of freedom. Future work is required to develop a model with deformable inner and outer rings in the radial directions. In addition, the model could be further improved to include the vibration response of the bearing housing, where the vibration is commonly measured.

### **7.2.3 Time-frequency signal processing algorithms**

In the research presented here, time-frequency analyses were used to detect the changes in the characteristic frequencies of the low frequency vibration pulses, and used to estimate the size of a defect. Future work may investigate if more advanced time-frequency analysis techniques can provide enhanced diagnostic results in detection of the changes in the characteristic frequencies of the low frequency vibration event.